An Upper-bound Analysis Of The Upset Forging Of Rectangular Strip And Solid Cylindrical Disc To Account For Bulge And Fold.

AN UPPER-BOUND ANALYSIS OF THE UPSET FORGING OF RECTANGULAR STRIP AND SOLID CYLINDRICAL DISC TO ACCOUNT FOR BULGE AND FOLD

by
Ronald Allen Kohser

A Dissertation

Presented to the Graduate Committee

of Lehigh University

in Candidacy for the Degree of

Doctor of Philosophy

in

Metallurgy and Materials Science

Lehigh University

1975

CERTIFICATE OF APPROVAL

Approved and recommended for acceptance as a dissertation in partial fulfillment of the requirements for the degree of Doctor of Philosophy.

MARCH 21, 75
(date)

Betzalel Amitzur
Professor in Charge

Accepted MARCH 21, 75
(date)

Special committee directing the doctoral work of Mr. Ronald Allen Kohser

Betzalel Amitzur
Chairman

Walter C. Hahn

Alan W. Perez

Edward N. Kottcamp

ACKNOWLEDGEMENTS

The author wishes to acknowledge the expert guidance and assistance of his advisor, Dr. Betzalel Avitzur, received during all stages of the investigation. Valuable assistance was also received from Dr. W. C. Hahn, Dr. A. W. Pense, and Dr. E. H. Kottcamp. The patience and understanding of Ms. Sharon Rader while typing the manuscript is gratefully acknowledged.

Financial support for the project was provided by the National Science Foundation through Grant No. GK-37536, and their backing is truly appreciated.

Final thanks go to my wife, Barbara, for her patience, support, and understanding throughout this graduate study.

TABLE OF CONTENTS

LIST OF TABLES

LIST OF FIGURES

ABSTRACT

With the assumption of a Mises perfectly plastic material and constant shear stress friction prevailing between the forge platens and deforming solid, the upper-bound analysis technique was applied to the upset forging of rectangular strip and solid cylindrical discs in an effort to incorporate the combined phenomena of bulge and fold. A two-zone two-parameter solution was developed for the strip geometry and successfully produced a lower upper-bound for conditions of high interface friction. A more general three-parameter solution was developed, but was abandoned when investigation showed the increase in complexity failed to yield any additional benefit. Turning to the disc geometry, a two-zone two-parameter solution was then developed. While failing to produce a lower upper-bound, the new solution comes sufficiently close to previous solutions to merit further refinement and additional investigation.

Both the strip and disc solutions were then applied in an incremental technique designed to model deformation with bulge and fold. The results appear most encouraging, and the relative simplicity of the technique when compared with present alternatives is quite attractive.

Extensive description and discussion is provided throughout and numerous references are included so that future investigators will be aware of the rationale behind all decisions and need not duplicate previous efforts.

INTRODUCTION AND BACKGROUND

The Process

The term "upset forging", when loosely applied, describes all forming processes in which a material is plastically compressed between flat opposing dies,[1,2] and therefore encompasses not only the basic deformation in open die forging, but also the initial stages of many closed die operations as well. In the work to be presented, investigation will be limited to the compression of simple geometrical solids - rectangular strips and solid cylindrical discs - between flat parallel platens.

Figure 1 depicts the process variables for rectangular strip forging in which a strip of thickness 2t, width 2w, and length ℓ is being compressed. (NOTE: To be considered a strip, it is assumed that the length ℓ is much greater than both the thickness and the width.) The platens move at a constant velocity, $\dot{U}$, reducing the thickness and increasing the width. Since platen velocity is constant, the analysis represents a press forging operation as opposed to the alternative impact or drop forging operations. Forging force is denoted by P, while p denotes a possible constraining pressure applied on the free surface. A complete listing of all notation is included in Table 1.

The process of disc forging is presented in a parallel form in Figure 2. Here a disc of radius R_o and height T is being compressed

in thickness with corresponding increase to the outer radius. Platen velocity is represented as $\dot{U}/2$.

The Problem

As with nearly all metal forming operations a knowledge and understanding of process fundamentals is basic to successful application and efficient implementation at the production level. It is not surprising, therefore, that considerable effort has been directed toward the development of adequate analytical representations for these simple forging operations.

Avitzur, in an unpublished treatise on limit analysis,[3] discusses the near impossibility of obtaining an exact solution in even the simplest of cases. Adherence of the stress and strain components to the differential equations of stress equilibrium, the yield criterion, conditions of flow continuity and obedience of stress-strain relations requires the simultaneous solution of fourteen differential equations at all points within the deforming body, subject also to the prescribed geometric and static boundary conditions. Furthermore, ". . . when one considers that in any actual forming process neither the material nor the geometry nor the friction can ever be closely specified, it is obvious that exact solutions are not really demanded for 'practical purposes'."[4] Thus, it is apparent that the most benefit will be obtained through alternate techniques of either an observational or approximation nature.

Techniques of Investigation

One of the simplest approaches to the study of inhomogeneous flow, such as in upset forging, is through direct experimental observations. In his state-of-the-art survey, Tardif[5] presents a number of available techniques including: visioplasticity and related marker methods, recrystallization studies, mechanical property observations, plasticine modeling, X-ray investigation, etc. Considering the numerous developments made subsequent to this 1957 article, one becomes aware of the wealth of experimental techniques available. These techniques by themselves, however, suffer from a common limitation in that each test involves only one set of process conditions. Considering the near infinite variations possible in materials, process geometries, interfacial frictions, etc., it becomes apparent that to obtain a fundamental understanding of a forming process through experiment alone would be a monumental task. What is thus desired is an adequate theoretical analysis supported by sufficient experimental verification.

Utilization of the applied theory of plasticity has enabled the development of techniques capable of modeling the deformation of an idealized material under restricted geometries such as those involving plane strain, plane stress, or cylindrical or spherical symmetry. Through recent efforts several of the above restrictions have been somewhat relaxed. Kobayashi and Thomsen[6] present an excellent survey of analytical techniques. As a first approximation, the slab or slug equilibrium method is often quite useful. Using a simplified

state of stress and permitting variation along one principal stress direction, a slug of deforming material is subjected to conditions of static equilibrium. Solution of the resulting differential equation then provides the stress component for that particular direction throughout the deforming body. Another first approximation can be obtained through the uniform deformation energy or ideal power of deformation approach. Utilizing the strains imparted in going from an initial to final geometry and assuming uniform deformation, the necessary work is computed. From the work, required power and stresses can be computed as desired. Since redundant work and friction losses are neglected, however, the method may be subject to considerable error.[6]

A more involved method of analysis applicable to plane strain problems and some involving axial symmetry is the slip line technique.[6] For a small volume element within the plastic region of a body, the state of stress is evaluated with respect to a set of coordinates, preferably those of a principal coordinate system. A slip line net is derived by locating the set of maximum shear stress lines consistent with the stress boundary conditions. Knowing the flow strength of the material being deformed, the forming force, work, power, etc. can then be computed.

This method, having shown great potential, has become an important analytical tool in the theory of plasticity, but suffers from the deficiency that there is no easy method of checking the validity of a solution and thus the amount of possible error remains unknown.[7]

Still another analytical approach is that of the finite element method, in which equilibrium conditions are applied to small volume increments within the body, consistent with the applied boundary conditions. By moving from one element to another in a building fashion, a description of the deformation throughout an entire deforming body can be achieved. Recently, this technique has been combined with use of a Lagrange multiplier and linearized stiffness equations to produce an approach known as the matrix method.[8,9,10] Finite element techniques are limited, however when the effects of process variables on the deformation characteristics are of major concern. Where large plastic deformations are involved, the finite element calculations require extensive utilization of computer time and facilities.[9] Each combination of friction, geometry, etc. must be solved as an individual problem.

As a final method of approximating the exact analytical solution of a metal forming process, consider the technique of limit analysis. Two approximate solutions are developed: one, an upper-bound and the other, a lower-bound. The exact forming pressure is never greater than the pressure predicted by the upper-bound, which requires flow to be described by a kinematically admissible velocity field, and never less than that predicted by the lower-bound, which requires a statically admissible stress field. Thus, the exact pressure is located between these limiting values, which converge toward the exact solution as the velocity field and the stress field respectively become more realistic.[11]

"Among various theoretical methods available for analyzing metal forming problems, the upper-bound method is the most practical technique for theoretical analysis of metal flow. For describing the metal flow, this method considers an admissible velocity field that satisfies the incompressibility, continuity, and velocity boundary conditions. Based on this velocity field, the deformation, the shear (if velocity discontinuities are present), and the friction energies are computed to give the total forming energy and also the forming load. Based on limit theorems,[12] this calculated forming load is necessarily higher than the actual load and it, therefore, represents an upper-bound to the actual forming load. Thus, the lower this upper-bound load, the better is the prediction. Often the velocity field considered includes one or more parameters that are determined by minimizing the total forming energy with respect to those parameters. Thus, the determined values of the parameters give a somewhat better upper-bound velocity field. In general, with an increasing number of parameters in the velocity field, the solution improves while the computations become more complex. Consequently, for practical use of the upper-bound method, practical compromises are made in selecting an admissible velocity field.'

'When applying the upper-bound method, the following assumptions are usually made:

1. The deforming material is isotropic and incompressible

2. The elastic deformations are neglected

3. The inertial forces are small and neglected

4. The friction shear stress, τ, is constant at the die-material interface and is given by a constant shear factor, f, or by a friction factor, m:

$$\tau = f\,\bar{\sigma} = \frac{m\,\bar{\sigma}}{\sqrt{3}}$$

[Note: we will use σ_o instead of $\bar{\sigma}$]

5. The material flows according to von Mises' flow rule

6. The flow stress, $\bar{\sigma}$ [here denoted as σ_o], is constant."[13]

Utilizing the above assumptions, the upper-bound approach will be applied in the following analyses.

Previous Analyses

Before discussing the need for an improved analysis and presenting the newly derived upper-bound solution, it is important to understand the state-of-the-art achieved by previous analyses. When one considers the potential applications such as modeling the upset test for forgeability[14] and providing the background necessary for theoretical calibration of the ring compression test (to be discussed later), it is not surprising that the work performed is quite extensive.

The original solution for plane strain compression of a slab between parallel flat dies was performed by Prandtl[15] in 1923, with subsequent work being performed by Geiringer and Prager[16] and Siebel.[17] These early slip-line type solutions were extended through the works of Hill,[18] Hill, Lee, and Tupper,[19] Alexander,[20] and Bishop.[21] The more recent works of Hill[4] and Shabaik[22,23] use slip-line techniques to predict the change in shape of the free surface as a function of the process variables. Paralleling the slip-line solutions, analyses using the upper-bound technique were performed for strip forging by: Johnson,[24] Johnson and Kudo,[25] Kudo,[26] and Avitzur.[27,28]

Since the slip-line technique is nominally restricted to plane strain problems, we find that the work on solid disc forging belongs primarily to the alternative techniques. Experimental studies have been conducted by Siebel,[29] Shaw,[30] and Kulkarni and Kalpakjian.[31] Schroeder and Webster[32] completed the earliest upper-bound analysis

in 1947 with subsequent contributions coming from Kudo,[33,34] Kobayashi,[35] Kobayashi and Thomsen,[36] Steck and Schmid,[37] and Avitzur.[27,28] The finite element technique was applied by Lee and Kobayashi[38] and the most recent matrix technique was used by: Kobayashi and Lee,[39,9] and Shah, et al.[8]

DEVELOPMENT OF THE UPPER-BOUND VELOCITY FIELD

Introduction

For describing metal flow during deformation, the upper-bound analysis begins by considering an admissible velocity field which satisfies incompressibility, continuity, and velocity boundary conditions. In general, the more accurately the proposed field models reality, the lower the resulting upper-bound solution. It has been noted, however, that such improved solutions usually come at the expense of increased mathematical complexity. A standard approach, therefore, is to produce a series of solutions of increasing complexity, wherein the simpler solutions become limiting conditions of the more complex. Such a sequence leading to the newly developed upper-bound solution for bulge and fold will now be presented. The process of strip forging (plane strain) will be used in the discussion with the disc forging analogues being obvious.

The Parallel Velocity Field

Figure 3 presents the parallel velocity field for rectangular strip forging.[27] The solid lines indicate the original strip which decreases in height and increases in width to produce the final profile indicated by the broken line. Since the velocity component in the X-direction is void of any Y-dependency, the originally straight contour of the free surface remains straight throughout the entire deformation. It has been observed that in the absence of friction at the workpiece-platen interfaces, the deformation of the body will

be everywhere uniform and the result will be a perfect cylinder of reduced height.[40] For such conditions, the parallel velocity field would be an ideal model.

Barreling or Bulging

Since a frictional resistance normally exists between the platens and the workpiece, the upper and lower surfaces of the specimen are not as free to move, the frictional forces opposing uniform deformation. The free spread of the ends of the specimen material is prevented, producing a convex or barrel-shaped contour.[1,40] Although "it is difficult to find much data about the extent of barreling during upsetting in the literature,"[31] it has been observed that the degree of bulge is a function of geometry and friction.[12] The results of one experimental study are presented in an article by Kulkarni and Kalpakjian.[31]

The Bulge Velocity Field

What is now desired, therefore, is to formulate a velocity field based on the parallel field, but modified to incorporate a possible bulge or barrel of the external free surface. Figure 4 depicts such a bulge velocity field as presented in section 13,2.2 of Reference 27. Here the velocity component in the X-direction is modified to include an exponential dependence on the term y/t, chosen so as to produce an exponential cusp type of free surface. Although this pointed cusp contour may be a poor representation of a convex bulge, the exponential term has the definite benefit of

mathematical simplicity when subjected to integration or differentiation. Furthermore, if b is set equal to zero, the bulge velocity field reduces to the previous parallel velocity field. Thus, the parallel field is simply a limiting case of the more general bulge flow field, in which b may assume all values greater than or equal to zero. By minimizing the final solution for required power with respect to b, the optimum rate of bulge formation may be determined. The larger the value of b, the larger the resulting bulge.

Evaluation of the Bulge Field - The Ring Test

In order to evaluate the relative merits and areas of deficiency in any solution, it is important to consider its performance in actual applications. Both of the velocity fields presented here have analogues for the solid cylindrical disc[27] and hollow cylindrical disc geometries.[27,41] The hollow disc solutions have both been applied to develop theoretical calibration curves for the ring compression test, a test useful in determining the flow stress of a deforming material and a quantitative measure of interface friction over a wide range of forming temperatures and strain rates. Since determination of these two values is necessary for all theoretical estimates of the force and energy required in forging,[42] a large amount of investigation has been performed.

The qualitative nature of the ring test can be understood through consideration of Figure 5. Figure 5a depicts the geometry of a cylindrical ring upset with good lubrication between the workpiece and the platens. Investigation of the free surface contours

indicates that there was a uniform outward expansion of the entire ring, resulting in an increase in the internal diameter. In comparison, Figure 5b shows the same specimen upset with poor interfacial lubrication. While the outer free surface still shows signs of outward expansion, the inner surface barrels inward, indicating a shrinking of the internal hole diameter. By upsetting identical ring specimens through identical reductions, varying only the lubrication, the investigator is qualitatively able to compare the various lubricants. The relative change in internal diameter determines the position in the relative rankings.

Since such a test is applicable over a wide range of temperatures, strain rates, amounts of deformation, lubrication, etc., and is directly suitable for evaluating hot working conditions, a major effort has been made to make the results quantitative. Using an appropriate theoretical analysis applied to a fixed ring geometry, calibration curves of percent change in internal diameter versus percent deformation are computed for various values of interfacial friction, as shown in Figure 6 [from Ref. 43]. An experimentally determined curve can then be fit to the theoretical calibration set to determine the appropriate value for interface friction. By knowing the friction factor, the theoretically computed forging force can then be equated to the experimentally observed value, enabling computation of the material flow stress, σ_o. A brief look at the history of the ring test calibrations will reveal the development

of the analytical studies. An investigation of any deficiencies in the present theory will expose areas of potential theoretical improvement.

The earliest efforts to obtain a quantitative ring test, as represented by the works of Male,[44] Male and Cockcroft,[45] Male,[46] and Burgdorf,[47] all utilize the coulomb coefficient of friction concept with the parallel field. When it was shown that the concept of constant interface friction factor [m] is more realistic than the concept of coefficient of friction for describing friction stresses in upset forging,[48] the parallel velocity field solution was modified to incorporate this change and the theoretical curves were recomputed. Solutions of the parallel field with constant shear friction are presented and used in works by: Hawkyard and Johnson,[49] Avitzur,[27] Saul, et al.,[50] Abdul and Bramley,[51] and Sauerwine.[11]

In 1970, Male and DePierre,[52] revealed the breakdown of the parallel velocity field solution for conditions of large thickness to diameter ratios (large compared to a thin disc but less than 1) and high values of friction. For these conditions, a solution was required that would incorporate the barreling or bulge phenomena. The bulge solution by Avitzur[53] opened the door for this improvement, which was ultimately found to be better than the parallel field solution in all cases.[11] Subsequent publications by Lee and Altan,[13] Liu,[54] DePierre and Gurney,[55] and DePierre, Gurney and Male[43] reflect the adaptation and development of the bulge solution. Since the solution is accurate only for the rate of bulge formation when a

bulge does not exist, it is assumed that any existing bulge does not influence the velocity field in the remainder of the specimen.[43]

Investigation of the present solutions for the bulge velocity field reveals an adequate correlation at low values of m.[13] When friction becomes high, however, the theoretical calibration appears to break down.[11] Experimental curves have been produced which lie entirely above the m = 1 calibration line.[56] Since m = 1 corresponds to a frictional shear stress of $\sigma_0/\sqrt{3}$, the maximum permitted by Mises Yield Criterion, values greater than one are unphysical and are indicative of a theoretical deficiency. As early as 1965, Male and Cockcroft observed that "compression of a ring under conditions of high friction is a complex process. Sliding of the original surfaces in contact with the dies tends to take place in addition to bulging of the free surfaces, and the degree of both of these is dependent upon μ and upon the amount of deformation imposed. When sufficient bulging takes place, material originally at the free surfaces comes into contact with the dies and adds to the area of the material tending to slide."[45] Lee and Altan[13] have proposed that it is the presence of the "foldover" phenomenon which destroys adequate calibration for high values of m.

The Foldover Phenomenon

Thus, while the bulge solutions were able to improve the results in the critical areas of high friction and relatively large thickness to diameter ratios, they were not able to completely overcome the

deficiencies. It has long been known that changes in lubrication change the stress pattern within the deforming body,[14] as has already been observed in the transition from the parallel field to the non-uniform deformation bulge velocity field. Shaw et al.[8] have observed that under conditions of high friction, "The complexity of nonuniform deformation is not only represented by barreling of the free surface, but further indicated by the fact that a part of the initially free surface comes into contact with the die during compression ("folding")." This type of flow is a function of geometry and friction[8] and becomes more pronounced with increasing frictional restraint.[9]

Figure 7 [From Ref. 30] presents a plasticine cylinder 2" in diameter and 4" in height, which has been compressed 50%. The grid lines originally on the cylindrical surface and now on the extended horizontal surface in contact with the platen show that the material has folded around the upper and lower corners of the specimen. Observations and discussion of such a flow occurring under conditions of high or "sticking" friction have been included in the recent works of: Kalpakjian,[17] and Jain,[58] as well as several publications of the AISI Committee of Hot Rolled and Cold Finished Bar Producers.[39,59] Unksov[60] has observed that the folding of material from the sides increases as friction and/or original height to diameter ratio is increased, precisely the areas where the bulge analysis appears to be deficient. Kobayashi[61] reports that while specimens with a larger initial height have more of the originally

free surface come into contact with the die for given reductions in height, "contact of originally free surface with the die begins even under lubricated conditions, when the height becomes small compared to the diameter".

One of the earliest attempts of incorporating foldover into a theoretical analysis was that of Lee and Kobayashi,[62] reported in May, 1971. The elastic - plastic finite element method was applied, but the results failed to show any tendency of folding up through a 33 percent reduction under conditions of complete sticking. Recently, however, several analyses have been presented which are capable of producing a near-continuous folding throughout the deformation. Shabaik[22,23] has published several works in which slip-line techniques are applied to a rectangular strip in plane strain. The only solutions available for the disc geometry are those using the matrix technique and are described in the publication of Lee and Kobayashi,[9,39] Shah, et al.,[8] and Kobayashi and Oh.[63] All of the techniques applied to-date, however, involve considerable mathematics and require extensive utilization of a computer. Each condition of geometry and friction must be computed individually from scratch, there being no general formulae, etc. The more general upper-bound method of analysis has yet to be applied to the problem of foldover, and it is precisely this lack which the present work attempts to fill.

Foldover in an Upper-Bound Velocity Field

Application of the upper-bound technique to the problem of upset forging with foldover is dependent upon the development of a kine-

matically admissible velocity field capable of modeling the phenomenon. That is, the proposed field must permit a downward moving ram or platen to overtake a slower moving outwardly sloped or barreled free surface. The velocity discontinuity between the ram and the slower moving surface coming into contact with the ram, i. e., being folded, is permissible only as a point discontinuity. Therefore, once folded, the material coming into contact with the platen must then assume the platen velocity. The geometry change must be noted and subsequent deformation computed from this new geometry in a step-by-step progression technique.

It has already been noted that the phenomena of barreling and foldover are closely linked, foldover being dependent on a prior barreling of the free surface. To obtain insight as to how these two might be presented in an admissible velocity field, consider several specimens upset under conditions of high friction. Figure 8[64] presents a bi-metal disc consisting of a copper alloy core inserted into a steel ring and subsequently upset under conditions of high friction. Investigation of the interface contour shows that the exponential cusp velocity field would be a good representation for flow in the interior region of the disc, the lack of symmetry arising due to differing friction conditions over the two platens. The outer free surface, however, shows that at the periphery the pointed cusp flow has blunted to produce a smooth convex bulge. Similar observations can be made from the bottom specimen of Figure 9, also provided by Mr. V. DePierre.[65] Here an OFHC copper cylinder

has been compressed 50% under conditions of poor lubrication. The interior flow seems to closely follow the exponential cusp velocity field. However, as we approach the periphery of the specimen the cusp becomes increasingly blunted, finally producing the smooth external bulge.

This differing of deformation depending on locality within the specimen has been noted as early as 1932 in work by Siebel.[29] Figure 10, taken from a more recent handbook,[2] depicts the three regions he observed. Area I depicts material adjoining the dies, which remains almost stationary as the deformation proceeds. The bulk of the deformation is concentrated in the region designated as Area II, with the material in Area III near the outer surface being deformed only as a result of the center material moving radially outward. By observing the distorted grid lines and using a minimum of imagination, Areas I and II can easily be envisioned as being a single region obeying the exponential bulge velocity field. Area III, near the periphery, obeys a modified velocity field which serves to blunt the internal cusp. Further evidence for the validity of this approach can be seen in Figure 11.[66] Here an aluminum split disc was compressed 20% with no lubrication. Under these sticking conditions, regions of little or no deformation were observed near the periphery causing the material to locally pull away from the plane of the split. The fact that such regions do not exist in well-lubricated specimens tends to indicate their possible involvement in both the blunting and foldover phenomena. The basic triangular shape

of the periphery region would produce the gradual blunting of the centerline cusp, and furthermore, would obey the point-type discontinuity necessary at the material - platen interface.

The Two-Zone Approach

With the preceding observations providing a basis, a two-zone velocity field is now proposed for the processes of disc and strip forging, utilizing the two-zone regions of Figure 12. An interior Zone I is proposed which will correspond to Siebel's[29] Areas I and II and will obey the exponential bulge velocity field. A peripheral Zone II is chosen to have a triangular geometry when cut in section and corresponds roughly to Siebel's Area III. A plane surface interface (straight line on a section) is chosen to divide the zones in order to provide for mathematical simplicity in the computation of both interzone shear losses and the Zone II velocity field. The size of Zone II is left as a pseudo-independent parameter, ξ, later to be determined by minimization of the resulting upper-bound solution.

The bulge or barrel phenomenon is incorporated in the interior Zone I. Zone II serves to blunt the cusp into a rounded barrel, and by selection of an appropriate velocity field, is capable of modeling the overtaking of an outwardly barreled surface by a faster moving ram necessary to produce "foldover".

THE TWO-ZONE TWO-PARAMETER SOLUTION FOR STRIP

Introduction

Noting that the required upper-bound computations are somewhat simpler in the Cartesian coordinate system than in the cylindrical coordinate system, the process of plane strain upset forging of rectangular strip was chosen for a preliminary investigation of the two-zone velocity field. As indicated in Figure 13, flow in the interior zone will obey the exponential bulge velocity field as presented by Avitzur in section 13.2.2 of Reference 27. This field is presently regarded as the best available upper-bound representation by those using the quantitative ring compression test, and has been shown to be an accurate modeling of flow in the interior of a deforming solid under conditions of high interface friction. The second zone, or fold zone, will be characterized by a new independent variable, ξ, and is restricted to obeying a simple shear type of flow pattern with flow being parallel to the platen surface, i.e., a constant height field. The size of Zone II will remain unspecified throughout the analysis and, along with the degree of bulge, will become an optimization parameter in the final solution. The ultimate values will be those that minimize the required power.

The Upper-Bound Approach

The analytical techniques to be applied in the following solutions parallel the standard upper-bound procedure as presented by Prager and Hodge[67] and used liberally in the text by Avitzur.[27] The basic theorem of the analysis states that among all kinematically

admissible velocity fields, the actual one minimizes the expression:

$$J^* = \frac{2}{\sqrt{3}}\sigma_o \int_V \sqrt{\frac{1}{2}\dot{\varepsilon}_{ij}\dot{\varepsilon}_{ij}}\, dV + \int_{S_\Gamma} \tau|\Delta v|dS - \int_{S_t} T_i v_i dS \qquad (1)$$

(Notation is described in Table 1)

Here, the first term expresses the power for internal deformation throughout the volume of the deforming body; the second term accounts for the shear power dissipated over surfaces of velocity discontinuity; and the final term considers power supplied by external body tractions.

Mathematical Description of the Two-Zone Regions

Before proceeding with the limit analysis, the various limits of integration, etc. must be established by mathematically describing the two-zone geometry. First, since symmetry can be applied with respect to both the X- and Y-axes, one need only consider a single quadrant of the strip and multiply the computed power by four to model the entire body. Thus, all computations will be performed in the upper right hand quadrant of the strip geometry presented in Figure 12.

Simple geometrical considerations will show that the interzone surface can be described by the equations:

$$y = \frac{t}{\xi}(x - w + \xi)$$

or (2)

$$x = w - \xi + \frac{\xi y}{t}$$

Thus, Zone I can be described as:

$$x: \quad \text{from } x = 0 \qquad \text{to} \qquad x = w - \xi + \frac{\xi y}{t}$$

$$y: \quad \text{from } y = 0 \qquad \text{to} \qquad y = t$$

and Zone II as:

$$x: \quad \text{from } x = w - \xi + \frac{\xi y}{t} \qquad \text{to} \quad x = w$$

$$y: \quad \text{from } y = 0 \qquad \text{to} \quad y = t$$

Zone I - Internal Power of Deformation

In Zone I, the mode of flow is described by the exponential bulge velocity field as presented in Reference 27. Equation 13.13c of this text presents the velocity components as:

$$\dot{U}_x = \frac{b}{1 - e^{-b}} \dot{U} \frac{x}{t} e^{-by/t}$$

$$\dot{U}_y = \frac{-1}{1 - e^{-b}} \dot{U} (1 - e^{-by/t}) \tag{3}$$

$$\dot{U}_z = 0$$

The strain rates components can then be computed by simple differentiation utilizing the relations:

$$\dot{\varepsilon}_{xx} = \frac{\partial \dot{U}_x}{\partial x} \qquad \dot{\varepsilon}_{yy} = \frac{\partial \dot{U}_y}{\partial y} \qquad \dot{\varepsilon}_{zz} = \frac{\partial \dot{U}_z}{\partial z}$$

$$\left.\begin{aligned}
\dot{\varepsilon}_{xy} &= \dot{\varepsilon}_{yx} = \frac{1}{2}\left(\frac{\partial \dot{U}_x}{\partial y} + \frac{\partial \dot{U}_y}{\partial x}\right) \\
\dot{\varepsilon}_{yz} &= \dot{\varepsilon}_{zy} = \frac{1}{2}\left(\frac{\partial \dot{U}_y}{\partial z} + \frac{\partial \dot{U}_z}{\partial y}\right) \\
\dot{\varepsilon}_{zx} &= \dot{\varepsilon}_{xz} = \frac{1}{2}\left(\frac{\partial \dot{U}_z}{\partial x} + \frac{\partial \dot{U}_x}{\partial z}\right)
\end{aligned}\right\} \quad (4)$$

Evaluating the strain rates of Zone I from the velocity field of Equation (3), we have the strain rates field presented as Eq. 13.14 of Reference 27:

$$\dot{\varepsilon}_{xx} = -\dot{\varepsilon}_{yy} = \frac{b}{1 - e^{-b}} \frac{\dot{U}}{t} e^{-by/t}$$

$$\dot{\varepsilon}_{xy} = \frac{1}{2} \frac{-b}{1 - e^{-b}} \dot{U} \frac{x}{t} \frac{b}{t} e^{-by/t} \quad (5)$$

$$\dot{\varepsilon}_{xz} = \dot{\varepsilon}_{xy} = \dot{\varepsilon}_{zz} = 0$$

The internal power of deformation can now be evaluated by use of the expression:

$$\dot{W}_i = \frac{2}{\sqrt{3}} \sigma_o \int_V \sqrt{\frac{1}{2} \dot{\varepsilon}_{ij} \dot{\varepsilon}_{ij}} \, dV \quad (6)$$

where σ_o is the flow stress of the material and V is the volume being deformed.

Substituting the strain rates of Equation (5) into the expression of Equation (6), the internal power of deformation in Zone I may be evaluated as follows:

$$\dot{W}_{iI} = \frac{2}{\sqrt{3}} \sigma_o \int_V \sqrt{\dot{\varepsilon}_{xx}^2 + \dot{\varepsilon}_{xy}^2}\, dV \tag{7}$$

Substituting and multiplying by four to include the four symmetrical regions:

$$\dot{W}_{iI} = \frac{4\sigma_o b^2 \dot{U}}{\sqrt{3}\, t^2 (1-e^{-b})} \int_{y=0}^{y=t} e^{-by/t} \left\{ \int_{x=0}^{x=w-\xi+\xi y/t} \sqrt{x^2 + \frac{4t^2}{b^2}}\, dx \right\} dy \tag{8}$$

Using the basic integral form of:

$$\int \sqrt{a^2 + x^2}\, dx = \frac{1}{2} \left[x \sqrt{x^2 + a^2} + a^2 \log_e (x + \sqrt{x^2 + a^2}) \right] \tag{9}$$

which appears as Integral 123 of Reference 68, the inside integral can be evaluated directly to yield:

$$\dot{W}_{iI} = A \left\{ (w - \xi) \int_{y=0}^{y=t} e^{-by/t} \sqrt{a + cy + fy^2}\, dy \right.$$

$$+ \frac{\varepsilon}{t} \int_{y=0}^{y=t} y e^{-by/t} \sqrt{a + cy + fy^2}\, dy$$

$$\left. + \frac{4t^2}{b^2} \int_{y=0}^{y=t} e^{-by/t} \ln \left(\frac{w-\xi+\xi y/t + \sqrt{a + cy + fy^2}}{2\ t/b} \right) dy \right\} \quad (10)$$

where:

$$A = \frac{2\sigma_o b^2 \dot{U}}{\sqrt{3}\ t^2 (1-e^{-b})}$$

$$a = \left\{ (w - \xi)^2 + \frac{4t^2}{b^2} \right\}$$

$$c = 2 \frac{\xi}{t} (w - \xi)$$

$$f = \xi^2/t^2$$

Being unable to evaluate the above integrals explicitly, an adequate approximation was sought that would conform to the upper-bound restrictions. As a first attempt, a series expansion of the exponential was attempted, terminating with a positive term to assure an upper-bound:

$$e^{-by/t} \approx 1 - \frac{by}{t} + \frac{b^2}{2t^2} y^2 - \frac{b^3}{6t^3} y^3 + \frac{b^4}{24t^2} y^2 - \ldots \quad (11)$$

This approximation was carried to completion, but resulted in an extremely lengthy and cumbersome expression. Seeking a simpler alternative, the possibility of approximating the $\sqrt{a + cy + fy^2}$ term was considered. Using the dimensionless notation of:

$$\begin{aligned} D &= t/w \\ S &= \xi/w \\ Y &= y/t \end{aligned} \quad (12)$$

the square root term becomes:

$$\sqrt{a + cy + fy^2} = w(1 - 2S + S^2 + \frac{4D^2}{b^2} + 2SY\ (1-S) + S^2Y^2)^{1/2} \quad (13)$$

Investigation of this term for the ranges of $b > 0$, $D > 0$, and $0 \leq S \leq 1$ (the range of variables for which the process is being modeled) reveals a continuous function with a positive second derivative [$d^2 f(y/t)/d(y/t)^2$] at all points from $y/t = 0$ to $y/t = 1$.

Thus, the function can be upper-bound approximated by straight line segments connecting points on the function line, as illustrated in Figure 14a. Aribtrarily selecting the points y/t = 0, y/t = 1/2, and y/t = 1 as end points for two straight line segments, the first two integrals of Equation (10) can be approximated directly. The term $\sqrt{a + cy + fy^2}$ will be replaced by the straight line approximations:

From y/t = 0 to y/t = 1/2:

$$\sqrt{a + cy + fy^2} \approx w\left\{\left(1 - 2S + S^2 + 4\,\frac{D^2}{b^2}\right)^{1/2} + \frac{y}{t}\left[\left(1 - S + \frac{S^2}{4} + 4\,\frac{D^2}{b^2}\right)^{1/2} - \left(1 - 2S + S^2 + 4\,\frac{D^2}{b^2}\right)^{1/2}\right]\right\}$$

From y/t = 1/2 to y/t = 1

$$\sqrt{a + cy + fy^2} \approx w\left\{\frac{3}{2}\left(1 - S + \frac{S^2}{4} + \frac{4D^2}{b^2}\right)^{1/2} - \frac{1}{2}\left(1 + 4\,\frac{D^2}{b^2}\right)^{1/2} + \frac{y}{t}\left[\left(1 + 4\,\frac{D^2}{b^2}\right)^{1/2} - \left(1 - S + \frac{S^2}{4} + 4\,\frac{D^2}{b^2}\right)^{1/2}\right]\right\} \quad (14)$$

By direct substitution and evaluation, the first two integrals of Equation(10)can be approximated as:

$$(w-\xi)\int_{y=0}^{y=t} e^{-by/t}\sqrt{a+cy+fy^2}\,dy + \frac{\xi}{t}\int_{y=0}^{y=t} y\,e^{-by/t}\sqrt{a+cy+fy^2}\,dy$$

$$\approx \left(1 - 2S + S^2 + 4\frac{D^2}{b^2}\right)^{1/2}\left\{\frac{w^2t}{b} - \frac{\xi wt}{b} - \frac{w^2t}{b^2} + \frac{2\xi wt}{b^2} - \frac{2\xi wt}{b^3}\right.$$

$$\left. + e^{-b/2}\left(\frac{\xi wt}{4b} - \frac{w^2t}{2b} - \frac{\xi wt}{b^2} + \frac{w^2t}{b^2} + \frac{2\xi wt}{b^3}\right)\right\}$$

$$+ \left(1 - S + \frac{S^2}{4} + 4\frac{D^2}{b^2}\right)^{1/2}\left\{\frac{w^2t}{b^2} - \frac{\xi wt}{b^2} + \frac{2\xi wt}{b^3} + e^{-b/2}\left(-\frac{\xi wt}{4b} - \frac{2w^2t}{b^2}\right.\right.$$

$$\left.\left. - \frac{4\xi wt}{b^3} + \frac{w^2t}{2b} + \frac{3}{2}\frac{\xi wt}{b^2}\right) + e^{-b}\left(-\frac{1}{2}\frac{w^2t}{b} + \frac{w^2t}{b^2} - \frac{1}{2}\frac{\xi wt}{b^2} + \frac{2\xi wt}{b^3}\right)\right\}$$

$$+ \left(1 + \frac{4D^2}{b^2}\right)^{1/2}\left\{e^{-b/2}\left(\frac{w^2t}{b^2} - \frac{1}{2}\frac{\xi wt}{b^2} + \frac{2\xi wt}{b^3}\right) + e^{-b}\left(-\frac{1}{2}\frac{w^2t}{b} - \frac{w^2t}{b^2}\right.\right.$$

$$\left.\left. - \frac{1}{2}\frac{\xi wt}{b^2} - \frac{2\xi wt}{b^3}\right)\right\} \qquad (15)$$

Consider now the third integral of Equation (10), which in the dimensionless notation of Equation (12) becomes:

$$\frac{4t^2}{b^2}\left\{\int_{y=0}^{y=t} e^{-by/t}\ \ell n\left(1 - S + \frac{y}{t}S\right.\right.$$

$$\left. + \sqrt{1 - 2S + S^2 + \frac{4D^2}{b^2} + \frac{y}{t}2S\,(1 - S) + \frac{y^2}{t^2}S^2}\ \right)\ dy$$

$$\left. - \ell n\left(\frac{2D}{b}\right)\int_{y=0}^{y=t} e^{-by/t}\ dy\right\} \qquad (16)$$

Since an explicit evaluation of the first integral does not appear possible, an adequate approximation is once again sought. An investigation of the troublesome log term over the prescribed range of process variables in this case shows a continuous function with a negative second derivative in the range of $y/t = 0$ to $y/t = 1$, as illustrated in Figure 14b. Thus, to preserve the upper-bound nature of the solution, the log term is replaced by a constant equal to the largest value the term attains over the integral of integration, which in this case is the value at the point $y/t = 1$.

The approximation becomes:

$$\ell n \left(1 - S + \frac{y}{t} S + \sqrt{1 - 2S + S^2 + \frac{4D^2}{b^2} + \frac{y}{t} 2S(1 - S) + \frac{y^2}{t^2} S^2}\right)$$

$$\approx \ell n \left(1 + \sqrt{1 + \frac{4D^2}{b^2}}\right) \tag{17}$$

Substituting this approximation into Equation (16), the third integral of Equation (10) can be approximated by:

$$\frac{4t^2}{b^2} \left\{ \int_{y=0}^{y=t} e^{-by/t} \quad \ell n \quad \left(1 - S + \frac{y}{t} S \right.\right.$$

$$\left. + \sqrt{1 - 2S + S^2 + \frac{4D^2}{b^2} + \frac{y}{t} 2S (1 - S) + \frac{y^2}{t^2} S^2} \right) dy$$

$$\left. - \ell n \left(\frac{2D}{b}\right) \int_{y=0}^{y=t} e^{-by/t} \quad dy \right\}$$

$$\approx \frac{4t^3}{b^3} (1 - e^{-b}) \left\{ \ell n \left(1 + \sqrt{1 + \frac{4D^2}{b^2}}\right) - \ell n \left(\frac{2D}{b}\right) \right\} \tag{18}$$

By substituting the approximations of Equations (15) and (18) into the expression of Equation (10), an upper-bound estimate of the internal power of deformation in Zone I can now be expressed in the dimensionless notation of Equation (12) as:

$$\dot{W}_{iI} \approx \frac{2\sigma_o \dot{U} w}{\sqrt{3}} \left\{ \frac{1}{(1 - e^{-b})bD} \right\} \left\{ (1 - 2S + S^2 + \frac{4D^2}{b^2})^{1/2} \right.$$

$$[b^2 - Sb^2 - b + 2Sb - 2S + e^{-b/2}(\frac{b^2 S}{4} - \frac{b^2}{2} - Sb + b + 2S)]$$

$$+ (1 - S + \frac{S^2}{4} + \frac{4D^2}{b^2})^{1/2} [b - Sb + 2S + e^{-b/2}$$

$$(\frac{b^2}{2} - \frac{b^2 S}{4} - 2b + \frac{3}{2} Sb - 4S) + e^{-b} (-\frac{b^2}{2} + b - \frac{Sb}{2} + 2S)]$$

$$+ (1 + \frac{4D^2}{b^2})^{1/2} [e^{-b/2} (b - \frac{Sb}{2} + 2S) + e^{-b} (-\frac{b^2}{2} - b - \frac{Sb}{2} - 2S)]$$

$$\left. + 4D^2 (1 - e^{-b}) [\ell n (1 + \sqrt{1 + \frac{4D^2}{b^2}}) - \ell n (\frac{2D}{b})] \right\} \qquad (19)$$

Friction Representation

Before leaving the Zone I region, we note that the entire length of contact between the platen and the deforming strip is simply the upper boundary of that zone. Since the strip is expanding in width

and is therefore sliding over the downward moving platen, power losses due to the overcoming of the frictional resistance must be included in our calculations. The major problem here involves the means used to model the shear stress arising due to frictional restraint.

Due to its presence and importance in numerous metal forming operations, friction during plastic deformation has been the subject of continuous study. In a purely experimental study of friction between a platen and a deforming cylinder, von Rooyen and Backofen[69] found a variation in μ with location and reduction and concluded that the assumption of constant μ was not valid except in conditions of low μ and small reductions. Subsequent work by Pearsall and Backofen[66] confirmed these results and shed considerable doubt on techniques developed to couple theory and experiment to calculate a constant coulomb coefficient of friction. Examples of such approaches are presented in works by Schroeder and Webster[32] in which the theoretical forging load is equated to the experimental and solved for μ, Alexander's[20] plane strain test with slip line analysis, and the early ring compression test of Male and Cockcroft.[45] DePierre, et al.,[48] through investigation of the ring test, found that the concept of constant interface shear factor, m, was more realistic as a quantitative index for friction stresses existing in metalworking processes. The combined forging-extrusion technique presented by Kobayashi[70] and the improved ring test calibration are

techniques using this approach. Unfortunately, the investigation of Pearsall and Backofen[66] showed that both μ and τ (shear stress) varied with position and reduction in a forging operation. Such a variation in τ has been included in lower-bound analyses and is presented in several works by Avitzur.[3,27] In the general work on limit analysis techniques,[27] Avitzur shows that a directional change necessitates that $\tau = 0$ at the centerline, and the presence of a free surface requires that τ go to zero at the periphery. Between these two end points, the shear stress is assumed to rise linearly to a constant value which may prevail over a substantial interim region. Such a distribution has been used in the most recent slip line and matrix techniques of Shabaik[22,23] and Kobayashi.[8,9] Both investigators, however, neglect the drop to zero at the periphery, and in so doing introduce a possible error in the analysis. The most recent approach to measuring friction has been developed by Kobayashi and Oh.[63] The displacement distributions at the interface are experimentally measured and, by means of the latest matrix method techniques, the frictional stress distribution is computed.

Friction Loss Computation

Equation (20) presents the mathematical form for the power losses due to friction as:

$$\dot{W}_f = \int_S \tau |\Delta v| dS \tag{20}$$

where:

τ is the shear stress at the surface or friction expression

Δv is the relative velocity of the sliding surfaces

S is the surface area over which friction losses are occurring

As has just been discussed, the present state of understanding is such that no accurate mathematical description exists for the frictional resistance during metal forming operations, the shear stress varying as a function of both position and reduction. In order to maintain valid upper-bound conditions and permit direct comparison with the previous single-zone bulge solution, the assumption of a constant friction factor will be made in the present analysis. Should an improved representation of friction become available, a benefit of the upper-bound technique becomes apparent in that only the single friction loss term need be recomputed.

Mises' yield criterion, presented in terms of stress components, can be written as:

$$\frac{1}{6}\left[(\sigma_{11}-\sigma_{22})^2 + (\sigma_{22}-\sigma_{33})^2 + (\sigma_{33}-\sigma_{11})^2\right] + \sigma_{12}^2 + \sigma_{23}^2 + \sigma_{31}^2 = \frac{\sigma_o^2}{3} \tag{21}$$

If all stress components with the exception of one shear stress are equal to zero, the expression states that the maximum shear stress a material may sustain while undergoing plastic deformation is:

$$\tau_{max} = \frac{\sigma_o}{\sqrt{3}} \tag{22}$$

Permitting frictional shear stress to vary from zero to maximum, the constant friction factor approach will be used as follows:

$$\tau = m \frac{\sigma_o}{\sqrt{3}} \tag{23}$$

where $0 \leq m \leq 1$

The value of $|\Delta v|$ in Equation (20) is simply the velocity discontinuity along the workpiece-platen interface. Since the platen has zero velocity in the X-direction, $|\Delta v|$ is simply the velocity of those points in Zone I lying at the interface:

$$\Delta v = \dot{U}_x \text{ (Zone I)} \Big|_{y=t} \tag{24}$$

$$= \frac{b}{1 - e^{-b}} \dot{U} \frac{x}{t} e^{-b}$$

Using symmetry conditions, the friction losses can be computed for a single quadrant and multiplied by four to give the total losses over both upper and lower platens.

$$\dot{W}_f = \int_S \tau |\Delta v| dS$$

$$= \frac{4m\sigma_o}{\sqrt{3}} \frac{b \dot{U} e^{-b}}{(1-e^{-b})t} \int_{x=0}^{x=w} x \, dx \tag{25}$$

$$\dot{W}_f = \frac{2m\sigma_o}{\sqrt{3}} \frac{b\ e^{-b}}{(1-e^{-b})} \frac{\dot{U}w^2}{t} \tag{25}$$

In the dimensionless notation of Equation (12), the power required to overcome friction becomes:

$$\dot{W}_f = \frac{2\sigma_o \dot{U}\ w}{\sqrt{3}} \frac{m\ b\ e^{-b}}{(1-e^{-b})\ D} \tag{26}$$

Velocity Field of Zone II

Having computed the powers associated with Zone I, the concepts of flow continuity perpendicular to an interface and volume constancy can now be applied to characterize the velocity field of Zone II. Coupled with the assumed mode of flow in this region,

$$\dot{U}_x = \dot{U}_x(x,y)$$
$$\dot{U}_y = \dot{U}_z = 0 \tag{27}$$

these concepts will enable complete specification of the velocity field for the entire volume of the zone.

The interzone boundary is first approached from Zone I, and the normal and tangential components of velocity are evaluated along this surface. Flow continuity then requires that the velocity com-

ponent normal to the interface must be continuous. Thus, the normal component of velocity on the Zone II side of the interface must be equal to that in Zone I. The value of this component coupled with the restriction of net flow being parallel to the X-axis enables the determination of the Zone II velocity field at points on the interzone surface. Volume constancy restrictions then enable the specification of the velocity field for the entire volume of Zone II. The details of this approach will now be presented.

The interzone boundary has already been determined by the relation of Equation (2):

$$x = w - \xi + \frac{\xi y}{t} \tag{2}$$

Evaluating the Zone I velocity field of Equation (3) for points along this boundary and summing the components of the X- and Y-velocities normal to the interface yields a normal velocity component of:

$$\dot{U}_N = \frac{\dot{U}\xi}{\sqrt{\xi^2+t^2}(1-e^{-b})} \left\{ e^{-by/t} \left(\frac{bw}{\xi} - b + \frac{by}{t} - 1\right) + 1 \right\} \tag{28}$$

This is also the component normal to the boundary in the Zone II region. Since both $\dot{U}_y$ and $\dot{U}_z$ are zero in this region, this net normal component must also be the normal component of the $\dot{U}_x$ term. Thus, the form of $\dot{U}_x$ evaluated along the interzone boundary must be:

$$\dot{U}_x\Big|_{bdy} = \frac{\dot{U}\xi}{t(1-e^{-b})} \left\{ e^{-by/t} \left(\frac{bw}{\xi} - b + \frac{by}{t} - 1\right) + 1 \right\} \qquad (29)$$

Volume constancy now requires that all points in the volume of Zone II must obey the restriction that:

$$\dot{\varepsilon}_{xx} + \dot{\varepsilon}_{yy} + \dot{\varepsilon}_{zz} = 0 \qquad (30)$$

Using the strain rate relations of Equation (4) applied to the Zone II velocity field of Equation (27), results in:

$$\dot{\varepsilon}_{xx} = \frac{\partial \dot{U}_x}{\partial x} \qquad \dot{\varepsilon}_{xy} = \frac{1}{2} \frac{\partial \dot{U}_x}{\partial y}$$

$$\dot{\varepsilon}_{yy} = \dot{\varepsilon}_{zz} = \dot{\varepsilon}_{yz} = \dot{\varepsilon}_{zx} = 0 \qquad (31)$$

Substituting into the volume constancy restriction of Equation (30):

$$\frac{\partial \dot{U}_x}{\partial x} = 0$$

or (32)

$$\dot{U}_x = f(y)$$

The $\dot{U}_x$ component has already been determined as a function of y only at the interzone boundary. Therefore, the domain of this relation, Equation (29), can now be extended to cover the entire volume of Zone II. The complete Zone II velocity field is thus:

$$\dot{U}_x = \frac{\dot{U}\xi}{t(1-e^{-b})} \left\{ e^{-by/t} \left(\frac{bw}{\xi} + \frac{by}{t} - b - 1\right) + 1 \right\}$$

$$\dot{U}_y = \dot{U}_z = 0 \tag{33}$$

Zone II - Internal Power of Deformation

From the velocity field of Equation (33), the strain rates components of Equation (4) can now be explicitly evaluated:

$$\dot{\varepsilon}_{xx} = \dot{\varepsilon}_{yy} = \dot{\varepsilon}_{zz} = \dot{\varepsilon}_{yz} = \dot{\varepsilon}_{zx} = 0 \tag{34}$$

$$\dot{\varepsilon}_{xy} = \frac{1}{2} \frac{\partial \dot{U}_x}{\partial y} = \frac{\dot{U}}{2(1-e^{-b})} e^{-by/t} \left(\frac{\xi b^2}{t^2}\right) \left\{ 1 + \frac{2}{b} - \frac{w}{\xi} - \frac{y}{t} \right\}$$

As with Zone I, the internal power of deformation may now be computed by use of the relation:

$$\dot{W}_{iII} = \frac{2}{\sqrt{3}} \sigma_o \int_V \sqrt{\frac{1}{2} \dot{\varepsilon}_{ij} \dot{\varepsilon}_{ij}} \, dV \tag{6}$$

Substituting the strain rates of Equation (34) and integrating over the volume of Zone II [four times the value of the quadrant being analyzed], this power can be expressed as:

$$\dot{W}_{iII} = \frac{2\sigma_o}{\sqrt{3}} \int_V \dot{\varepsilon}_{xy}\, dV$$

$$= \frac{4\sigma_o \dot{U}\xi\, b^2}{\sqrt{3}(1-e^{-b})t^2} \int_{y=0}^{y=t} e^{-by/t} \left\{1 + \frac{2}{b} - \frac{w}{\xi} - \frac{y}{t}\right\} dy \int_{x=w-\xi+\xi\, y/t}^{x=w} dx$$

$$\dot{W}_{iII} = \frac{4\sigma_o \dot{U}\xi^2 b^2}{\sqrt{3}(1-e^{-b})t^2} \int_{y=0}^{y=t} e^{-by/t} \left\{ (1 + \frac{2}{b} - \frac{w}{\xi}) \right.$$

$$\left. + \frac{y}{t}\left(\frac{w}{\xi} - 2 - \frac{2}{b}\right) + \frac{y^2}{t^2} \right\} dy \qquad (35)$$

The term within the braces in the above integral is simply the product $(1 + 2/b - w/\xi - y/t)\,(1 - y/t)$ and it is possible for the first of these expressions to change sign in the range of $y/t = 0$ to $y/t = 1$. If the sign of this term is constant throughout the entire range of integration, a straight-forward evaluation of the integral is possible (Case A) with the absolute value of the result being the total power. If a sign transition exists within the range of integration, the integral must be broken at the transition point

[$y/t = 1 + 2/b - w/\xi$] forming two component integrals over the y/t range. (Case B).

The direct evaluation of Case A can be performed as follows:

CASE A:

$$W_{iII} = \frac{4\sigma_o \dot{U}\xi^2 b^2}{\sqrt{3}(1-e^{-b})t^2} \left\{ \left(1 + \frac{2}{b} - \frac{w}{\xi}\right) \int_{y=0}^{y=t} e^{-by/t}\, dy \right.$$

$$\left. + \left(\frac{w}{\xi} - 2 - \frac{2}{b}\right) \frac{1}{t} \int_{y=0}^{y=t} y\, e^{-by/t}\, dy + \frac{1}{t^2} \int_{y=0}^{y=t} y^2 e^{-by/t}\, dy \right\} \quad (36)$$

Evaluating the integrals yields:

$$\dot{W}_{iII} = \frac{4\sigma_o \dot{U}\xi b w}{\sqrt{3}(1-e^{-b})t} \left| \left\{ \frac{\xi}{w} - 1 + \frac{1}{b} - \frac{e^{-b}}{b} \right\} \right| \quad (37)$$

In the dimensionless notation of Eq. (12):

$$\dot{W}_{iII} = \frac{4\sigma_o \dot{U} w}{\sqrt{3}(1-e^{-b})} \left| \left\{ \frac{bS^2}{D} - \frac{bS}{D} + \frac{S}{D} - \frac{e^{-bS}}{D} \right\} \right| \quad (38)$$

For the case of the sign transition, the integral relation of:

$$\int_{y/t=0}^{y/t=f(y)} (\ ) + \int_{y/t=f(y)}^{y/t=1} -(\ ) = \int_{y/t=0}^{y/t=f(y)} (\ ) + \int_{y/t=1}^{y/t=f(y)} (\ ) \quad (39)$$

may be applied to produce the Zone II internal power expression:

CASE B:

$$\dot{W}_{iII} = \frac{4\sigma_o \dot{U} \xi^2 b^2}{\sqrt{3}(1-e^{-b})t} \left\{ (1 + \frac{2}{b} - \frac{w}{\xi}) \right.$$

$$\left[\int_{y/t=0}^{y/t=1+2/b-w/\xi} e^{-by/t} \, d(y/t) + \int_{y/t=1}^{y/t=1+2/b-w/\xi} e^{-by/t} \, d(y/t) \right]$$

$$+ (\frac{w}{\xi} - 2 - \frac{2}{b}) \left[\int_{y/t=0}^{y/t=1+2/b-w/\xi} \frac{y}{t} e^{-by/t} \, d(\frac{y}{t}) + \int_{y/t=1}^{y/t=1+2/b-w/\xi} \frac{y}{t} e^{-by/t} \, d(\frac{y}{t}) \right]$$

$$\left. + \left[\int_{y/t=0}^{y/t=1+2/b-w/\xi} (\frac{y}{t})^2 e^{-by/t} \, d(y/t) + \int_{y/t=1}^{y/t=1+2/b-w/\xi} (\frac{y}{t})^2 e^{-by/t} \, d(y/t) \right] \right\} \quad (40)$$

Evaluating the integrals and collecting terms yields:

$$\dot{W}_{iII} = \frac{4\sigma_o \dot{U}\xi bw}{\sqrt{3}(1-e^{-b})t} \left| \left\{ \frac{\xi}{w} - 1 + \frac{1}{b} + \frac{e^{-b}}{b} \right.\right.$$

$$\left.\left. + e^{(-b - 2 + \frac{bw}{\xi})} \left[\frac{2}{b} - \frac{8\xi}{b^2 w} \right] \right\} \right| \tag{41}$$

which, in dimensionless notation, becomes:

$$\dot{W}_{iII} = \frac{4\sigma_o \dot{U}w}{\sqrt{3}(1-e^{-b})} \left| \left\{ \frac{bS^2}{D} - \frac{bS}{D} + \frac{S}{D} + \frac{e^{-bS}}{D} \right.\right.$$

$$\left.\left. + e^{(-b - 2 + b/S)} \left[\frac{2S}{D} - \frac{8S^2}{bD} \right] \right\} \right| \tag{42}$$

Interzone Shear Losses

The only interior power term remaining to be computed is the power lost in shear over the surface separating the two zones. Recall that when determining the velocity field for Zone II, velocity continuity was required normal to the interzone surface. The tangential components need not be the same, however, and this leads to a tangential velocity discontinuity and shear occurring along this surface. Equation (20) represented friction losses as:

$$\dot{W}_f = \int_S \tau |\Delta v| dS \tag{20}$$

and the same expression holds for interzone shear. In the case of internal shear, however, upper-bound analyses set $\tau = \sigma_o/\sqrt{3}$ as a result of Mises' yield criterion with only one shear stress component being non-zero [as already presented in Equations (21) and (22)]. In actuality, additional stress components are likely to be non-zero at the interface and hence the assumed value for τ may be a gross overestimate. At present, however, no alternative method has been accepted as producing a rigorous upper-bound solution and the representation of $\tau = \sigma_o/\sqrt{3}$ will be used to characterize internal shear in the present analysis.

From the velocity fields of Zones I and II, presented as Equations (3) and (33), elementary vector analysis can determine the tangential components along the interzone boundary. The velocity discontinuity is simply the difference between the tangential components and is computed to be:

$$|\Delta v| = \frac{\sqrt{\xi^2 + t^2}}{t} \left\{ \frac{\dot{U}(1-e^{-by/t})}{(1-e^{-b})} \right\} \tag{43}$$

Substituting for τ and $|\Delta v|$ in Equation (20), the power required to overcome interzone shear becomes:

$$\dot{W}_{s\ I\text{-}II} = \frac{\sigma_o}{\sqrt{3}} \frac{\sqrt{\xi^2 + t^2}}{t(1-e^{-b})} \dot{U} \int_S (1-e^{-by/t})dS \tag{44}$$

The integration over the sloping surface can be simplified by using the similarity of a differential triangle and the triangle of Zone II to show:

$$\int_S (\ )dS = 4 \int_{y=0}^{y=t} (\ ) \frac{\sqrt{\xi^2 + t^2}}{t} dy \tag{45}$$

Thus:

$$\dot{W}_{sI-II} = \frac{4\sigma_o(\xi^2 + t^2)\dot{U}}{\sqrt{3}\, t^2(1-e^{-b})} \int_{y=0}^{y=t} (1 - e^{-by/t})\ dy$$

$$= \frac{4\sigma_o(\xi^2 + t^2)\dot{U}}{\sqrt{3}\, t\, (1-e^{-b})} \left\{ 1 - \frac{1}{b} + \frac{e^{-b}}{b} \right\} \tag{46}$$

In the dimensionless notation of Equation (12), the interzone shear losses can be represented as:

$$\dot{W}_{sI-II} = \frac{4\sigma_o\, \dot{U}\, w}{\sqrt{3}(1-e^{-b})D} \left\{ (S^2 + D^2)\ (1 - \frac{1}{b} + \frac{e^{-b}}{b}) \right\} \tag{47}$$

Power to Overcome Imposed Body Tractions

The possible body tractions for strip forging are limited to a simple external pressure applied to the free surface area. The power associated with this external pressure is simply the rate at which work must be performed to overcome it or $P\dot{dV}$, the pressure

times the rate at which volume is being displaced against this pressure. Both platens are moving at velocity $\dot{U}$ and are acting on an area 2w in width by a unit length. Thus, for a unit length of strip, the volume rate at which material is being displaced, $\dot{V}$, is just $\dot{V} = 4\dot{U}w$. The power to overcome the external pressure, p, is simply:

$$\dot{W}_p = 4p\dot{U}w \tag{48}$$

This result can also be obtained by direct evaluation of the third term of Equation (1), integrating the $\dot{U}_x$ velocity of Zone II over the free surface, but the mathematics are considerably more involved. The fact that the same result is obtained serves as an internal check for possible errors in computing the Zone II velocity field.

Total Power Required

In upper-bound analyses, the total power required is simply the sum of all contributing terms. Thus, for the present analysis:

$$\dot{W}_{TOT} = \dot{W}_{iI} + \dot{W}_{iII} + \dot{W}_{sI-II} + \dot{W}_f + \dot{W}_p \tag{49}$$

Using the dimensionless notation of Equation (12), these terms have been developed as follows:

$\dot{W}_{iI}$:

$$\dot{W}_{iI} = (2\sigma_o\dot{U}w) \cdot \left(\frac{b^2}{\sqrt{3}(1-e^{-b})}\right)\left\{\left(\frac{1}{D} - \frac{S}{D}\right) \int_{Y=0}^{Y=1} e^{-bY} \sqrt{\quad} \, dY \right|$$

(cont.)

$$+ \frac{S}{D} \int_{Y=0}^{Y=1} Y\, e^{-bY} \sqrt{\quad}\, dY + \frac{4D}{b^2} \int_{Y=0}^{Y=1} e^{-bY}\, \ell n \left[\frac{1-S+SY+\sqrt{\quad}}{2\ D/b}\right] dY \Bigg\} \Bigg| \qquad (50)$$

where:

$$\sqrt{\quad} = w \cdot \sqrt{1 - 2S + S^2 + \frac{4D^2}{b^2} + 2SY\ (1-S) + Y^2S^2} \qquad (51)$$

$\dot{W}_{iI}$ has also been approximated by Equation (19).

$\dot{W}_{iII}$:

This term has two possible cases which are presented explicitly as Equations (38) and (42).

$\dot{W}_{sI-II}$:

Interzone shear losses are presented explicitly in Equation (47).

$\dot{W}_f$:

Power required to overcome friction is given as Equation (26).

$\dot{W}_p$

The power to overcome imposed body tractions is computed through Equation (48).

Relative Average Forging Pressure

The external power being supplied by the platens is simply the force times the platen velocity or the average pressure times the platen area times the platen velocity. Thus, for a unit length of

strip, the applied power is simply:

$$J^* = 4w\, p_{ave}\, \dot{U} \tag{51}$$

By equating the power supplied by the platens to the power required to deform the strip, an expression can be developed to compute the relative average forging pressure, p_{ave}/σ_o. For a unit length of strip:

$$\frac{p_{ave}}{\sigma_o} = \frac{1}{4\, w\, \dot{U}\, \sigma_o}\, \dot{W}_{TOT} \tag{52}$$

Single Zone Bulge Solution

In order to evaluate the merits of the two-zone solution just developed, the results must be compared to those of alternative solutions. Provided all solutions being compared are rigorous upper-bounds and use the same friction representation, that solution producing the lowest value for $\dot{W}_{TOT}$ and p_{ave}/σ_o is regarded as being superior. Since the single-zone upper-bound of Avitzur[27,28] is concise and presently accepted, and since the present solution should converge to it when Zone II disappears, it is to this solution that the present expressions will be compared.

In the dimensionless notation of Equation (12), the relative average forging pressure for the single-zone bulge solution can be written as:

$$\left.\frac{p_{ave}}{\sigma_o}\right|_{\text{single zone}} = \frac{1}{\sqrt{3}}\left\{\sqrt{1+\frac{b^2}{4D^2}} + \frac{2D}{b}\,\ell n\left[\frac{b}{2D} + \sqrt{1+\frac{b^2}{4D^2}}\right]\right\} \tag{53}$$

(cont)

$$+ \left. \frac{m\, b\, e^{-b}}{2(1-e^{-b})D} \right\} + \frac{p}{\sigma_o} \Bigg|$$

Comparison of the Solutions

An inspection of Equation (53) shows that the relative average forging pressure for the single zone solution is a function of four variables: the strip dimension ratio (D = t/w), the platen-strip friction factor (m), imposed external pressure (p/σ_o), and the degree of bulging (b). Of these, the first three, called the independent parameters, are preset and describe the conditions of the forging being performed. The fourth, b, cannot be preset and assumes that value which will minimize the result of Equation (53), i.e., which will produce the lowest upper-bound for the single zone solution. Although expressions have been developed to compute b_{opt} as a function of the other process variables,[27,28] such as:

$$b_{opt} \approx \frac{3}{1 + (\frac{2}{m})\ (\frac{1}{D})} \quad , \tag{54}$$

these expressions are only approximate in nature and, although convenient in reducing the mathematical difficulty in using the results, tend to compromise the true value of the solution. Since a valid comparison of the two solutions is desired, Equation (53) was used directly in an optimization search routine [the Lehigh Optimum Parameter Routine -LOPER- a canned optimization routine available

at the Lehigh University Computer Center] to determine the best values of b_{opt} and $p_{ave}/\sigma_o|_{single\ zone}$ for a wide range of geometries and frictions.

Analysis of the new solution of Equation (52) with all terms being substituted reveals a function of five variables: the four discussed previously and an additional one, the relative zone size parameter, S. As before, D, m, and p/σ_o are preset, and the values for b and S are determined by process optimization. Equation (19) is used to approximate the internal power of deformation in Zone I, $\dot{W}_{iI}$, in the optimization search routine, thereby enabling a rapid determination of b_{opt} and S_{opt}. These optimum values of b and S are then substituted into Equation (50) and an improved value of $\dot{W}_{iI}$ is then computed by numeric integration. [The interval of integration, $y/t = 0$ to $y/t = 1$, is broken into 200 increments and the integrand of each component integral is evaluated at both end-points of each increment. To maintain the upper-bound quality of the solution, the higher value of the two end-points is taken to be the constant value of the integrand over that increment. Summing the contributions of all 200 increments then produces an upper-bound numeric integration of Equation (50).] This improved value of $\dot{W}_{iI}$ is then coupled with the previously determined remaining power terms to compute the relative average forging pressure through Equation (52). Values of b_{opt}, S_{opt}, and $p_{ave}/\sigma_o|_{two\ zone}$ have thus been computed for a wide range of process geometries and frictions, with the assumption that the external pressure on the free surface is zero.

The results produced by these techniques are therefore: the best possible solution for the one zone velocity field and a near-best for the two-zone approach, since an approximation is used to determine b_{opt} and S_{opt}. Since any compromise will occur as an overestimate in the two-zone solution, a valid evaluation of the new results should be possible. [NOTE: In several cases, a rigorous assessment of the two-zone solution was conducted by replacing the approximation of Equation (19) with numeric integration of Equation (50) in the LOPER optimization routine. In all cases, the net improvement in p_{ave}/σ_o was less than .3% and in most cases substantially less. The minimal improvement failed to justify the substantial increase in computer time and expense as the cost-per-data point rose from $\approx$ 9¢ to nearly $4.00. The technique of using an analytic approximation in the optimization search and subsequently performing a numeric integration to improve the solution seemed quite adequate for the present investigation.]

Results

To present the results of the various investigations and facilitate easy comparison of the solutions, tables such as Table 2 were prepared. For a constant value of friction, m, the thickness to width ratio was varied from 0.9 to 0.1 in increments of 0.1 and from 0.10 to 0.01 in increments of 0.01. Column 1 presents the single-zone bulge solution with b approximated by Equation (54), i.e., the simplest and most direct solution available. Column 2 presents this same solution with b free to assume that value which

minimizes the solution with no approximations. Columns 3 and 4 present the two parameter solution. The results of the optimization with the approximated Zone I power are in Column 3, with the improvement produced by numeric integration being reflected in Column 4. A complete set of these tables covering m values of 1.00, 0.95, 0.90, 0.85, 0.80, 0.75, 0.70, 0.69, 0.68, and 0.67 is on file at the Institute for Metal Forming at Lehigh University.

From these tables, figures were prepared to graphically depict the results of the study. Figure 15 presents the optimal value of the bulge parameter, b_{opt}, for the two-zone two-parameter solution. As can be seen, for constant friction, a variation in thickness to width ratio or process geometry produces a smooth continuous variation in b_{opt}. A change in friction produces a near-uniform displacement of the curve. Similar results are observed for the optimal value of the zone size parameter, S_{opt}, in Figure 16. As will be seen in a later section, such behavior is useful in enabling these analytically determined points for b_{opt} and S_{opt} to be approximated by a polynomial curve fit. Continuous modeling of the deformation process can then be performed without a dependence on the optimization routine. Extremely fine increments can be considered without requiring excessive computer time and expense.

Figure 17 presents the relative average forging pressure computed by numeric integration about the approximated optimum as previously discussed. Comparison with Figure 18, derived from the early work of Schroeder and Webster[32] (1949) and Figure 19, from the

analysis of Bishop[21] (1958) shows that the basic form of the graph is far from surprising. Although these early works used the coulomb coefficient of friction concept in place of the present shear factor approach, the results are quite similar.

The benefit of the present analysis, however, becomes apparent when one compares the results from a least upper-bound approach. Recall that in the upper-bound technique, that field which produces the lowest prediction of power and forging pressure is regarded as the superior solution. Figure 20, prepared from charts such as presented in Table 2, graphically depicts the domains of superiority for the two solutions being evaluated: the optimized single-zone bulge solution and the two-zone two-parameter bulge plus fold solution with numeric integration. As expected, the two-zone solution is superior for the high friction conditions where foldover is observed. Furthermore, since the two-zone solution contains a possible overestimate of the shear losses incurred on the interzone surface (as discussed earlier), the actual domain of superiority is likely to be greater than that presented.

Figure 21 presents the amount of improvement provided by the two-zone solution as a percentage of the previous one-zone value. Although this improvement fails to exceed 3%, it is significant to note that it was obtained by use of a markedly different velocity field acting in the region near the free surface. Furthermore, a comparison of the values of b_{opt} in Table 2 shows that the rate of bulge formation is considerably greater for the two-zone solution

than for the single-zone. Thus, even the similar velocity fields in the interior region adopt markedly different values. Nevertheless, in spite of the significant differences in velocity fields, these two solutions produce remarkably similar upper-bound results, lending support to the possible validity of the new solution as a good representation of the actual velocity distribution.

Since the two velocity fields considered differ markedly in detail yet produce similar net results, it seems indeed possible that, should a continuous transition be provided between them, an interim point may very well be superior to either of the present solutions. Such a transition has been provided and will be presented in the following section.

INTRODUCTION OF THE TWO-ZONE THREE-PARAMETER APPROACH AND ITS FAILURE TO PROVIDE AN IMPROVED SOLUTION

Past Solutions

It has already been noted that a standard approach of applying the upper-bound technique to a complex problem is to produce a series of solutions of increasing complexity, with the simpler solutions becoming limiting cases of the more complex. For the process of strip forging in plane strain, such a sequence has already been developed. Figure 3 presented the parallel velocity field, wherein a rectangular strip is deformed into a thinner, wider rectangular strip with no bulge or fold. The solution is direct with no optimization parameters being included, and only a single deforming region is considered.

To this field, the possibility of a bulge was added to produce the bulge velocity field of Figure 4. A minimization parameter, b, has been added to the solution, but as before, only a single deforming region need be considered. When b is set equal to zero, the bulge velocity field reduces to the previous parallel deformation.

Most recently, the possibility of a foldover accompanying bulge formation was included through the addition of a second zone and with it, a second minimization parameter, S, the zone size parameter. This field, known as the two-zone two-parameter velocity field, was presented in Figure 13. The previous bulge velocity field is applied to the interior region of Zone I. To permit the modeling of the

foldover phenomenon, however, the vertical velocity of the point in Zone II which contacts the platen must have a value less than the vertical velocity of the platen. In the two-parameter solution, this condition was met by requiring that all points in the Zone II region have a vertical velocity component of zero.

The Fold Parameter, F, and the Two-Zone Three-Parameter Approach

The restriction that the vertical component of velocity for all points in Zone II be equal to zero is extremely severe, for the foldover condition only requires that the vertical velocity of the point where Zone II contacts the platen be less than the vertical velocity of the platen itself. The appropriate relaxing of this $\dot{U}_y = 0$ condition for Zone II provides the key to development of a general solution in which the parallel, single-zone bulge, and two-zone two-parameter solutions are all limiting cases and a continuous transition exists between them. Consider a two-zone solution in which the vertical velocity in Zone II is simply F times the vertical velocity in Zone I, where F is free to assume any value between zero and 1:

$$\dot{U}_{y\ (\text{Zone II})} = F \cdot \dot{U}_{y\ (\text{Zone I})} \tag{55}$$

$$\text{where } 0 \leq F \leq 1$$

If the form of $\dot{U}_{y\ (\text{Zone I})}$ is chosen as its form in the bulge solution, i.e.,:

$$\dot{U}_{y\ (\text{Zone I})} = \frac{-1}{1 - e^{-b}} \dot{U} \left(1 - e^{-by/t}\right), \tag{56}$$

the proposed value of $\dot{U}_{y(\text{Zone II})}$ then obeys the necessary boundary condition that $\dot{U}_y|_{y=0} = 0$, yet permits non-zero but still reduced values throughout the remainder of the zone. Thus, the proposed term meets both the boundary requirements and the conditions for foldover, while providing added flexibility to the solution through a variable rate of fold. Figure 22 presents this improved field, which will be known as the two-zone three-parameter solution.

Graphical Visualization of Solution Development

In order to visually depict the development of the various velocity fields, consider the three component coordinate system of Figure 23, in which each axis corresponds to one of the three proposed minimization parameters. In its most general application, the bulge parameter, b, is free to assume any positive value. The fold parameter, F, as recently presented, is restricted to positive values between zero and 1. The zone size parameter, $S = \xi/w$, is also restricted to positive values between zero and 1: zero corresponding to the absence of Zone II and one producing a field where the two Zone II triangles share a common apex at the geometrical center of the strip. Thus, the developed coordinate system can easily serve as a map on which to consider the permissible domains of the various solutions.

The parallel field is the most restricted of the solutions and is depicted in Figure 24. No bulge is permitted, so b is restricted to zero. In addition, the solution is applied to a single deforming region, which can be represented by requiring that F = 1. This in

essence permits the single zone field to be represented by two zones with identical velocity fields, the imaginary surfaces dividing the zones being free to assume any permissible configuration. The fact that the solution applies to a single zone can thus be represented by: F = 1 and $0 \leq S \leq 1$. On the coordinate system of Figure 24, the parallel velocity field is therefore restricted to the domain of the heavy line at b = 0 and F = 1, for which the computed value of p_{ave}/σ_o for D = t/w = 0.2 and m = 1.0 is: $p_{ave}/\sigma_o = 3.1824$.

By permitting a bulge to occur, b is now free to assume any positive value, as illustrated in Figure 25. The fact that the solution applies only to a single zone, however, again requires that F = 1 and $0 \leq S \leq 1$, thereby restricting the domain of the bulge solution to the shaded region of Figure 25. For the process conditions specified previously, the optimum value of p_{ave}/σ_o is 2.49281 and occurs at $b_{opt} = .313$. Comparison of the two relative average forging pressures clearly reveals the advantage gained by expanding the solution.

In a similar manner, the two-zone two-parameter solution is depicted in Figure 26. Both the bulge parameter, b, and the zone size parameter, S, are free to assume their entire range of values. The fold parameter, F, however, is restricted to F = 0. Thus, the domain of the two-parameter solution is limited to the shaded area of Figure 26. For the specified conditions of D = 0.2 and m = 1.0, the optimum value of p_{ave}/σ_o is 2.48722 and occurs at $b_{opt} = .558$ and $S_{opt} = .231$.

Thus, the bulge solution and two-zone two-parameter solution occupy domains which form the opposing faces of an open-ended volumetric solid and are capable of producing nearly equivalent predictions of relative average forging pressure for conditions of high friction and a wide range of strip geometry. Figure 20 has already presented information indicating the various domains of superiority of the two solutions. Information as to whether the transition between the two solutions occurs gradually or abruptly and whether a still better solution exists for points between the two schematic surfaces depends on the development of a solution valid for all points within the imaginary volume.

Development and Failure of the Three-Parameter Field

This most general velocity field, known as the two-zone three-parameter field and presented in Figure 22, was developed in spite of a significant increase in mathematical complexity and need for substantial use of upper-bound approximation and numeric integration. The results obtained, however, fail to justify the effort required.

Figure 27 graphically depicts the results of a typical investigation. For the conditions previously considered, i.e., D = 0.2 and m = 1.0, an optimization search of the solution domain produced two end-point minima, the ultimate point of convergence depending on the starting point of the search. Moreover, these two minima corresponded to none other than the previously presented bulge and two-parameter solutions. A second study designed to check the results

of the optimization search considered sections cut through the search domain at constant values of F. Contour maps of the resulting b - S planes revealed that all points in the intervening volume produced values of p_{ave}/σ_o greater than that of the nearer end-point minimum. Thus, the additional effort and considerable increase in mathematical complexity required to produce the continuous three-parameter solution failed to produce any significant benefit. Direct computation of the two "limiting case" solutions is much simpler and provides more accurate results since less approximation is required. Moreover, since a two-parameter optimization search is far more efficient than a three-parameter search, abandonment of the general solution in favor of the two limiting solutions is the more economical alternative. Details of the two-zone three-parameter solution are provided for reference in Appendix I.

THE TWO-ZONE TWO-PARAMETER SOLUTION FOR DISC

Introduction

As can be seen through a comparison of the schematics of Figures 1 and 2, the processes of strip and disc forging show remarkable similarities. In both cases, a geometrical solid is being reduced in height with a corresponding expansion in either the width or diameter. In addition, the same basic phenomena, such as bulging or possible foldover of the free surface, have been observed for both configurations.

Unlike the slip line technique, which is primarily limited to plane strain problems, the upper-bound approach is free to make use of the observed process similarities. By simply shifting from the Cartesian to cylindrical coordinate systems, analyses can be developed for the disc geometry which parallel those previously presented for strip. Avitzur, in Chapter 7 of his text: Metal Forming: Processes and Analysis,[27] presents both the parallel and bulge solutions for disc forging. As with the strip geometry, however, no previous upper-bound analysis has successfully accounted for the foldover phenomenon accompanying bulge.

The two-zone velocity field approach appeared to pave the way for such a solution, and it was originally intended to use the experience gained from the strip analysis to move directly to a two-zone three-parameter approach for discs. With the apparent failure of the three-parameter strip solution, the goal for the disc geometry was revised to successful development of the simpler two-

zone two-parameter solution, and it is this solution which will now be presented. Since the solution is simply a parallel of the two-zone two-parameter analysis presented for strip, much of the description and discussion will be omitted. Concentration will be focused on the mathematical details of the solution development.

Background

As with the strip solution, a two-zone velocity field will be applied to the solution following the basic schematic of Figure 12b. Flow in the interior, Zone I, will obey the exponential bulge velocity field for discs as presented in section 7.5 of the text by Avitzur.[27] The second zone or fold zone is restricted to a simple shear type of flow parallel to the platen with $\dot{U}_y = 0$ for all points in that region. Both the rate of bulge formation, b, and size of Zone II, ξ, remain unspecified throughout the analysis and serve as minimization parameters to optimize the final solution. The upper-bound expression of Equation (1) will serve as the basic foundation of the analysis.

Mathematical Description of the Two-Zone Regions

As with the previous two-zone solution, the various limits of integration, etc. must first be determined through mathematical description of the geometry and the utilization of symmetry with respect to the R-axis. Geometrical consideration will show that the interzone surface can be described by the equations:

$$y = \frac{T}{2\xi}(R - R_o + \xi)$$

$$R = R_o - \xi + \frac{2\xi y}{T} \tag{57}$$

Thus, Zone I can be described as:

R: from $R = 0$ to $R = R_o - \xi + \frac{2\xi y}{T}$

y: from $y = 0$ to $y = T/2$

and Zone II as:

R: from $R = R_o - \xi + \frac{2\xi y}{T}$ to $R = R_o$

y: from $y = 0$ to $y = T/2$

Zone I - Internal Power of Deformation

In the region of Zone I, the mode of flow is described by the exponential bulge velocity field as presented by Equation 7.25 of Reference 27:

$$\dot{U}_R = \frac{1}{4}\frac{b}{1 - e^{-b/2}}\dot{U}\frac{R}{T}e^{-by/T}$$

$$\dot{U}_y = -\frac{\dot{U}}{2}\frac{1 - e^{-by/T}}{1 - e^{-b/2}} \tag{58}$$

$$\dot{U}_\theta = 0$$

From this field, the strain rates components can be computed by simple differentiation using the relations for cylindrical coordinates:

$$\dot{\varepsilon}_{RR} = \frac{\partial \dot{U}_R}{\partial R} \qquad \dot{\varepsilon}_{\theta\theta} = \frac{\dot{U}_R}{R} + \frac{1}{R}\frac{\partial \dot{U}_\theta}{\partial \theta} \qquad \dot{\varepsilon}_{yy} = \frac{\partial \dot{U}_y}{\partial y}$$

$$\dot{\varepsilon}_{R\theta} = \frac{1}{2}\left(\frac{1}{R}\frac{\partial \dot{U}_R}{\partial \theta} + \frac{\partial \dot{U}_\theta}{\partial R} - \frac{\dot{U}_\theta}{R}\right) \tag{59}$$

$$\dot{\varepsilon}_{\theta y} = \frac{1}{2}\left(\frac{\partial \dot{U}_\theta}{\partial y} + \frac{1}{R}\frac{\partial \dot{U}_y}{\partial \theta}\right)$$

$$\dot{\varepsilon}_{yR} = \frac{1}{2}\left(\frac{\partial \dot{U}_R}{\partial y} + \frac{\partial \dot{U}_y}{\partial R}\right)$$

Evaluating the strain rates of Zone I from the velocity field of Equation (58), we have the strain rates field presented as Equation 7.26 of Reference 27:

$$\dot{\varepsilon}_{RR} = \dot{\varepsilon}_{\theta\theta} = -\frac{1}{2}\,\dot{\varepsilon}_{yy} = \frac{1}{4}\,\frac{b}{1 - e^{-b/2}}\,\frac{\dot{U}}{T}\,e^{-by/T}$$

$$\dot{\varepsilon}_{Ry} = -\frac{1}{8}\,\frac{b^2}{1 - e^{-b/2}}\,\frac{\dot{U}R}{T^2}\,e^{-by/T} \tag{60}$$

$$\dot{\varepsilon}_{R\theta} = \dot{\varepsilon}_{\theta y} = 0$$

Substituting these strain rates into the expression for internal power of deformation, Equation (6), the internal power of deformation for Zone I becomes:

$$\dot{W}_{iI} = \frac{2}{\sqrt{3}} \sigma_o \int_V \sqrt{3 \dot{\varepsilon}_{RR}^2 + \dot{\varepsilon}_{Ry}^2} \; dV \tag{61}$$

Substituting for the strain rates and multiplying the integrals for the upper half of the disc by two to include the entire solid, this expression becomes:

$$\dot{W}_{iI} = \frac{2\pi\sigma_o}{\sqrt{3}} \frac{\dot{U}}{T} \frac{b}{1 - e^{-b/2}} \int_{y=0}^{y=T/2} e^{-by/T} \left\{ \int_{R=0}^{R=R_o - \xi + \frac{2\xi y}{T}} R \sqrt{3 + \frac{b^2 R^2}{4T^2}} \; dR \right\} dy \tag{62}$$

Applying Integral 130 of Reference 68, which states that:

$$\int x \sqrt{x^2 + a^2} \; dx = \frac{1}{3} (x^2 + a^2)^{3/2} , \tag{63}$$

the integral with respect to R can be evaluated directly to yield:

$$\dot{W}_{iI} = A \left\{ \int_{y=0}^{y=T/2} e^{-by/T} (a + cy + fy^2)^{3/2} \; dy - \int_{y=0}^{y=T/2} e^{-by/T} \left(\frac{12T^2}{b^2}\right)^{3/2} dy \right\} . \tag{64}$$

where:

$$A = \frac{\pi\sigma_o \dot{U} b^2}{3\sqrt{3}\, T^2(1-e^{-b/2})}$$

$$a = (R_o - \xi)^2 + \frac{12T^2}{b^2}$$

$$c = 4 \frac{\xi}{T} (R_o - \xi)$$

$$f = 4 \frac{\xi^2}{T^2}$$

Evaluating the second of the integrals of Equation (64), we have:

$$W_{iI} = A \left\{ \int_{y=0}^{y=T/2} e^{-by/T} (a + cy + fy^2)^{3/2} dy \right.$$

$$\left. - \frac{T}{b} \left(\frac{12T^2}{b^2}\right)^{3/2} (1 - e^{-b/2}) \right\} \qquad (65)$$

In the dimensionless notation of:

$$D = T/R_o$$
$$S = \xi/R_o \qquad (66)$$
$$Y = y/T$$

Equation (65) becomes:

$$\dot{W}_{iI} = \pi R_o^2 \sigma_o \dot{U} \left(\frac{b^2}{3\sqrt{3}\, D(1-e^{-b/2})}\right) \left\{ \int_{Y=0}^{Y=1/2} e^{-bY}[1 - 2S + S^2 + \frac{12D^2}{b^2} + 4S(1-S)\, Y + 4\, S^2Y^2]^{3/2}\, dY - \frac{24\sqrt{3}\, D^3}{b^4}(1 - e^{-b/2}) \right\} \qquad (67)$$

Being unable to evaluate the remaining integral explicitly, an adequate upper-bound approximation is now sought. Investigation of the $[\ ]^{3/2}$ term for the range of integration reveals characteristics similar to those presented in Figure 14a. Thus, pursuing an approach similar to that used in the strip solution, the term is approximated by two straight line segments, one running from Y = 0 to Y = 1/4 and the second, from Y = 1/4 to Y = 1/2. Replacing the $[\ ]^{3/2}$ term by the forms of the two straight line segments and evaluating the resulting integrals, the internal power in Zone I can be approximated as:

$$\dot{W}_{iI} \approx \frac{\pi R_o^2 \sigma_o \dot{U}}{3\sqrt{3}\, D\, (1-e^{-b/2})} \left\{ (1-S + \frac{S^2}{4} + 12\, \frac{D^2}{b^2})^{3/2} (1-2\, e^{-b/4} + e^{-b/2} + \frac{3}{4} b\, e^{-b/4} - \frac{3}{4} b\, e^{-b/2}) + (1 - 2S + S^2 + \frac{12D^2}{b^2})^{3/2} (b + e^{-b/4} - \frac{3}{4} b\, e^{-b/4} - 1) + (1 + 12\, \frac{D^2}{b^2})^{3/2} \right.$$

(cont.)

$$\cdot \left(e^{-b/4} - e^{-b/2} - \frac{b}{4}\, e^{-b/2}\right) - 24\sqrt{3}\, \frac{D^3}{b^2}\left(1 - e^{-b/2}\right) \Bigg\} \qquad (68)$$

As the results section will show, however, the approximation of Equation (68) is an unnecessary exercise. Even with numeric integration applied to Equation (67), the disc solution fails to produce a lower-upper bound. The details and explanation of this result will be presented in a subsequent section.

Friction Losses

Friction losses over the workpiece - platen interfaces can now be computed through Equation (20) with the assumption of a constant shear factor approach to friction, presented in Equation (23). The value of $|\Delta v|$ is simply the velocity of those points in Zone I lying at the interface, for the platen has no horizontal velocity. Thus:

$$\Delta v = \dot{U}_R \text{ (Zone I)} \Big|_{y=T/2}$$

$$= \frac{1}{4}\, \frac{b}{1 - e^{-b/2}}\, e^{-b/2}\, \dot{U}\, \frac{R}{T} \qquad (69)$$

Noting the condition of vertical symmetry, the friction losses are computed for one surface and doubled to give the total power loss for both platens:

$$\dot{W}_f = \int_S \tau |\Delta v| dS$$

where $dS = 2\pi R dR$

$$\dot{W}_f = \frac{m\sigma_o}{\sqrt{3}} \frac{b\, e^{-b/2}}{(1 - e^{-b/2})} \frac{\dot{U}\pi}{T} \int_{R=0}^{R=R_o} R^2 dR$$

Evaluating the integral and using the dimensionless notation of Equation (66), we have:

$$\dot{W}_f = \pi R_o^2 \sigma_o \dot{U} \frac{mb}{3\sqrt{3}D} \frac{e^{-b/2}}{(1 - e^{-b/2})} \tag{70}$$

Velocity Field of Zone II

The concepts of flow continuity perpendicular to an interface and volume constancy are now coupled with the assumed mode of flow,

$$\begin{aligned} \dot{U}_R &= \dot{U}_R(R,y) \\ \dot{U}_y &= \dot{U}_\theta = 0 \end{aligned} \tag{71}$$

to completely characterize the velocity field of Zone II.

Evaluating the Zone I velocity field components at the inter-zone boundary, $R = R_o - \xi + 2\xi y/T$, and summing their normal contributions produces a normal component of the Zone I velocity field at the boundary of:

$$\dot{U}_N = \frac{\dot{U}\xi}{2\sqrt{\xi^2 + T^2/4}\,(1-e^{-b/2})} \left\{ e^{-by/T}\left(\frac{bR_o}{4\xi} + \frac{by}{2T} - \frac{b}{4} - 1\right) + 1 \right\} \tag{72}$$

Flow continuity then requires that this must also be the normal component along the boundary in the Zone II region. Since both $\dot{U}_y$ and

$\dot{U}_\theta$ are zero, the net normal component must be the normal component of the $\dot{U}_R$ term. The form of $\dot{U}_R$ having Equation (72) as its normal component is:

$$\dot{U}_R\Big|_{bdy} = \frac{\dot{U}\xi}{T(1-e^{-b/2})} \left\{ e^{-by/T}\left(\frac{bR_o}{4\xi} + \frac{by}{2T} - \frac{b}{4} - 1\right) + 1 \right\} \tag{73}$$

Volume constancy for cylindrical coordinates requires that all points within a deforming region must obey the restriction that:

$$\dot{\varepsilon}_{RR} + \dot{\varepsilon}_{\theta\theta} + \dot{\varepsilon}_{yy} = 0 \tag{74}$$

For our assumed velocity field of Equation (71), the strain rates components of Equation (59) become:

$$\dot{\varepsilon}_{RR} = \frac{\partial \dot{U}_R}{\partial R} \qquad \dot{\varepsilon}_{\theta\theta} = \frac{\dot{U}_R}{R}$$

$$\dot{\varepsilon}_{yR} = \frac{1}{2}\frac{\partial \dot{U}_R}{\partial y} \tag{75}$$

$$\dot{\varepsilon}_{yy} = \dot{\varepsilon}_{R\theta} = \dot{\varepsilon}_{\theta y} = 0$$

Volume constancy then requires:

$$\left.\begin{aligned} &\frac{\partial \dot{U}_R}{\partial R} + \frac{\dot{U}_R}{R} = 0 \\ &\frac{1}{R}\left\{\frac{\partial}{\partial R}(\dot{U}_R R)\right\} = 0 \end{aligned}\right\} \tag{76 (cont.)}$$

$$\left.\begin{aligned} \frac{\partial}{\partial R}(\dot{U}_R R) &= 0 \\ \dot{U}_R &= \frac{f(y)}{R} \end{aligned}\right\} \qquad (76)$$

Thus, there now exists a general form for $\dot{U}_R$ in Zone II, Equation (76), and a specific expression for its value along the boundary at $R = R_o - \xi + 2\xi y/T$, presented as Equation (73). Evaluation of the general expression of Equation (76) at the boundary will enable determination of f(y):

$$\dot{U}_R\Big|_{bdy} = \frac{f(y)}{R_o - \xi + \frac{2\xi y}{T}}$$

$$\therefore f(y) = \left(R_o - \xi + \frac{2\xi y}{T}\right) \cdot \dot{U}_R\Big|_{bdy} \qquad (77)$$

Substituting Equation (77) into Equation (76) and replacing $\dot{U}_R\Big|_{bdy}$ by its form in Equation (73), the velocity field for the entire Zone II region can be presented as:

$$\dot{U}_R = \frac{\left(R_o - \xi + \frac{2\xi y}{T}\right)\dot{U}\xi}{R\,T\,(1-e^{-b/2})} \left\{ e^{-by/T}\left(\frac{bR_o}{4\xi} + \frac{by}{2T} - \frac{b}{4} - 1\right) + 1 \right\}$$

$$\dot{U}_y = \dot{U}_\theta = 0 \qquad (78)$$

Zone II - Internal Power of Deformation

From the velocity field of Equation (78), the strain rates field for Zone II can be evaluated through the relations of Equation (59):

$$\dot{\varepsilon}_{RR} = -\dot{\varepsilon}_{\theta\theta} = \frac{-\dot{U}\xi(R_o - \xi + \frac{2\xi y}{T})}{R^2 T(1-e^{-b/2})} \left\{ e^{-by/T} \left(\frac{bR_o}{4\xi} + \frac{by}{2T} - \frac{b}{4} - 1 \right) + 1 \right\}$$

$$\dot{\varepsilon}_{yy} = \dot{\varepsilon}_{R\theta} = \dot{\varepsilon}_{\theta y} = 0$$

$$\dot{\varepsilon}_{yR} = \frac{1}{2}\frac{\partial \dot{U}_R}{\partial y} = \frac{\dot{U}\xi^2}{2RT^2(1-e^{-b/2})} \left[2 + e^{-by/T} \left\{ -2 - 2b + \frac{4by}{T} \right.\right.$$

$$\left.\left. + \frac{b^2 y}{T} - \frac{b^2}{4} - \frac{b^2 y^2}{T^2} + \frac{2bR_o}{\xi} + \frac{b^2 R_o}{2\xi} - \frac{b^2 y R_o}{T\xi} - \frac{R_o^2 b^2}{4\xi^2} \right\} \right] \qquad (79)$$

Substituting the non-zero strain rates of Equation (79) into the basic internal power expression of Equation (6) and integrating over the volume of Zone II [two times the integral over the upper half-disc] yields:

$$\dot{W}_{iII} = \frac{2\sigma_o}{\sqrt{3}} \int_V \sqrt{\dot{\varepsilon}_{RR}^2 + \dot{\varepsilon}_{yR}^2}\, dV$$

where $dV = 2\pi R dR dy$

$$\dot{W}_{iII} = \frac{8\pi\sigma_o}{\sqrt{3}} \int_{y=0}^{y=T/2} \left\{ \int_{R=R_o-\xi+2\xi y/T}^{R=R_o} R \sqrt{\dot{\varepsilon}_{RR}^2 + \dot{\varepsilon}_{yR}^2}\, dR \right\} dy \qquad (80)$$

Substituting the explicit forms of the strain rate terms and manipulating:

$$\dot{W}_{iII} = \frac{8\pi\sigma_o \dot{U}\xi}{\sqrt{3}\, T(1-e^{-b})} \int_{y=0}^{y=T/2} r(y) \left\{ \int_{R=R_o-\xi+2\xi y/T}^{R=R_o} \frac{1}{R} \sqrt{R^2 + \left\{\frac{s(y)}{r(y)}\right\}^2}\, dR \right\} dy \qquad (81)$$

where:

$$r(y) = \frac{\xi}{2T} \left\{ 2 + e^{-by/t} (\ell y^2 + my + n) \right\}$$

$$\ell = -b^2/T^2$$

$$m = \left(\frac{4b}{T} + \frac{b^2}{T} - \frac{b^2 R_o}{T\xi}\right)$$

$$n = \left(-2 - 2b - \frac{b^2}{4} + \frac{2bR_o}{\xi} + \frac{b^2 R_o}{2\xi} - \frac{R_o^2 b^2}{4\xi^2}\right)$$

$$s(y) = \left(R_o - \xi + \frac{2\xi y}{T}\right) \left\{ 1 + e^{-by/T} (py + q) \right\}$$

$$p = b/2T$$

$$q = \left(\frac{bR_o}{4\xi} - \frac{b}{4} - 1\right)$$

Applying the integral relation presented as No. 241.01 in the text by Dwight:[72]

$$\int_x \frac{1}{x}\sqrt{x^2 + a^2}\, dx = \sqrt{x^2 + a^2} - a\, \ell n \left| \frac{a + \sqrt{x^2 + a^2}}{x} \right| \quad (82)$$

the integral with respect to R can be evaluated directly to produce:

$$\dot{W}_{iII} = \pi R_o^2 \sigma_o \dot{U} \left(\frac{8\,S}{\sqrt{3}\,(1-e^{-b/2})}\right) \int_{Y=0}^{Y=1/2} \left\{ \sqrt{\{r(y)\}^2 + \{t(y)\}^2} \right.$$

$$- \sqrt{(1 + 2SY - S)^2 \{r(y)\}^2 + \{t(y)\}^2} - t(y) \cdot$$

$$\left[\ell n \left| \frac{t(y)}{r(y)} + \sqrt{1 + \left\{\frac{t(y)}{r(y)}\right\}^2} \right| - \ell n \left| \right.\right.$$

$$\left.\left. \frac{\left\{\frac{t(y)}{r(y)}\right\} + \sqrt{(1 + 2SY - S)^2 + \left\{\frac{t(y)}{r(y)}\right\}^2}}{(1 + 2SY - S)} \right| \right] \Bigg\} dY \quad (83)$$

where:

$$t(y) = \frac{s(y)}{R_o}$$

$$= (1 + 2SY - S) \left\{1 + e^{-bY} \left(\frac{bY}{2} - \frac{b}{4S} - \frac{b}{4} - 1\right)\right\}$$

$$r(y) = \frac{S}{2D} \left\{2 + e^{-bY} \left[-b^2Y^2 + \left(4b + b^2 - \frac{b^2}{S}\right) Y \right.\right.$$

$$\left.\left. + \left(-2 -2b - \frac{b^2}{4} + \frac{2b}{S} + \frac{b^2}{2S} - \frac{b^2}{4S^2}\right)\right]\right\}$$

In lieu of attempting an upper-bound approximation of the remaining integral, numeric integration will be used in the preliminary investigation of the final solution. Should the results prove such that extensive utilization would seem likely, an approximation would then be pursued.

Interzone Shear Losses

The remaining interior power term is that for shear losses over the interzone surface. Elementary vector analysis applied to the velocity fields of Equations (58) and (78) will produce a velocity discontinuity along the boundary of:

$$\Delta v = \frac{\sqrt{\xi^2 + T^2/4}}{T} \cdot \left\{\frac{\dot{U}(1-e^{-by/T})}{(1-e^{-b/2})}\right\} \qquad (84)$$

As discussed in the earlier strip solution, the shear stress resisting this motion must be represented by $\tau_{max} = \sigma_o/\sqrt{3}$.

Substituting these expressions into the general power expression of Equation (20) produces an integral expression for the interzone shear losses:

$$\dot{W}_{sI\text{-}II} = \frac{\sigma_o}{\sqrt{3}} \frac{\sqrt{\xi^2 + T^2/4}\ \dot{U}}{T(1-e^{-b/2})} \int_S (1 - e^{-by/T})\ dS \qquad (85)$$

Using the similarity of a differential triangle and the triangle of Zone II, the differential surface element can be simplified as follows:

$$dS = 2\pi R d\ell$$

$$= 2\pi(R_o - \xi + \frac{2\xi y}{T}) \frac{d\ell}{dy}\ dy$$

$$= 2\pi(R_o - \xi + \frac{2\xi y}{T}) \frac{\sqrt{\xi^2 + T^2/4}}{T/2}\ dy \qquad (86)$$

Substituting the expression of Equation (86) into Equation (85) and integrating, the interzone shear losses can be computed explicitly:

$$\dot{W}_{sI\text{-}II} = \frac{8\pi\sigma_o \dot{U}(\xi^2+T^2/4)}{\sqrt{3}\ T^2(1-e^{-b/2})} \int_{y=0}^{y=T/2} (1-e^{-by/T})\ (R_o - \xi + \frac{2\xi y}{T})\ dy \qquad (87)$$

(cont.)

$$\dot{W}_{sI-II} = \frac{8\pi\sigma_o \dot{U}(\xi^2 + T^2/4)}{\sqrt{3}\, T\, (1-e^{-b/2})} \left\{ \frac{R_o}{2} - \frac{\xi}{4} + \frac{\xi}{b} - (1-e^{-b/2})[\frac{R_o}{b} + \frac{2\xi}{b^2}] \right\} \quad (87)$$

In the dimensionless notation of Equation (66), the result becomes:

$$\dot{W}_{sI-II} = \pi R_o^2 \sigma_o \dot{U} \left\{ \frac{8D\ (\frac{S^2}{D^2} + \frac{1}{4})}{\sqrt{3}\ (1-e^{-b/2})} \cdot [\ \frac{1}{2} - \frac{S}{4} + \frac{S}{b} \right.$$

$$\left. - \ (1 - e^{-b/2})\ (\frac{1}{b} + \frac{2S}{b^2})] \right\} \quad (88)$$

Power Required to Overcome Imposed Body Tractions

As with the strip geometry, the possible body tractions for disc forging are limited to an external pressure on the free surface area. The power associated with this pressure is simply the value of the pressure times the rate at which volume is being displaced against it. Since each platen displaces material at a rate equal to the area of the disc in contact with the platen times the platen velocity, the net rate of volume displacement for both platens is simply $\pi R_o^2 \dot{U}$. Multiplying by the pressure, the power required to overcome the external restraint becomes:

$$\dot{W}_p = \pi R_o^2 \dot{U}p \quad (89)$$

A check in which the velocity of the free surface was integrated to compute volume rate produced the identical result, providing proof

that no errors were made in determining the Zone II velocity field.

Total Power Required

Summing all of the contributing terms, the upper-bound of the total power required is:

$$\dot{W}_{TOT} = \dot{W}_{iI} + \dot{W}_{iII} + \dot{W}_{sI-II} + \dot{W}_{f} + \dot{W}_{p} \tag{49}$$

In the dimensionless notation of Equation (66), these terms have been developed as follows:

$\dot{W}_{iI}$:

This term has been presented explicitly as Equation (67) with one integral remaining in the expression, and in approximate form with no integrals by Equation (68).

$\dot{W}_{iII}$:

Equation (83) presents the internal power of deformation with one integral remaining unsolved.

$\dot{W}_{sI-II}$:

The interzone shear losses are presented explicitly by Equation (88).

$\dot{W}_{f}$:

Power required to overcome friction is given as Equation (70).

$\dot{W}_{p}$:

The power to overcome imposed body tractions (pressure applied to the free surface) is computed through Equation (89).

Relative Average Forging Pressure

The external power being supplied by the platens is simply the force times the platen velocity, and force is the average pressure times the area on which it is acting. Considering both upper and lower platens, the applied power is simply:

$$J^* = \pi R_o^2 \, p_{ave} \, \dot{U} \tag{90}$$

By equating the power supplied by the platens and the power required to deform the disc, the relative average forging pressure may be computed as:

$$\frac{p_{ave}}{\sigma_o} = \frac{1}{\pi R_o^2 \, \dot{U} \, \sigma_o} \, \dot{W}_{TOT} \tag{91}$$

Single Zone Bulge Solution

In order to evaluate the merits of the solution just developed, the results must be compared to those of alternative solutions and evaluated from the viewpoint of least upper-bound. As with the strip geometry, the single zone upper-bound with bulge of Avitzur[27,28] provides the best field for comparison. In the dimensionless notation of Equation (66), the relative average forging pressure for the single-zone bulge solution can be written as:

$$\left.\frac{p_{ave}}{\sigma_o}\right|_{\text{single zone}} = 8 \frac{b}{D} \left\{ \left[\frac{1}{12} + \frac{D^2}{b^2} \right]^{3/2} - \frac{D^3}{b^3} \right. \tag{92 (cont.)}$$

$$- \frac{m}{24\sqrt{3}} \left. \frac{1}{1 - e^{-b/2}} \right\} + \frac{p}{\sigma_o} \tag{92}$$

Comparison of Solutions

Inspection of Equation (92) reveals a function of four variables: the three independent variables of D, m, and p/σ_o, and the variable of optimization, b. As with the strip geometry, an expression has been derived to approximate b_{opt} as a function of the independent process variables:[27,28]

$$b_{opt} \approx \frac{4\left(\frac{m}{\sqrt{3}}\right) D}{1 + \frac{2}{3}\left(\frac{m}{\sqrt{3}}\right) D} \tag{93}$$

Still further approximations produce an explicit form of the relative average forging pressure with all variables being independent:

$$\frac{p_{ave}}{\sigma_o} = \frac{1 + \frac{2}{3}\left(D + \frac{1}{D}\right)\frac{m}{\sqrt{3}} + \frac{1}{9}\left(\frac{m}{\sqrt{3}}\right)^2}{1 + \frac{2}{3}\left(\frac{m}{\sqrt{3}}\right) D} \tag{94}$$

These approximations are extremely useful in reducing the mathematical difficulty necessary to apply the solution and are surprisingly accurate. Nevertheless, since a valid comparison of solution capabilities is desired, Equation (92) was used directly in the LOPER optimization search routine to determine the best values of b_{opt} and $p_{ave}/\sigma_o|_{\text{single zone}}$, Equation (93) serving to establish the starting point for the search.

For the two-zone two-parameter solution of Equation (91), an additional minimization parameter has been added in the form of the zone size parameter, S. Equation (67) is used to represent the internal power of deformation in Zone I, since the parallel term for Zone II contains an unsolved integral and requires the use of numeric integration as previously described in the strip presentation. Thus, with upper-bound numeric integration of both the $\dot{W}_{iI}$ and $\dot{W}_{iII}$ terms included within the two parameter optimization search routine of LOPER, the two-zone two-parameter approach is given its best chance of producing a superior solution.

Results

Reasoning that the newly-proposed two-zone solution has its greatest chance of success for the highest possible interface friction, m was set equal to one and the results of Table 3 were computed to enable a comparison. The three columns for the single-zone solution provide results of increasing accuracy. In column 1, Equation (94) is computed directly. Column 2 computes b_{opt} through the approximation of Equation (93) and substitutes this value into Equation (92). The solution in column 3 subjects Equation (92) to an optimization routine which determines the best values of b_{opt} and $p_{ave}/\sigma_o|_{\text{single zone}}$ possible for the bulge solution. Column 4 presents the results of the two-zone solution of Equation (91) as obtained by a two-parameter optimization search with upper-bound numeric techniques being applied to all unsolved integrals.

Comparison of the results reveals that for all conditions of geometry investigated, the single-zone solution produced the lower value for power and relative average forging pressure, and was thus the superior solution. Reasons for the apparent anomaly of an improved solution for strip but not for disc will be presented in the following section. Figure 28 presents the optimal value of the bulge parameter, b_{opt}, as a function of disc geometry for the two-zone solution with m = 1. A similar curve for S_{opt} is presented in Figure 29.

DISCUSSION: STRIP SOLUTION vs. DISC SOLUTION

Strip Solution

In order to facilitate a clear explanation of the apparent failure of the two-zone disc analysis, a more complete understanding of the strip solution is required. Table 4 presents a comparison of the one-zone and two-zone solutions for a single value of geometry, friction, and imposed pressure, chosen to be representative of those conditions in which the two-zone field is superior. The contributions of the various power terms to the net p_{ave}/σ_o are designated by the various subscripts.

TABLE 4

COMPARISON OF STRIP SOLUTIONS

$D = t/w = 0.5$

$m = 1.0$

$p/\sigma_o = 0$

TERM	ONE-ZONE	TWO-ZONE
b_{opt}	.6577	1.6732
S_{opt}	--	.4962
$p_{ave\ iI}/\sigma_o$	1.2332	.9575
$p_{ave\ iII}/\sigma_o$	--	.0487
$p_{ave\ sI\text{-}II}/\sigma_o$	--	.3629
Total of Above Pressures	1.2332	1.3691
$p_{ave\ f}/\sigma_o$	.4081	.2231
$p_{ave\ p}/\sigma_o$	0	0
p_{ave}/σ_o	1.6413	1.5922

Upon studying Table 4, several observations become apparent:

1) The optimum value of the bulge parameter, b_{opt}, is considerably larger for the two-zone solution.
2) For the case of m = 1.0, the value of S_{opt}, the optimum size of Zone II, is approximately equal to the value of D (see Figure 16). Referring to Figure 13, we see that this is equivalent to requiring $\xi \approx t$ and thus, the inclination of the interzone shear surface is approximately 45°.
3) The addition of a second zone and accompanying interzone shear surface serves to raise the amount of power necessary to deform the interior volume of the strip. In the example shown the relative average pressure related to deformation of the interior regions increases from 1.2332 to 1.3691 as we go from one-zone to two-zones.
4) The power required to overcome the platen-workpiece friction, however, decreases for the two-zone velocity field. This can be related to the value of b_{opt}, since a larger degree of bulging will produce a corresponding decrease in velocity along the platen surfaces.
5) The net effect on the total power required and relative average forging force depends upon the magnitude of the two significant changes: a) the increase in the power required to deform the interior of the strip due primarily to shear over the interzone surface and b) the decrease

in power required to overcome friction along the workpiece-platen interfaces. For those conditions where the decrease dominates the increase, the two-zone field will produce a superior solution.

Disc Solution

Consideration of a similar table for the disc geometry, Table 5, shows similar trends occurring.

TABLE 5

COMPARISON OF DISC SOLUTIONS

$D = T/R_o = 0.1$

$m = 1.0$

$p/\sigma_o = 0$

TERM	ONE-ZONE	TWO-ZONE
b_{opt}	.2577	.2993
S_{opt}	--	.0198
$p_{ave\ iI}/\sigma_o$	1.1277	1.1430
$p_{ave\ iII}/\sigma_o$	--	.0051
$p_{ave\ SI\text{-}II}/\sigma_o$	--	.0340
Total of Above Pressures	1.1277	1.1821
$p_{ave\ f}/\sigma_o$	3.6063	3.5681
$p_{ave\ p}/\sigma_o$	0	0
p_{ave}/σ_o	4.7340	4.7502

As with the strip solutions, a larger value of b_{opt} is produced by the two-zone approach, leading to a decrease in the power

required to overcome platen-workpiece friction. The introduction of an interzone surface of shear produces a net increase in the power required to deform the interior of the disc. For the disc geometry, however, the region for which power increases is much larger than for the strip. The surface of interzone shear now wraps around the entire circumference of the disc as opposed to only the two free surfaces for strip. In contrast, the areas experiencing a drop in power, the areas where the workpiece contacts the platens, remains relatively similar. The change in geometry shifts the balance in such a way that the increased power demand for internal deformation dominates the decrease in power to overcome friction for all goemetries and frictions studied. S_{opt} becomes much smaller than that observed for strip in an effort to decrease the size of the interzone shear surface, but is unable to sufficiently reduce the power. Thus, the one-zone velocity field is always superior for the process of disc forging.

Possible Improvements to the Disc Solution

In order to produce a superior two-zone solution for the disc geometry, the power required to overcome the interzone shear losses must be decreased. As noted during the development of this term for the strip geometry, the assumed value of the shear stress opposing motion, $\tau = \sigma_o/\sqrt{3}$, may be a considerable overestimate of the actual. Should an alternative representation be accepted as producing a valid upper-bound solution, it is possible that the contribution of this term would be diminished to such an extent

that the two-zone solution may indeed by superior. In the absence of such an improved representation, a possible alternative is to modify the velocity field in Zone II so as to reduce the magnitude of the interzone velocity discontinuity. It has already been noted that the two-zone velocity field bears considerable resemblance to what has been observed in reality and it should not be totally abandoned as a result of the present "failure".

APPLICATION OF SOLUTIONS TO MODELING DEFORMATION

Introduction

The successful development of the two-zone two-parameter solutions and subsequent optimization of relative average forging pressure has provided the values of b_{opt} and S_{opt} for specified conditions of friction and process geometry. Since these values are all that is required to completely characterize the velocity of all points within the deforming body at a given instant, it seems likely that by incrementing the downward motion of the platen and applying the instantaneous velocity field for a given increment, the entire deformation process may be adequately modeled. Moreover, since the analysis has been designed to permit foldover, it is expected that the development of a fold with increased deformation may be modeled.

How the Approach Permits Foldover

To understand the mechanism by which the upper-bound solution models foldover, consider the sequence of Figure 30. The upper sketch of Figure 30a depicts the optimum two-zone geometry when initial contact is made with the platen. If the platen is now lowered an increment, Δy, the exponential bulge velocity field will act to distort Zone I to the configuration of Zone I'. Zone II is restricted to a lamellar shear flow parallel to the platen and thus shears to produce Zone II' with a net bulge of the free surface. The interzone surface is now repositioned to correspond to the optimal location for the new geometry, with any external bulge being

ignored, and an additional deformation increment is considered as in Figure 30b. In this increment, however, the ram will be overtaking a slightly inclined surface and a small amount of foldover will occur. In addition, Zone I will produce additional bulge and thereby increase the amount of foldover developed in the next increment. By proceeding step by step in this manner an entire deformation may be modeled; the smaller the increment of deformation, the more accurate the results.

Polynomial Curve Fit of b_{opt} and S_{opt} Curves

To successfully model the deformation, it is necessary to characterize the optimal velocity field for each increment of motion, and this requires a knowledge of both b_{opt} and S_{opt} as a function of process geometry. Figures 15 and 16 present this information for the strip solution and Figures 28 and 29 apply to discs. Each data point on these figures, however, is the result of an optimization search of all possible b or S values for the particular conditions of friction and geometry. For such a search to be conducted at each increment of a deformation modeling, the required computer utilization would be extensive.

Fortunately, the necessary data already exists and produces the continuous smooth curves observed in the figures. Furthermore, extremely accurate curve fit routines are available to replace an experimental curve with an approximating equation. Such a routine from the ISIS statistical package [POLREG subroutine of the Interactive Statistical Instructional System - a statistical program

available at the Lehigh University Computer Center] was selected to perform a polynomial regression curve fit of the form:

$$b_{opt} \text{ or } S_{opt} = C_o + C_1 D + C_2 D^2 + C_3 D^3 + C_4 D^4 + \ldots \quad (95)$$

Degree of fit is available in increasing order up to 9 or n-1 (where n is the number of data points), whichever is less, and a plot is available to show any possible deviation from the desired curve.

This routine was applied to all curves in the previous figures and all orders of fit from one to nine were produced. The results were plotted and that order which produced the best fit with no abnormal behavior between data points was selected. In the case of the strip geometry, an eighth order approximation was chosen for both b_{opt} and S_{opt}. For discs, S_{opt} was approximated by eighth order, while b_{opt} showed improved characteristics for the extreme ninth order. Tables 6 and 7 present the coefficients for Equation (95).

Approach to Modeling

Even with the simplified determination of b_{opt} and S_{opt}, the incremental modeling of a deformation sequence would be a monumental task if the path of each point in the body must be followed. Fortunately, however, the relevant information on foldover and bulge profile can be obtained by following only a select family of points. Consider the schematics presented in Figure 31. The upper diagram depicts the deforming body in its original geometry with a series

of points laid out at intervals along the free surface. The point labeled 0 will belong to the Zone I region and serves to mark the location of the original corner. All other points belong to the Zone II region and determine the amount of foldover and contour of the free surface.

If the platen is now displaced an increment Δy, the material must undergo a finite amount of deformation. Points along the upper surface of Zone I move down with the platen and expand outward. In Zone II, however, no downward velocity is permitted so the area of triangle 011' is "lost", the line 1'1 shearing horizontally such that point 1 now forms the new corner of the body. [NOTE: In the strip solution, the area of the "lost" triangle is added as a uniform skin to the free surface for each increment of deformation to preserve a constant volume]. Thus, the lower sketch of Figure 31 depicts the body after the third increment of deformation. Point 0 marks the original corner and Point 3, the present corner of the body. Points with numbers greater than three map the contour of the free surface. During the next deformation increment, the "loss" of triangle 344" will be compensated.

Studies for the Strip Geometry

For the strip solution, the velocity fields have already been determined to show that the non-zero components are:

Zone I:

$$\dot{U}_x = \dot{U} \frac{b}{1-e^{-b}} \frac{x}{w} \frac{1}{D} e^{-by/t} \qquad (3)$$

(cont.)

$$\dot{U}_y = -\dot{U} \frac{1}{1-e^{-b}} (1 - e^{-bY}) \tag{3}$$

Zone II:

$$\dot{U}_x = \dot{U} \frac{S}{D} \frac{1}{1-e^{-b}} \left\{ e^{-bY} \left(\frac{b}{S} + bY - b - 1 \right) + 1 \right\} \tag{33}$$

where:

$$D = \frac{t}{w}$$

$$S = \frac{\xi}{w}$$

$$Y = \frac{y}{t}$$

Since the only point to be considered in Zone I is always in contact with the platen where $Y = y/t = 1$, Equation (3) reduces to:

$$\dot{U}_x = \dot{U} \frac{b\, e^{-b}}{1-e^{-b}} \frac{x}{wD}$$

$$\dot{U}_y = -\dot{U} \tag{96}$$

Noting that the components presented are velocity components and not displacements, the relation that displacement = velocity x time is applied. Multiplying all components by an unspecified increment of time Δt and replacing the product $\dot{U}\Delta t$ by Δy (since the downward displacement of the point in Zone I in contact with the platen is desired to be Δy for each increment of deformation) the velocity components of Equations (33) and (96) become the required displacement field.

An initial geometry of $t_{orig} = 2.0$, $w_{orig} = 4.0$, $D = t/w = 0.5$ was selected for study, and the free surface height was divided into 1000 increments, such that 1% deformation corresponded to 10 deformation increments. Deformation was then allowed to proceed and the geometry was computed through a 95% reduction in height for friction values of m = 1.00, 0.90, 0.80, and 0.70.

Results and Observations for Strip

Figure 32 presents a typical deformation sequence, which in this particular case corresponds to maximum interface friction or m = 1. The small arrow on the top surface indicates the location of the original corner and serves to determine the relative amounts of top surface spread and foldover. Since only the upper-right quadrant is being presented, the inward slope of the free surface where it approaches the center-line indicates a double bulge formation. Such a phenomenon is not an unphysical one; however, most reports in the literature reveal its occurrence in the compression of solid discs. Kulkarni and Kalpakjian[31] and Tarnovskii[73] both report double bulge formation during the deformation of high cylinders. Shah, Lee, and Kobayashi[8] report additional observations by Kudo and Aoi[74] and Nagamatsu, et al.,[75] and in their own work observe a transition between single bulge and double bulge for an original height to diameter ratio $\approx$ 1.6. For samples with initial ratios of 2.0 and 2.5, a double bulge formed in the early stages of deformation giving way to a single bulge as deformation continues.

Additional discussion has been provided by Hsu[76] and pictures of such deformation have been presented by Berkowitz and Kuhn.[77]

Such a phenomenon has only been observed in discs with a height to diameter ratio greater than one, however, and here appears in the model of a strip with thickness to width of only 0.5. Theoretically, this can be explained by comparison of the values of S_{opt} for the disc and strip geometries. For strip, S_{opt} is considerably larger and the deeper penetration of this Zone II region serves to blunt the exponential cusp. For disc, however, the size of Zone II is considerably smaller and the exponential cusp of Zone I dominates the free surface. This observation will become even clearer when a deformation sequence for the disc geometry is presented. Unfortunately, no experimental observations have been reported which would either validate or invalidate the strip prediction.

Figure 33 illustrates the effect of a variation in friction by comparing identical reductions (50%) for friction factors from $m = 1.0$ through $m = 0.7$. While the overall geometry shows little variation, the relative contributions of the original top surface and folded side surface which combine to form the new surface of contact differ noticeably. Increased foldover is produced by the higher interface friction. Figures 34 and 35, from Reference 78, illustrate these same phenomena in the upsetting of pure aluminum discs. With good lubrication the new contact surface is formed almost entirely by radial spreading of the original. In the unlubricated sample, significant foldover is observed with little radial spread.

Figure 36 presents a blow-up of the free surface for a 30% deformation with both m = 1.0 and m = 0.7. The results correspond well with the observation of Kobayashi and Lee[39] that an increase in interface friction produces an increase in the curvature of the bulge, but the change is not a large one. The contour for m = 1.0 clearly indicates a double bulge.

Other Techniques to Model Strip

Nearly all previous work on analytically modeling bulge and foldover in plane-strain upsetting was performed by Shabaik and co-workers. Figures 37a and 37b were taken from an early work [Ref. 78] in which visioplasticity studies were conducted to produce experimental distorted grids which were then computer analyzed to determine the instantaneous velocity for all points. An attempt was made to approximate the velocities by an analytical expression, but no complete solution was provided.

In subsequent efforts aimed at the determination of the bulge profile as a function of deformation, Shabaik[22,23] used these distorted grid studies to determine the shear stress distribution across the interface and observed that τ is a function of location, friction, and amount of deformation. As an approximation, he assumed that $\tau = 0$ at the center and increases to a maximum as the free surface is approached and proceeded to develop a corresponding slip line net. The resulting predictions for normal pressure and load showed good experimental agreement, so an incremental deformation was applied to model the geometrical changes in plane-strain upsetting.

Such an approach is indeed a valid one, although the neglect of τ approaching zero at the free surface is subject to question. The primary disadvantage lies in the extensive computer utilization required for each investigation. The slip line net must be totally recomputed for each increment of deformation, so unless considerable computer time is available, the increments must be large. In contrast, the upper-bound solution provides a single set of optimized equations which describe the motion of all points within the body and requires little time to compute an increment. Much smaller increments can be considered with a corresponding reduction in both expense and complexity. Unfortunately, since the new solution is invalid for thickness-to-width ratios greater than one [alternate approaches produce a lower upper-bound], no attempt could be made to provide a comparison with the experimental Figure 37 and a difference in friction assumptions precludes comparison of analytical results.

Studies for the Disc Geometry

Although the two-zone two-parameter analysis for the disc geometry failed to produce a lower upper-bound, its potential merits for modeling deformation when compared to those of alternate techniques justify a further presentation.

For the disc geometry, the velocity fields for the two zones show non-zero components of:

Zone I:

$$\dot{U}_R = \frac{\dot{U}}{4} \frac{b}{1-e^{-b/2}} \frac{R}{T} e^{-by/T} \qquad (58)\ (\text{cont.})$$

$$\dot{U}_y = -\frac{\dot{U}}{2}\,\frac{1-e^{-by/T}}{1-e^{-b/2}} \tag{58}$$

Zone II:

$$\dot{U}_R = \frac{\dot{U}}{2}\left(\frac{2}{1-e^{-b/2}}\right)\frac{R_o}{R}\,\frac{S}{D}\,(1+2YS-S)$$

$$\left\{e^{-bY}\left(\frac{b}{4S}+\frac{b}{2}Y-\frac{b}{4}-1\right)+1\right\} \tag{78}$$

where

$$D = T/R_o$$

$$S = \xi/R_o$$

$$Y = y/T$$

Since the only point to be considered in Zone I is always in contact with the platen where $y = T/2$, Equation (58) reduces to:

$$\dot{U}_R = \frac{\dot{U}}{2}\,\frac{1}{2}\,\frac{b\,e^{-b/2}}{1-e^{-b/2}}\,\frac{R}{T}$$

$$\dot{U}_y = -\frac{\dot{U}}{2} \tag{97}$$

Moreover, since the velocity field of Zone II will be applied only to points for which $R = R_o$ (a result of a technique to be discussed), the ratio R_o/R may be omitted from Equation (78). Multiplying all velocities by Δt and setting $\dot{U}/2\ \Delta t = \Delta y$ where Δy is the increment of deformation, the velocity equations are transformed to those for

displacement.

Modified Deformation Model

The basic deformation model of Figure 31 still applies, but several modifications must be incorporated for the disc geometry since points in Zone II have velocities dependent on their radial position. Moreover, the velocity field for Zone II was derived with the assumption of a straight vertical free surface and is subject to question when extended into an already barreled segment. Thus, after each increment of deformation, a vertical line is dropped from the new end point of contact (point 3 in the lower sketch of Figure 31) and the points of further consideration are repositioned on this line. The distances from these new points to the free surface, such as 44', 55', etc., are stored for future use.

If the platen is now displaced another increment, Δy, the displacement field can be applied to compute the new location of the primed points. The new point 4' forms the corner of the deformed unit and the remaining points describe the contour. Concurrent with the deformation of the imaginary surface, however, the material in the pre-existing bulge must also move outward. This increase in radial position increases the circumference of the bulge ring and must be compensated by thinning or decrease in the length between the primed and unprimed points. Accurate computation of this thinning to consider a finite length between the primed and unprimed points and its addition to a variable contour

produced by the incremental deformation would be quite complex, so an acceptable approximation was developed.

Viewing the lower sketch of Figure 31 from above, the line segments 4'4, 5'5, etc. take the form of thin rings with an inner radius equal to that of the corner point 3. If the length of segment 4'4 is small and equal to $\Delta_{4'4}$, the area of its ring before deformation is simply $2\pi R_3 \Delta_{4'4}$. The area of the ring after deformation should be equal to its original area, but the inner radius is now the new location of point 4'.

Thus:

$$\Delta_{4'4(new)} = \frac{\Delta_{4'4(old)} R_3}{R_{4'(new)}} \tag{98}$$

Since the increment of deformation is small, the new radius of the remaining primed points should not differ substantially from that of point 4', so the form of Equation (98) can be generalized to:

$$\Delta_{i'i(new)} = \frac{\Delta_{i'i(old)} \; R_{j-1(old)}}{R_{j'(new)}} \tag{99}$$

where j is the increment of deformation being computed and $i > j$. The assumptions in the approximation all tend to produce an increase in total volume, but if compensation of the "lost" area of triangles such as 344" in Figure 31 is omitted, the errors tend to cancel and a workable first approximation is produced.

Results and Observations for Disc

Using initial conditions of $T_{orig} = 3.2$, $R_{orig} = 4.0$, and $m = 1.0$, the deformation of a disc was computed through a 95% re-

duction. Eight hundred increments comprised the total height of the original free surface such that 8 increments corresponded to a 1% deformation. Figure 32 depicts part of the resulting deformation sequence with the arrow again indicating the position of the original corner. As discussed previously, the lower value of S_{opt} for the disc geometry results in a dominance of the exponential bulge, which in the current example appears unblunted on the free surface. A volume check performed by integrating over the free surface contour showed only a 0.05% gain at 25% reduction and 0.6% loss at a reduction of 50%. Thus, the first order approximation technique appears to produce a workable model.

Other Techniques Applied to Disc

Such an approach to modeling disc deformation with foldover is admittedly only an initial step toward a workable solution, but its value can be appreciated when compared to the alternate techniques currently available. Figure 39 [From Ref. 59] depicts results obtained from the primary means of investigation, that of direct experiment. The position of the original end-face diameter, which corresponds to the arrow in the figures presented for the new model, is compared to the theoretical position computed for uniform deformation [the parallel field]. Various lubricants are considered for an entire sequence of deformation. The difference between the observed curve and the theoretical is due to the combined phenomena of bulge and fold.

Kobayashi and co-workers have thus far developed the only other analytical technique capable of successfully modeling foldover in disc forging. The method, known as the matrix method, follows the basic elastic-plastic finite-element approach in which the deforming body is divided into elements which are each evaluated by limit analysis extremum conditions. The matrix name is derived through the use of a Lagrange multiplier with linearized stiffness equations.

In the earliest related publication,[39] deformation of cylinders with thickness to diameter ratios of 0.75 and 1.0 was modeled with increments corresponding to 1.0 - 1.2% compression being used. When coupled with a fracture criterion, the limiting reduction in height was computed for various process geometries and frictions. Variation in strain-hardening ability resulted in increased foldover for non-hardening materials. Thus, the method was clearly able to predict the free surface barreling and foldover phenomena, long known but previously never shown by a theoretical calculation. In more recent publications, Reference 9 presents results for thinner discs, and Reference 8 modifies the matrix approach to consider tall cylinders with height-to-diameter ratios of 2.0 and 2.5. Nevertheless, the method suffers from several significant disadvantages, such as the high degree of mathematical complexity and extensive utilization of computer techniques. Should the upper-bound velocity field approach be improved, its advantages would be distinct.

CONCLUSIONS, RECOMMENDATIONS, AND APPLICATIONS

A new capability has been added to the upper-bound technique of analysis. The proposed two-zone two-parameter velocity field for strip forging appears to be an adequate upper-bound solution for describing the combined phenomena of bulge and fold. A lower upper-bound is produced for the expected conditions of friction and geometry, and application of the solution through an incremental deformation technique provides an acceptable model of the forging process. Modeling of deformation with foldover has previously been accomplished only by far more complex and costly techniques, such as the slip line or matrix methods.

The parallel analysis for the disc geometry is only a qualified success, however. A lower upper-bound was not obtained, most likely due to the necessary overestimation of the shear losses over the interzone surface. Power minimization results in attempts to minimize the contribution of this component and forces the solution to assume low values for the optimum size of the Zone II region. When this optimum value is then applied in the modeling of deformation, the Zone II region has insufficient size to produce the desired blunting of the exponential cusp formed in the interior.

Nevertheless, the concepts behind the development of the two-zone approach are valid and it is postulated that further refinements may well produce a superior solution. In the absence of an acceptable alternative for describing interzone shear, a

modification of the velocity field in Zone II and contour of the interzone shear surface is suggested. Moreover, since a major hurdle in the three-parameter solution for strip occurred in handling the Zone II region, a modification of the velocity field may well simplify the "general solution" to a competitive level of complexity.

The work does provide the necessary background for the incorporation of foldover into an upper-bound analysis of the upset forging of hollow rings. This could lead to a possible improvement in the theoretical calibration curves used to determine friction and flow stress conditions during the deformation of a solid. Such ring test determinations are particularly useful for conditions of high temperature workpieces and high strain rates.

The results of Figure 33 indicate another possible application of this work in developing a simplified technique for quantifying high friction in forging operations. After a substantial increment of deformation, the relative amounts of spread of the original surface of contact with the platen (the position of the original corner being indicated by the small arrow) and material coming into contact with the platen due to the foldover phenomenon (to the right of the arrow) show a definite variation with interface friction. With theoretical support to provide the necessary calibration, the use of solid specimens and possibly a single measurement could well replace the hollow ring test to measure high friction. The ring test now requires a sequential deform and measure cycle to produce

an experimental percent change in internal diameter vs. percent reduction in thickness curve. Although additional requirements would be required before an improved test could be calibrated, the concept and initial groundwork has been provided.

Table 1

NOMENCLATURE

b	bulge parameter
bdy	subscript denoting evaluation along the interzone boundary
b_{opt}	value of b which produces minimum required power
D	dimension ratio (t/w or T/R_o)
F	fold parameter
f( )	function of ( )
J*	externally supplied power to deform the solid
	upper-bound on energy consumption
ℓ	length of the strip
m	constant shear stress friction factor
P	forging force
p	external pressure applied on the free surface of the material (free from platens)
p_{ave}	average forging pressure
p_{ave}/σ_o	relative average forging pressure
R,θ,y	cylindrical coordinate system
R_o	radius of the disc
S	surface area (in integrals)
	zone size parameter (ξ/w or ξ/R_o)
S_{opt}	value of S which produces minimum required power
S_t	surface over which tractions are prescribed
S_Γ	surface of velocity discontinuity

T	thickness of the disc
T_i	prescribed applied surface tractions
t	half thickness of the strip
$\dot{U}$	velocity vector
	platen velocity or multiple thereof (see Figs. 1 & 2)
$\dot{U}_i$	component of a velocity vector
$\dot{U}_N$	normal component of velocity
V	volume
$\dot{V}$	volume rate of material being deformed
v	velocity
$\dot{W}_f$	power required to overcome friction
$\dot{W}_i$	internal power of deformation
$\dot{W}_{iI}$	internal power of deformation for Zone I
$\dot{W}_{iII}$	internal power of deformation for Zone II
$\dot{W}_p$	power required to overcome imposed body tractions
$\dot{W}_{sI-II}$	power required to overcome shear along the interzone surfaces
$\dot{W}_{TOT}$	upper-bound on total power required to deform the body
w	half width of the strip
x,y,z	Cartesian coordinate system
Y	dimensionless parameter (y/t or y/T)
Δv	velocity difference or discontinuity
Δy	increment of deformation
$\dot{\varepsilon}_{ij}$	components of strain rate tensor
μ	coulomb coefficient of friction

ξ	depth of penetration of Zone II along the disc or strip centerline
σ_{ij}	component of stress tensor
σ_o	flow stress in a uniaxial tensile test of a round rod
τ	shear or friction stress

TABLE 2

COMPARISON OF SOLUTIONS - STRIP

m = 0.90

D	TERM	SINGLE-ZONE BULGE		TWO-ZONE TWO-PARAMETER	
		APPROX.	OPTIMUM	APPROX.	NUMERIC
0.90	p_{ave}/σ_o	1.37932	1.37913	1.54381	1.39949
	b_{opt}	.8648	.9167	2.3315	
	S_{opt}	--	--	.5898	
0.80	p_{ave}/σ_o	1.41320	1.41298	1.54362	1.41360
	b_{opt}	.7941	.8446	2.1912	
	S_{opt}	--	--	.5721	
0.70	p_{ave}/σ_o	1.45720	1.45694	1.55602	1.44180
	b_{opt}	.7186	.7677	1.9966	
	S_{opt}	--	--	.5460	
0.60	p_{ave}/σ_o	1.51647	1.51616	1.58691	1.48961
	b_{opt}	.6378	.6852	1.7539	
	S_{opt}	--	--	.5100	
0.50	p_{ave}/σ_o	1.60026	1.59988	1.64646	1.56673
	b_{opt}	.5510	.5961	1.4695	
	S_{opt}	--	--	.4613	
0.40	p_{ave}/σ_o	1.72709	1.72661	1.75431	1.69206
	b_{opt}	.4576	.4995	1.1472	
	S_{opt}	--	--	.3952	
0.30	p_{ave}/σ_o	1.94023	1.93960	1.95456	1.90877
	b_{opt}	.3568	.3938	.7995	
	S_{opt}	--	--	.3066	

TABLE 2 (cont.)

D	TERM	SINGLE-ZONE BULGE		TWO-ZONE TWO-PARAMETER	
		APPROX.	OPTIMUM	APPROX.	NUMERIC
0.20	p_{ave}/σ_o	2.36953	2.36870	2.37653	2.34609
	b_{opt}	.2477	.2772	.4634	
	S_{opt}	--	--	.1985	
0.10	p_{ave}/σ_o	3.66447	3.66333	3.66708	3.65195
	b_{opt}	.1292	.1471	.1917	
	S_{opt}	--	--	.0900	
0.09	p_{ave}/σ_o	3.95271	3.95154	3.95493	3.94134
	b_{opt}	.1168	.1332	.1691	
	S_{opt}	--	--	.0800	
0.08	p_{ave}/σ_o	4.31311	4.31190	4.31494	4.30289
	b_{opt}	.1042	.1192	.1473	
	S_{opt}	--	--	.0702	
0.07	p_{ave}/σ_o	4.77661	4.77536	4.77803	4.76752
	b_{opt}	.0916	.1050	.1264	
	S_{opt}	--	--	.0606	
0.06	p_{ave}/σ_o	5.39475	5.39346	5.39577	5.38679
	b_{opt}	.0789	.0906	.1062	
	S_{opt}	--	--	.0513	

TABLE 2 (cont.)

D	TERM	SINGLE-ZONE BULGE		TWO-ZONE TWO PARAMETER	
		APPROX.	OPTIMUM	APPROX.	NUMERIC
0.05	p_{ave}/σ_o	6.26032	6.25900	6.26093	6.25347
	b_{opt}	.0660	.0760	.0867	
	S_{opt}	--	--	.0422	
0.04	p_{ave}/σ_o	7.55890	7.55753	7.55909	7.55315
	b_{opt}	.0531	.0612	.0680	
	S_{opt}	--	--	.0333	
0.03	p_{ave}/σ_o	9.72350	9.72208	9.72327	9.71883
	b_{opt}	.0400	.0462	.0500	
	S_{opt}	--	--	.0246	
0.02	p_{ave}/σ_o	14.05316	14.05169	14.05249	14.04954
	b_{opt}	.0268	.0310	.0327	
	S_{opt}	--	--	.0162	
0.01	p_{ave}/σ_o	27.04307	27.04155	27.04195	27.04049
	b_{opt}	.0134	.0156	.0160	
	S_{opt}	--	--	.0080	

TABLE 3

COMPARISON OF SOLUTIONS - DISC

m = 1.00

D	TERM	SINGLE-ZONE BULGE			TWO-ZONE NUMERIC
		EQN. (92)	EQN.(90)App.	EQN. (90)	
0.90	p_{ave}/σ_o	1.34514	1.34264	1.34230	1.46078
	b_{opt}	--	1.5437	1.6528	6.2615
	S_{opt}	--	--	--	.3083
0.80	p_{ave}/σ_o	1.39617	1.39344	1.39304	1.50199
	b_{opt}	--	1.4126	1.5192	5.0518
	S_{opt}	--	--	--	.2625
0.70	p_{ave}/σ_o	1.46233	1.45932	1.45886	1.55415
	b_{opt}	--	1.2735	1.3772	4.3879
	S_{opt}	--	--	--	.2407
0.60	p_{ave}/σ_o	1.55124	1.54791	1.54735	1.63235
	b_{opt}	--	1.1257	1.2255	3.4492
	S_{opt}	--	--	--	.1971
0.50	p_{ave}/σ_o	1.67662	1.67291	1.67222	1.74637
	b_{opt}	--	.9683	1.0628	2.6648
	S_{opt}	--	--	--	.1571
0.40	p_{ave}/σ_o	1.86596	1.86179	1.86094	1.92344
	b_{opt}	--	.8005	.8872	1.8468
	S_{opt}	--		--	.1071

TABLE 3 (cont.)

D	TERM	SINGLE-ZONE BULGE			TWO-ZONE NUMERIC
		EQN. (92)	EQN.(90)App.	EQN. (90)	
0.30	p_{ave}/σ_o	2.18339	2.17867	2.17759	2.22635
	b_{opt}	--	.6211	.6966	1.1536
	S_{opt}	--	--	--	.0696
0.20	p_{ave}/σ_o	2.82133	2.81595	2.81457	2.84725
	b_{opt}	--	.4289	.4881	.6664
	S_{opt}	--	--	--	.0422
0.10	p_{ave}/σ_o	4.74201	4.73584	4.73404	4.75024
	b_{opt}	--	.2224	.2577	.2994
	S_{opt}	--	--	--	.0198
0.09	p_{ave}/σ_o	5.16928	5.16303	5.16117	5.17573
	b_{opt}	--	.2009	.2332	.2668
	S_{opt}	--	--	--	.0177
0.08	p_{ave}/σ_o	5.70346	5.69712	5.69521	5.70814
	b_{opt}	--	.1792	.2085	.2350
	S_{opt}	--	--	--	.0157
0.07	p_{ave}/σ_o	6.39038	6.38395	6.38198	6.39328
	b_{opt}	--	.1574	.1835	.2037
	S_{opt}	--	--	--	.0136

TABLE 3 (cont.)

D	TERM	SINGLE-ZONE BULGE			TWO-ZONE NUMERIC
		EQN. (92)	EQN.(90)App.	EQN. (90)	
0.06	p_{ave}/σ_o	7.30640	7.29988	7.29786	7.30753
	b_{opt}	--	.1354	.1582	.1730
	S_{opt}	--	--	--	.0116
0.05	p_{ave}/σ_o	8.58899	8.58238	8.58030	8.58834
	b_{opt}	--	.1133	.1327	.1429
	S_{opt}	--	--	--	.0096
0.04	p_{ave}/σ_o	10.51308	10.50637	10.50423	10.51066
	b_{opt}	--	.0910	.1068	.1133
	S_{opt}	--	--	--	.0077
0.03	p_{ave}/σ_o	13.72016	13.71336	13.71116	13.71597
	b_{opt}	--	.0685	.0805	.0842
	S_{opt}	--	--	--	.0057
0.02	p_{ave}/σ_o	20.13475	20.12785	20.12558	20.12878
	b_{opt}	--	.0458	.0540	.0557
	S_{opt}	--	--	--	.0038
0.01	p_{ave}/σ_o	39.37933	39.37233	39.37000	39.37160
	b_{opt}	--	.0230	.0272	.0276
	S_{opt}	--	--	--	.0019

TABLE 6

POLYNOMIAL CURVE FIT FOR b_{opt}

$$b_{opt} = C_o + C_1 D + C_2 D^2 + C_3 D^3 + C_4 D^4 + \ldots + C_9 D^9$$

STRIP m	C_0	C_1	C_2	C_3	C_4	C_5	C_6	C_7	C_8
1.00	-.00210	2.01555	-1.16219	59 .36152	-242 .73143	450 .51978	-445 .25242	226 .38725	-46 .43054
0.95	-.00153	1.83296	- .02807	38 .86645	-139 .06257	204 .34619	-135 .09058	25 .06154	6 .69242
0.90	-.00104	1.66084	1.01815	21 .63847	- 57 .07887	18 .53316	90 .75261	-117 .63310	43 .62315
0.85	-.00058	1.50995	1.58857	11 .47865	- 14 .72876	-59 .94720	163 .28448	-148 .84586	48 .00797
0.80	-.00029	1.36961	2.10281	3.01491	18 .17412	-117 .11420	212 .83808	-168 .70406	50 .51481
0.75	.00000	1.24316	2.36982	-2.09051	34 .77289	-136 .52283	216 .22211	-159 .62806	45 .67285
0.70	.00019	1.12869	2.47449	-4.96351	41 .18572	-134 .48344	196 .33911	-137 .95009	38 .15640

DISC m	C_0	C_1	C_2	C_3	C_4	C_5	C_6	C_7	C_8	C_9
1.00	-.00885	3.66992	-26 .95058	409 .36219	-2945 .46268	11982 .02477	-27880 .15887	36794 .98940	-25617 .58349	7301 .84497

TABLE 7

POLYNOMIAL CURVE FIT FOR S_{opt}

$$S_{opt} = C_0 + C_1D + C_2D^2 + C_3D^3 + C_4D^4 + \ldots + C_8D^8$$

STRIP m	C_0	C_1	C_2	C_3	C_4	C_5	C_6	C_7	C_8
1.00	-.00053	.96426	-.20971	21 .16876	-121 .78247	292 .97541	-365 .68671	234 .04533	-60 .89473
0.95	-.00053	.89741	-.18328	17 .48580	-94 .35690	214 .13667	-253 .48919	154 .62099	-38 .51751
0.90	-.00042	.82836	-.00513	12 .85268	-65 .00901	134 .67212	-143 .95558	78 .60221	-17 .38154
0.85	-.00037	.76317	.14908	9 .21533	-43 .51155	80 .06505	-72 .98073	31 .90666	-5 .00852
0.80	-.00028	.70013	.31874	5 .93571	-25 .60466	37 .02203	-19 .54181	-1 .86494	3 .62130
0.75	-.00018	.63840	.50934	2 .94903	-10 .80574	3 .92616	19 .06668	-24 .95475	9 .24195
0.70	-.00008	.57937	.66488	.69990	-.57721	-16 .74467	40 .47508	-36 .07098	11 .52365

DISC m	C_0	C_1	C_2	C_3	C_4	C_5	C_6	C_7	C_8
1.00	.00181	.03530	3.55754	-32 .13452	147 .44912	-361 .97710	494 .90315	-356 .94380	105 .78011

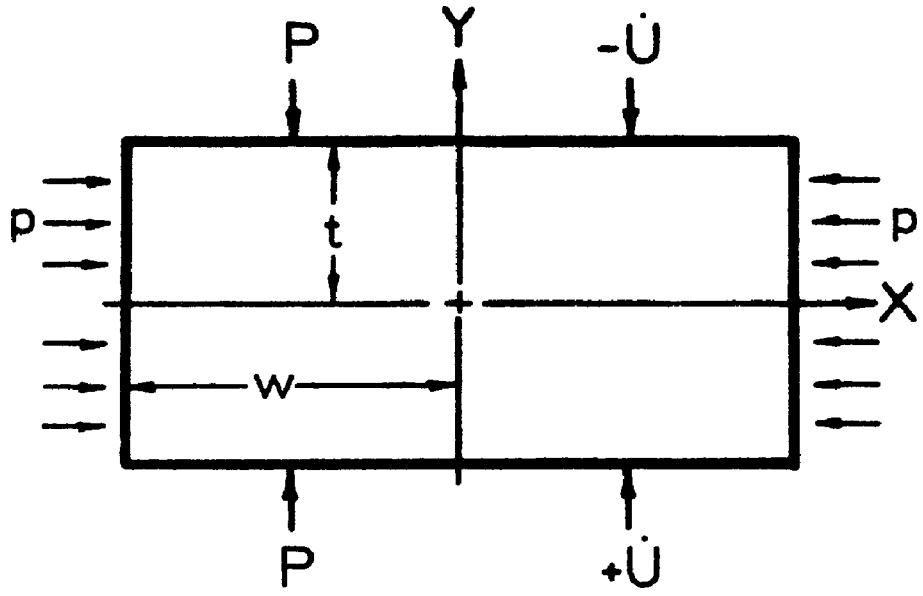

FIG.1 STRIP FORGING

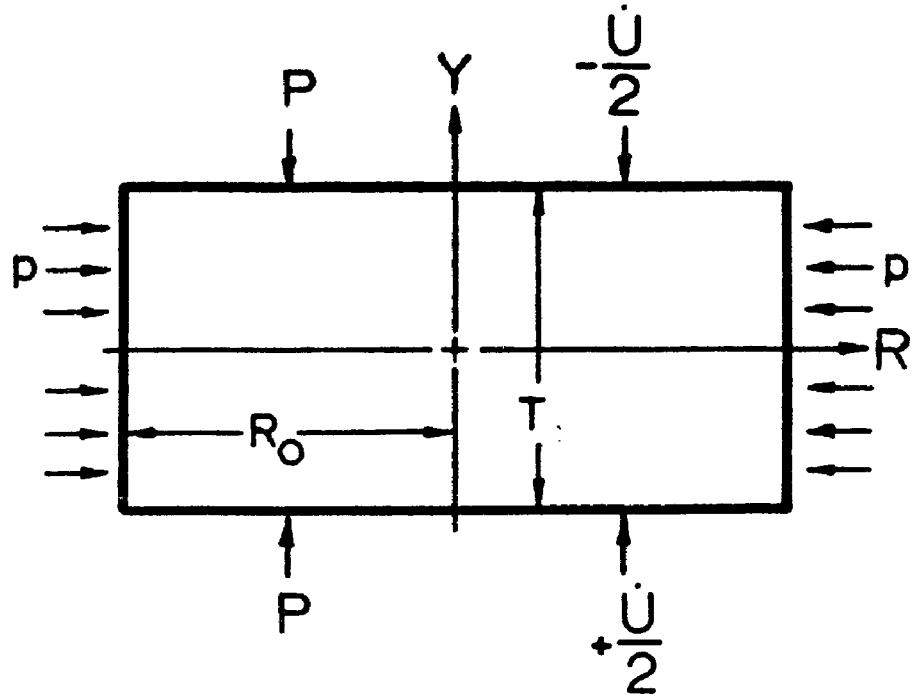

FIG. 2 DISC FORGING

PARALLEL VELOCITY FIELD

$$\dot{U}_x = \frac{x}{t}\dot{U}$$

$$\dot{U}_y = \frac{-y}{t}\dot{U}$$

$$\dot{U}_z = 0$$

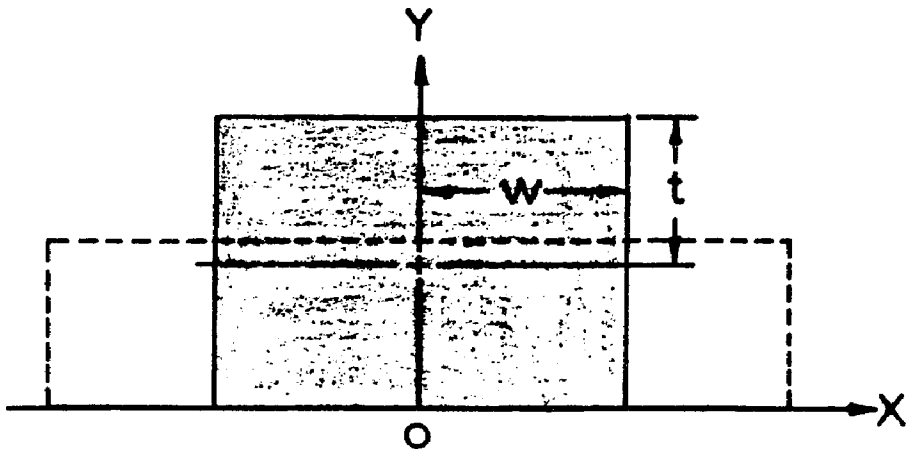

FIG. 3. THE PARALLEL VELOCITY FIELD

BULGE VELOCITY FIELD

$$\dot{U}_x = \frac{b}{1-e^{-b}} \dot{U} \frac{x}{t} e^{-by/t}$$

$$\dot{U}_y = \frac{-b}{1-e^{-b}} \dot{U} \left[1 - e^{-by/t}\right]$$

$$\dot{U}_z = 0$$

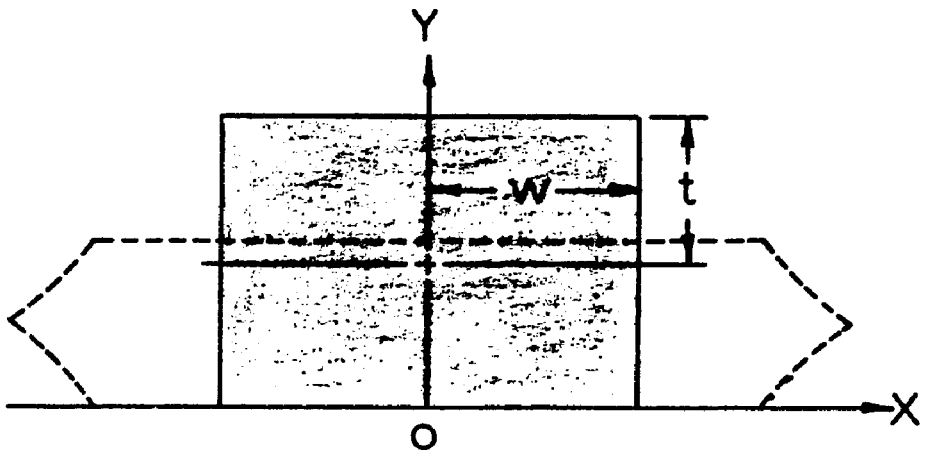

—— initial geometry

------- final geometry

FIG. 4 THE BULGE VELOCITY FIELD

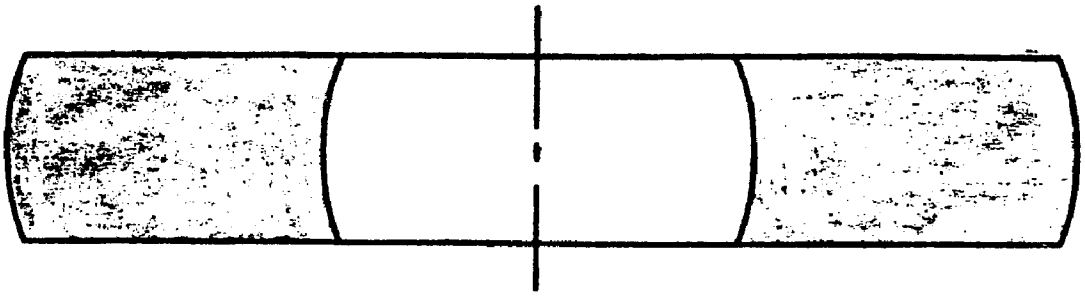

GOOD LUBRICATION

a.

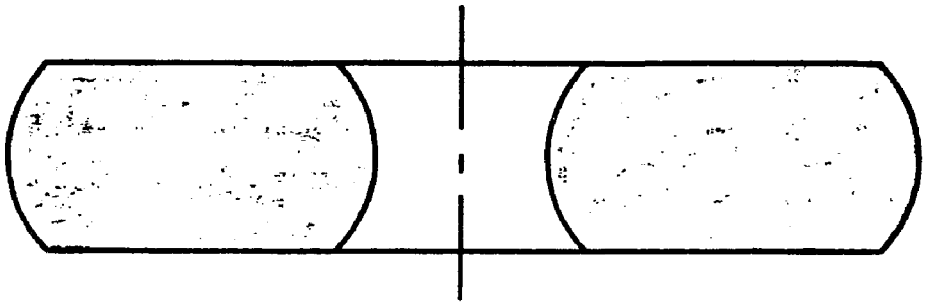

POOR LUBRICATION

b.

FIG. 5 RING PROFILES

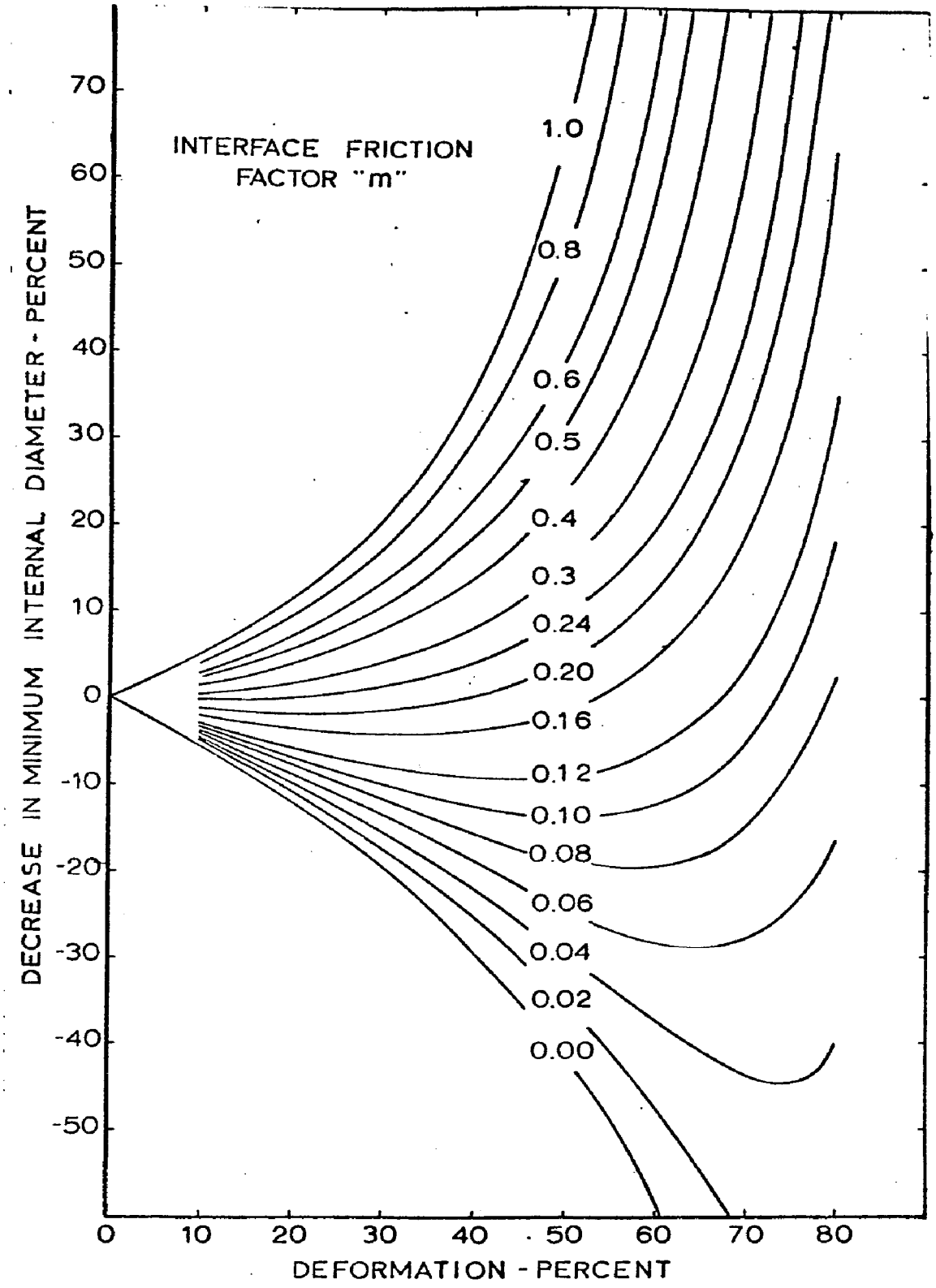

FIG. 6 CALIBRATION CURVES
(WITH BULGE)

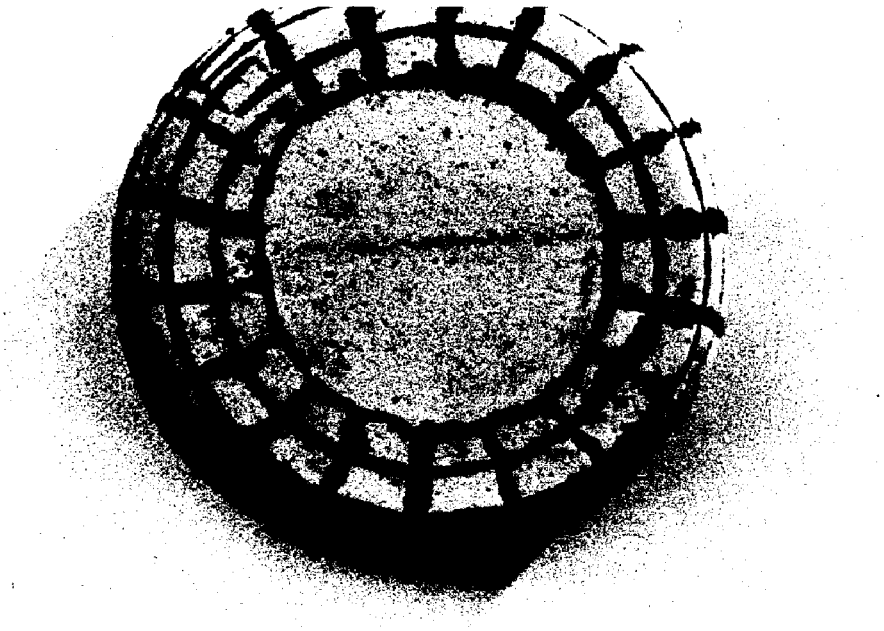

FIG. 7 PLASTICINE DISC SHOWING FOLD From Ref. [30]

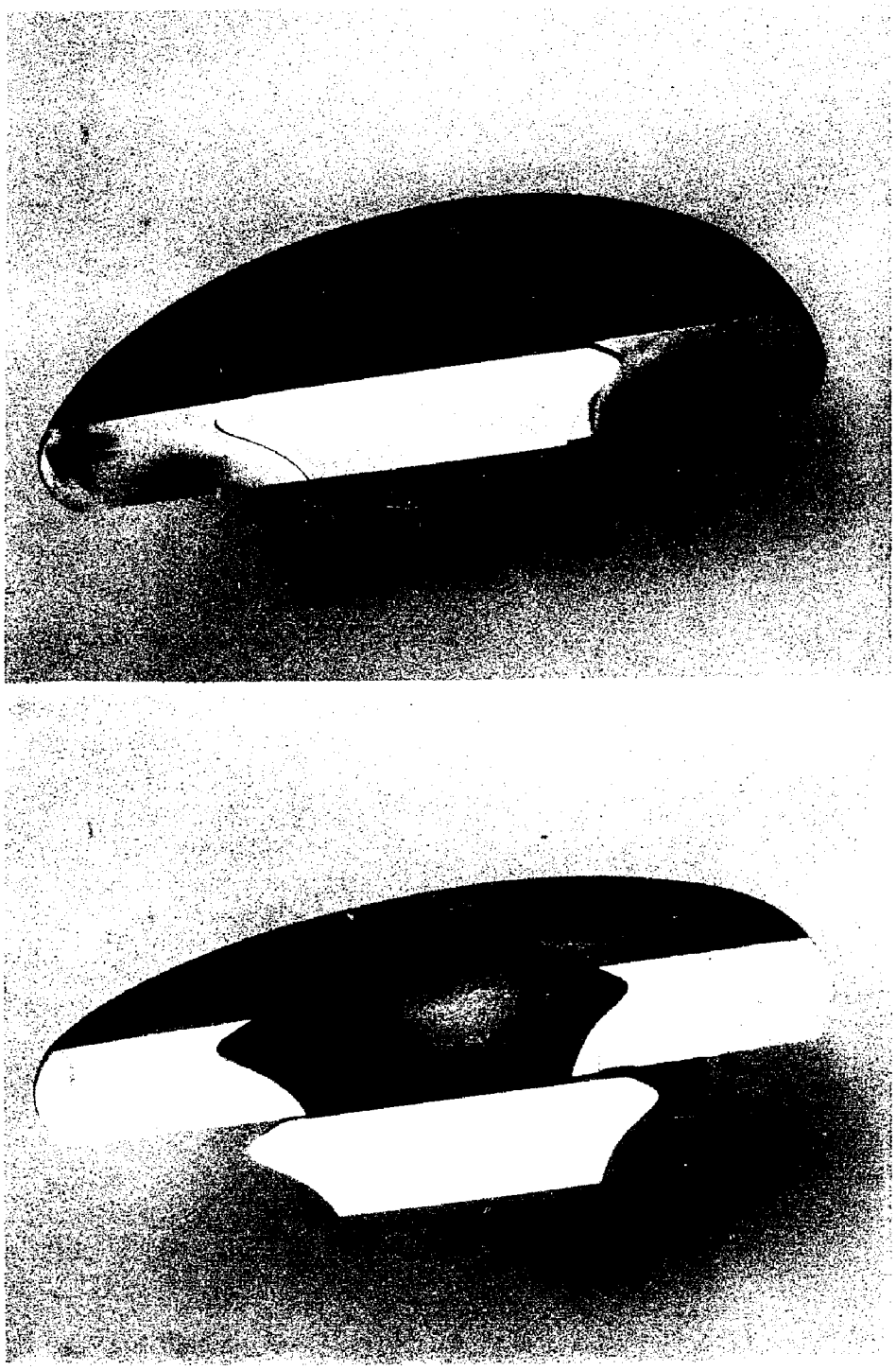

FIG. 8 BI-METAL DISC

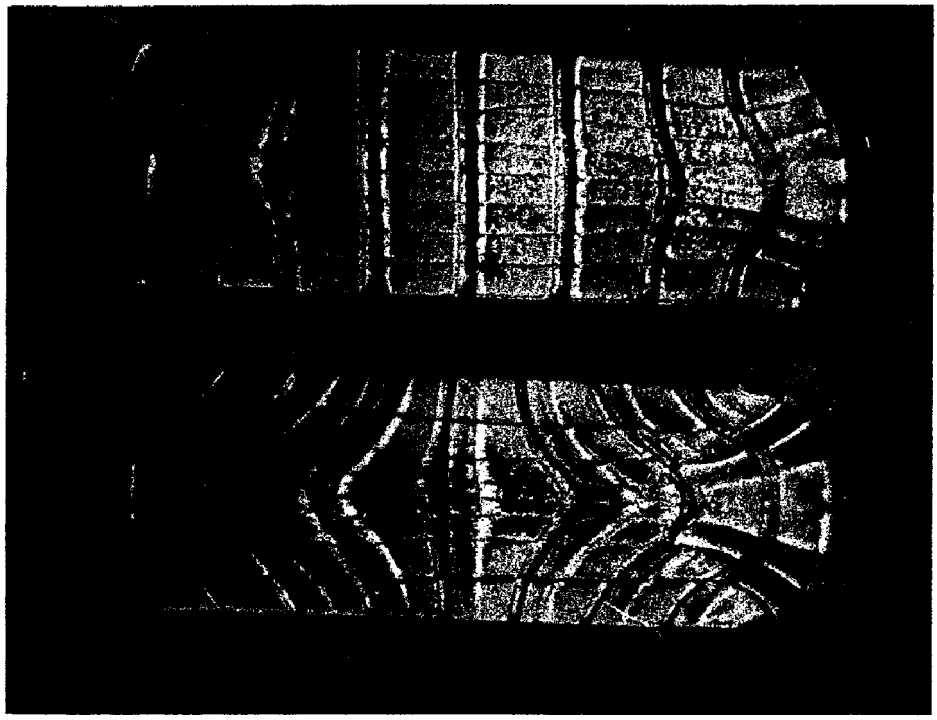

OFHC Copper Cylinders Compressed 50%
Top: Good Lubrication
Bottom: Poor Lubrication
(Courtesy of V. DePierre)

FIG. 9 DISC FORGING

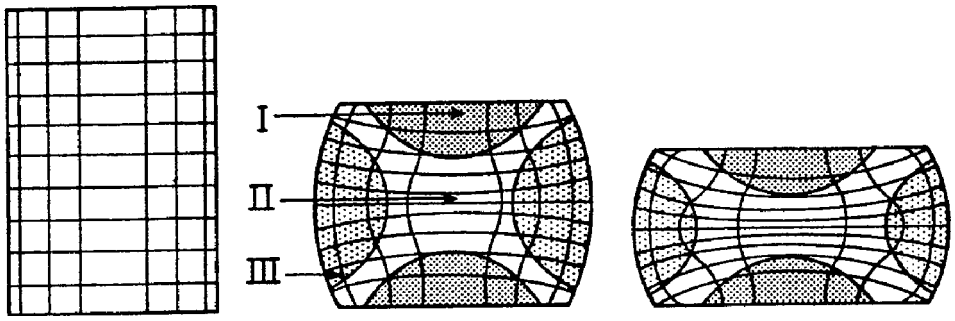

FIG.10 PROGRESSIVE FORGING OF A DISC WITH FRICTION

Fig. 8 Distortion of an originally square grid on a diametral plane of an aluminum disk which was split, gridded, put together, and compressed 20 per cent with no lubrication; $R_0/h_0 = 2$, $R_0 = 1.00$ in. Note the regions near the periphery in which metal tended not to deform, resulting in separation across the plane of the split. Magnification 1.5×.

FIG.11 ALUMINUM SPLIT DISC From Ref. [66]

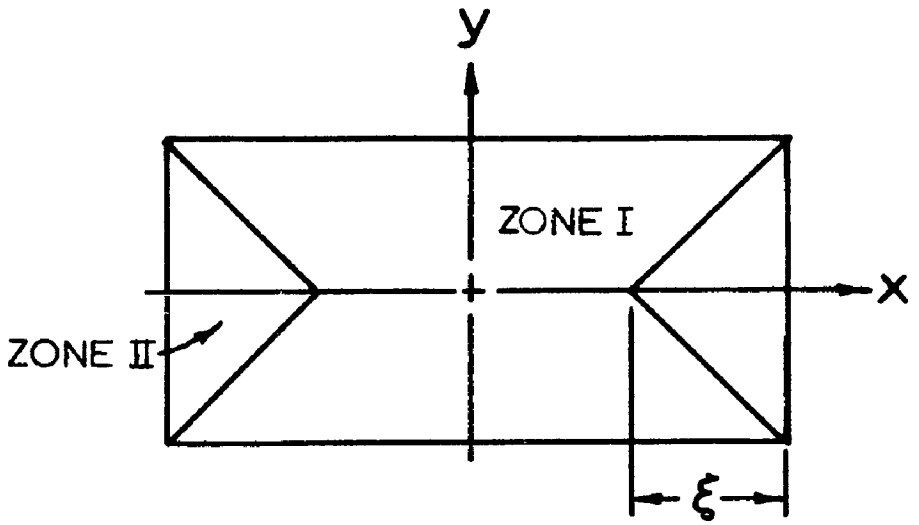

FIG. 12a STRIP

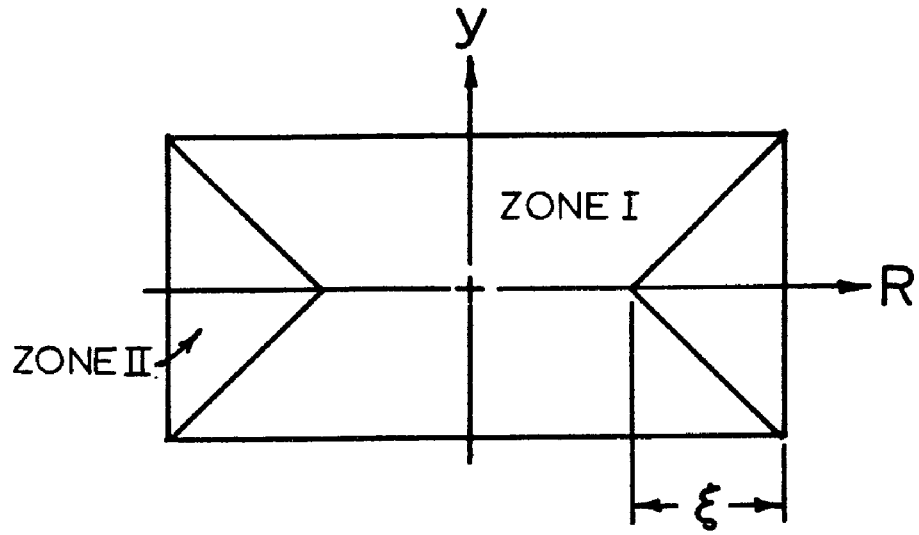

FIG. 12b DISC

FIG. 12 TWO-ZONE REGIONS

2-PARAMETER
VELOCITY FIELD

zone 1	zone 2
SAME AS BULGE	$\dot{U}_x = \dot{U}_x(x,y)$
	$\dot{U}_y = 0$
	$\dot{U}_z = 0$

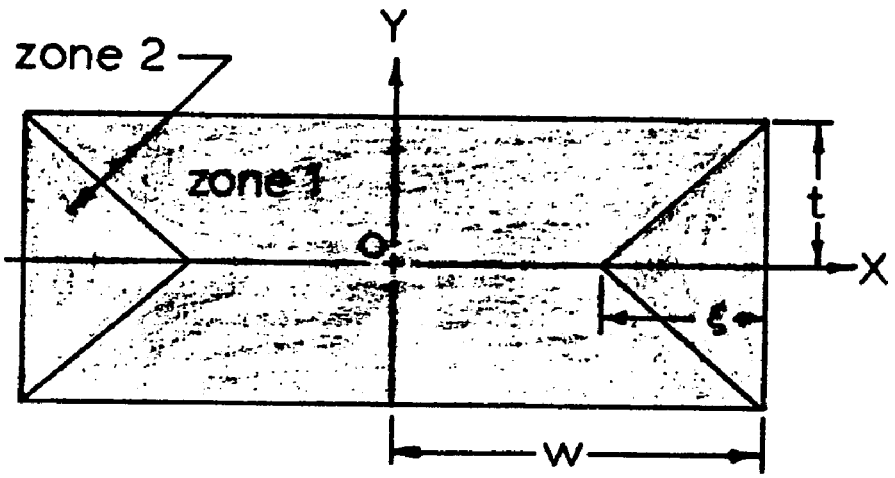

$$D = \frac{t}{w}$$

$$S = \frac{\xi}{w}$$

FIG.13 2-ZONE
2-PARAMETER
VELOCITY FIELD

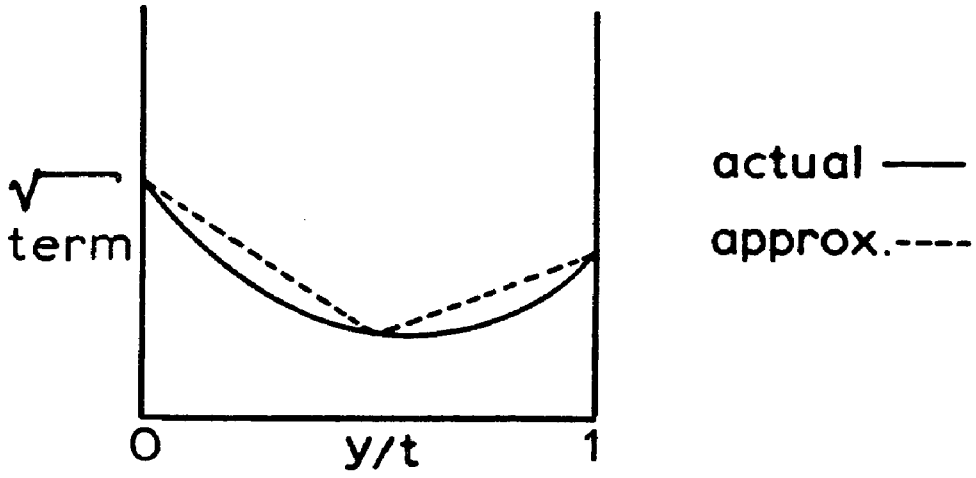

FIG. 14a

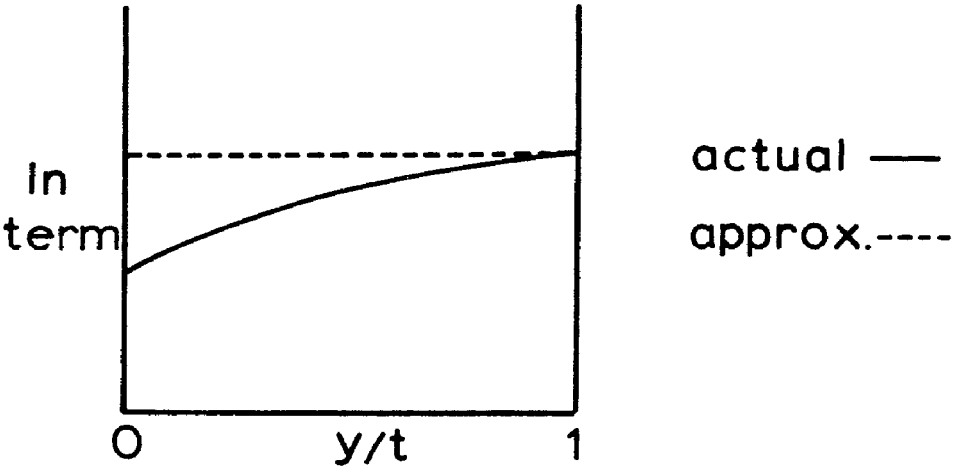

FIG. 14b

FIG. 14 UPPER-BOUND APPROXIMATIONS

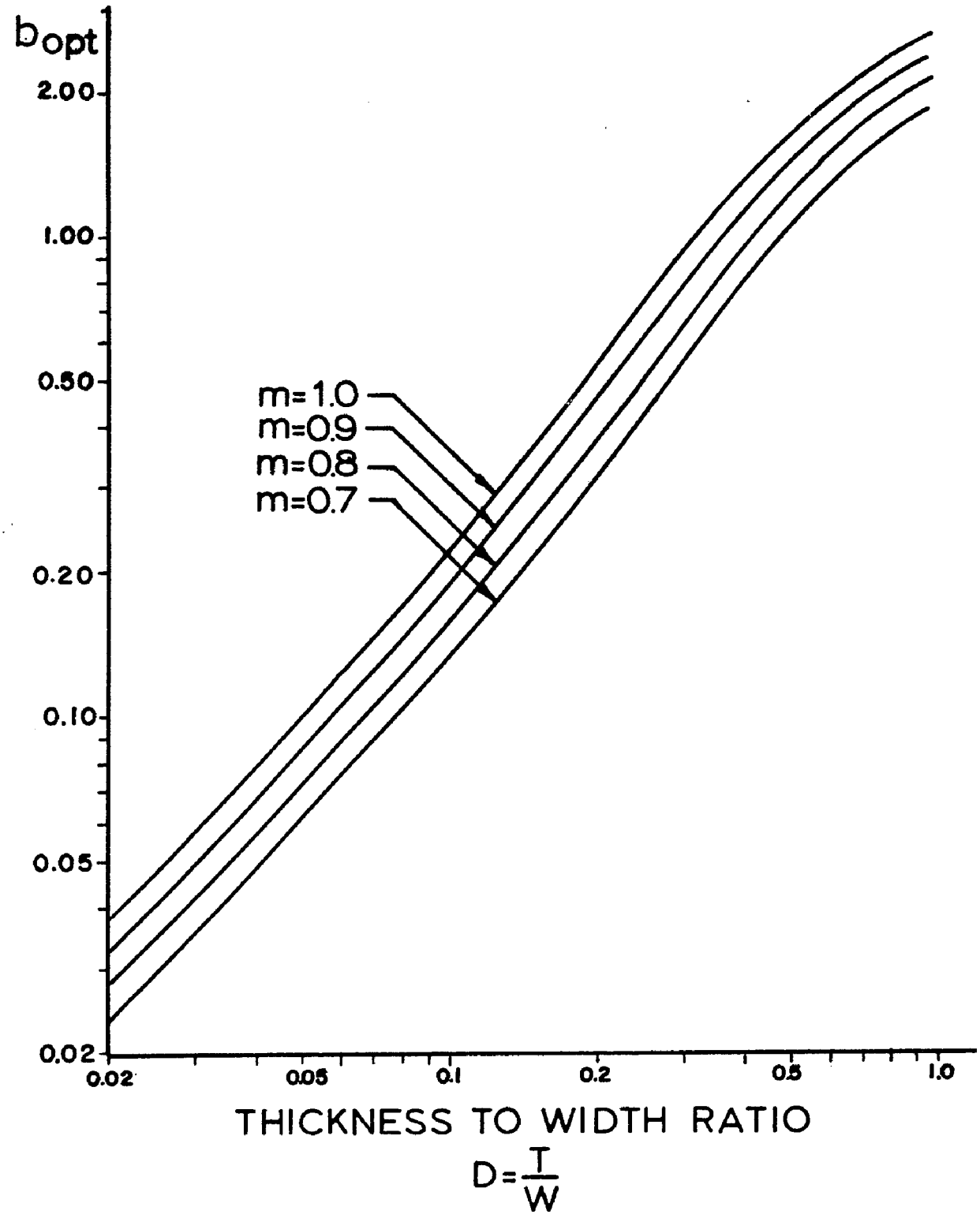

FIG. 15 OPTIMAL VALUE OF THE BULGE PARAMETER

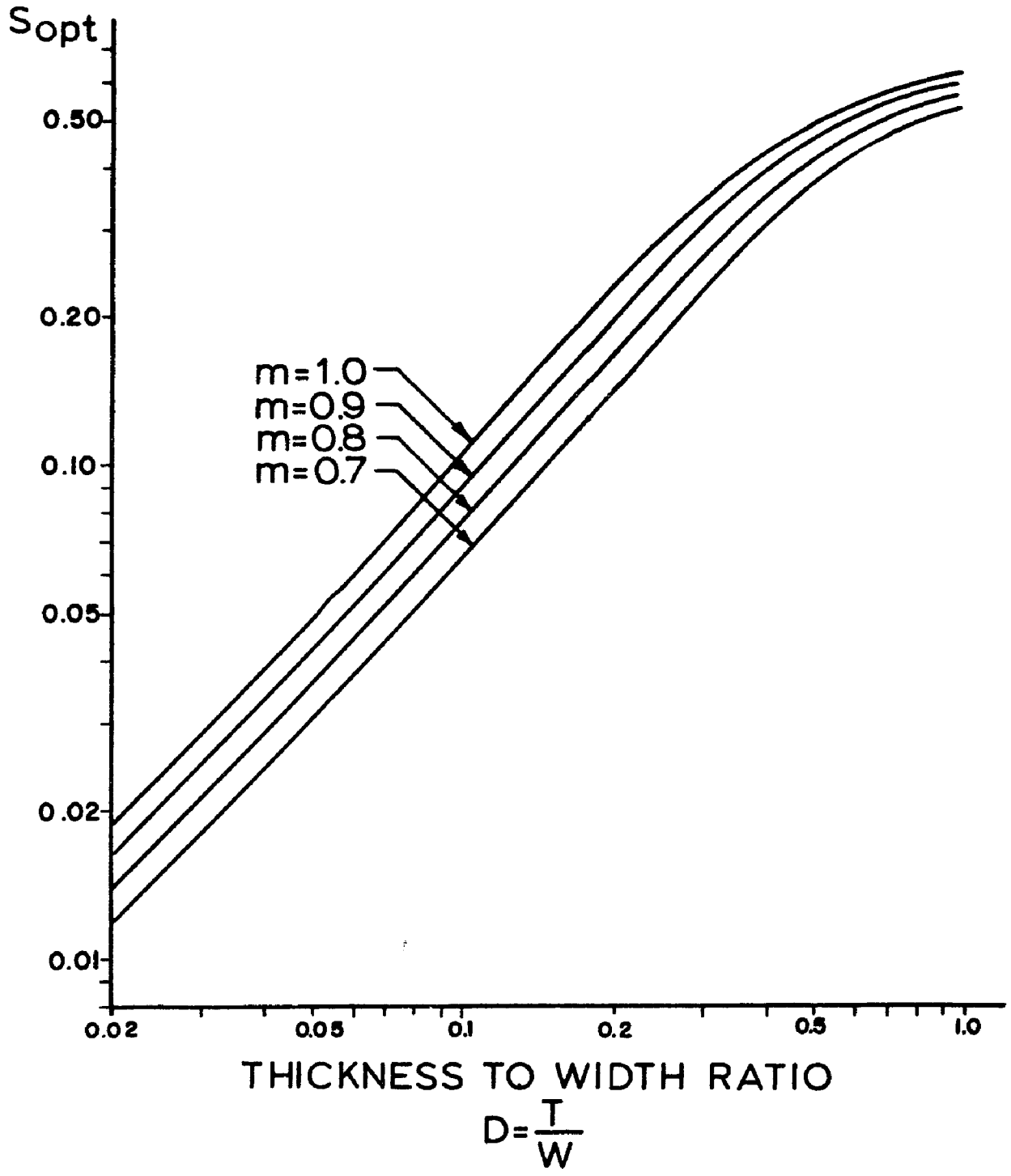

FIG. 16 OPTIMAL VALUE OF THE ZONE SIZE PARAMETER

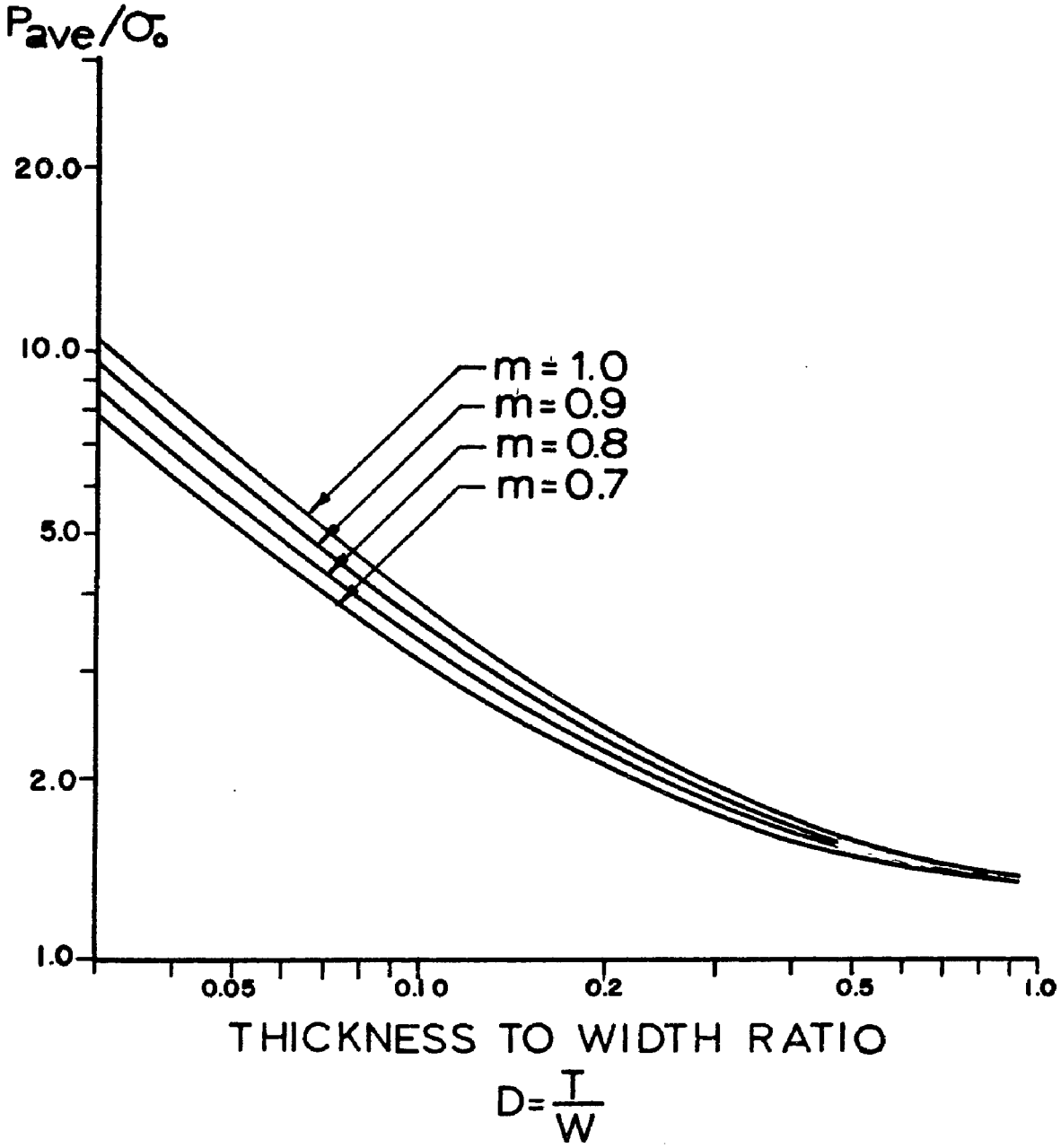

FIG. 17 RELATIVE AVERAGE FORGING PRESSURE

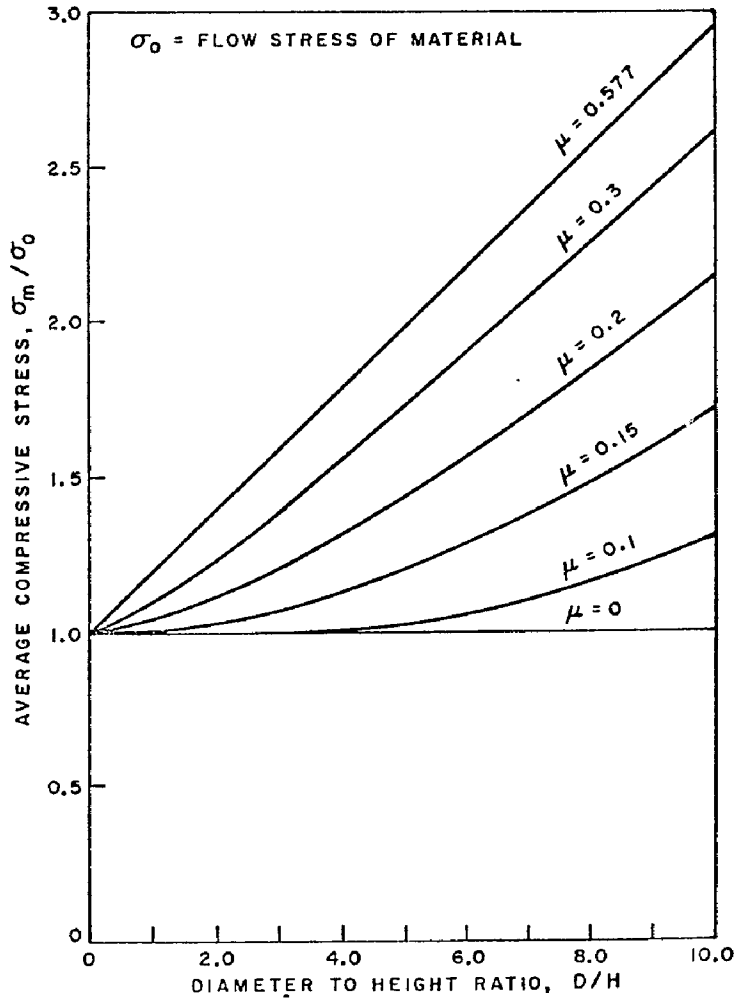

Theoretical Relationship Between Average Compressive Stress and Diameter/Height Ratio in Simple Upsetting (After Thomsen, et al.).

FIG.18 EARLY SOLUTION OF SCHROEDER AND WEBSTER [32] - From Ref. [12]

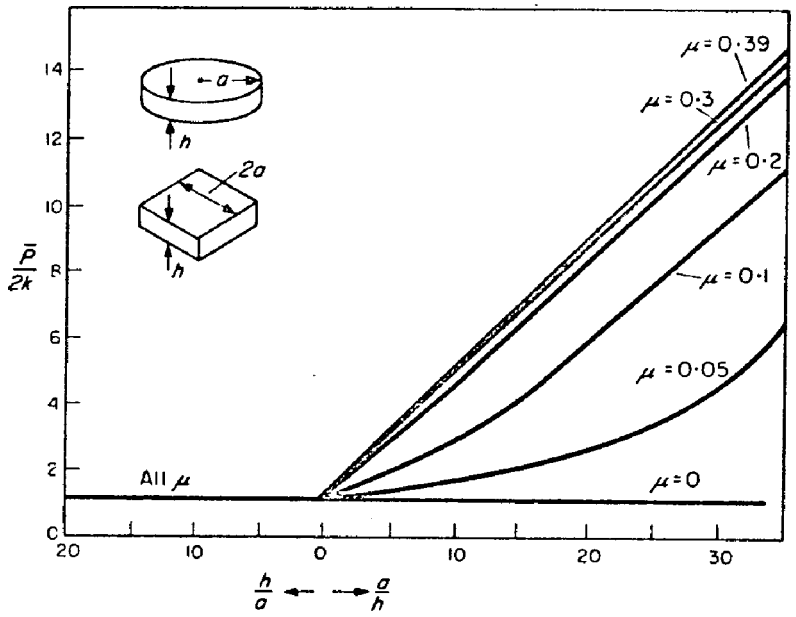

Variation of mean pressure with a/h ratio for cylindrical and square billets (Bishop, J. Mechanics and Physics Solids)

FIG.19 EARLY SOLUTION BY BISHOP [21]
From Ref.[71]

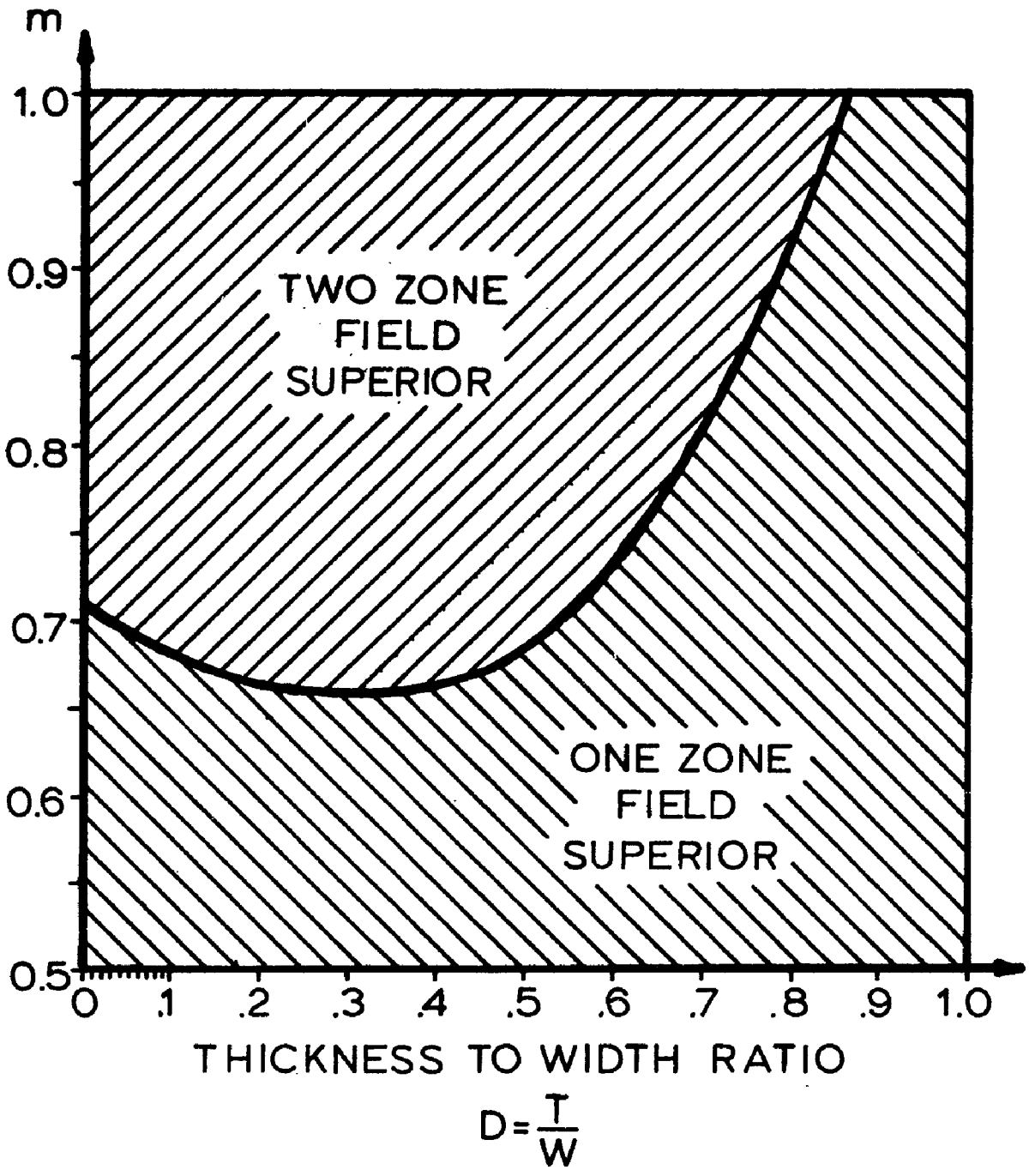

FIG. 20 DOMAIN OF IMPROVEMENT FOR STRIP

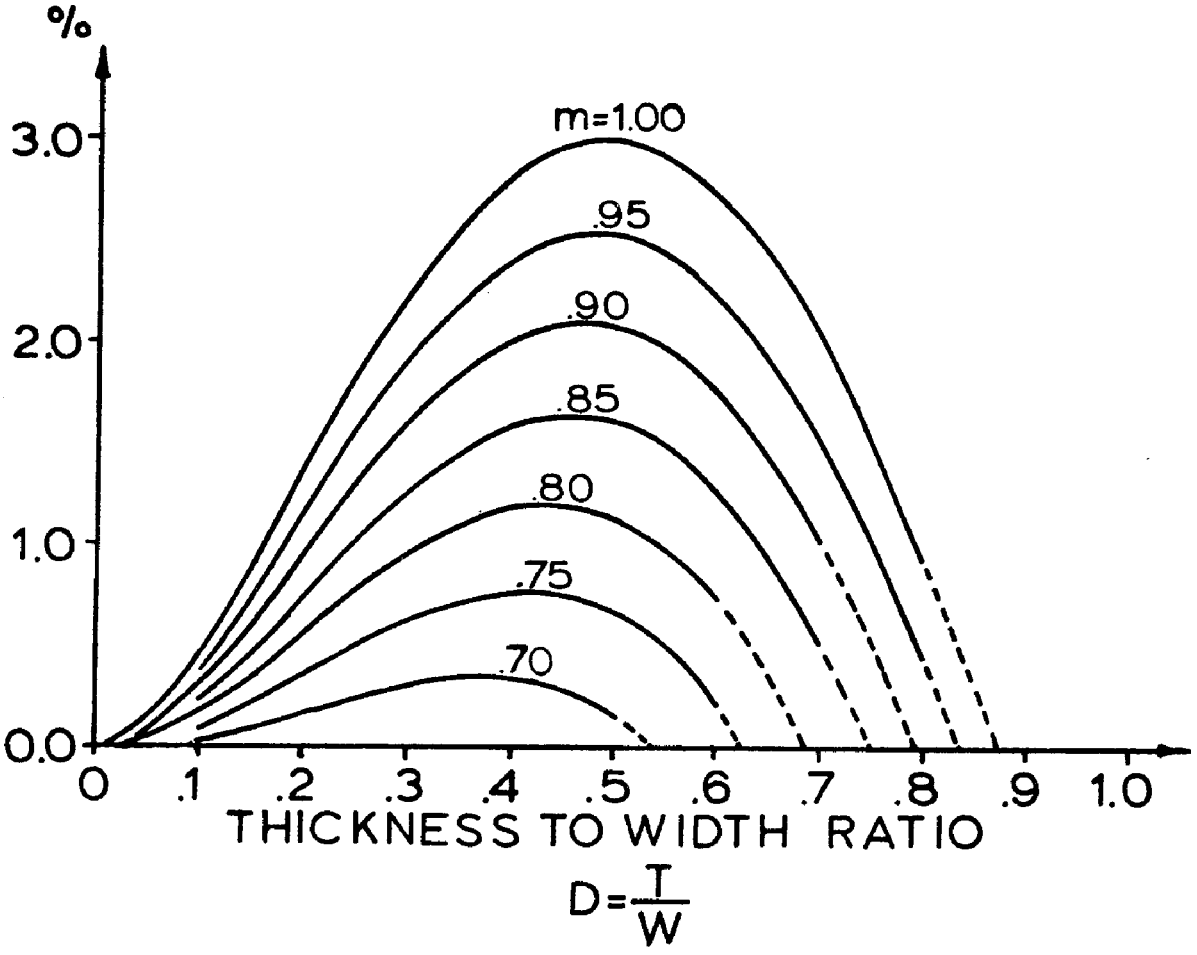

FIG. 21 PERCENT IMPROVEMENT OVER SINGLE-ZONE FIELD

3-PARAMETER
VELOCITY FIELD

zone 1	zone 2
SAME AS BULGE	$\dot{U}_x = \dot{U}_x(x,y)$
	$\dot{U}_y = F \cdot \dot{U}_{y(\text{zone 1})}$
	$\dot{U}_z = 0$

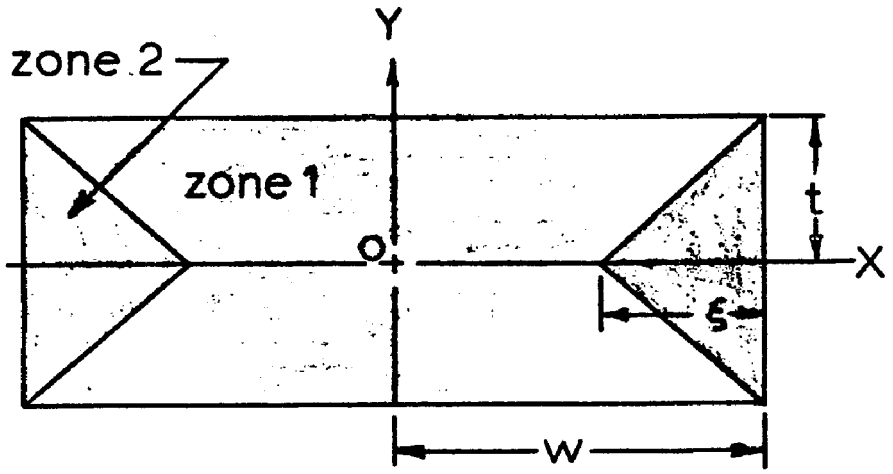

$$D = \frac{t}{w}$$

$$S = \frac{\varepsilon}{w}$$

FIG. 22 2-ZONE
3-PARAMETER
VELOCITY FIELD

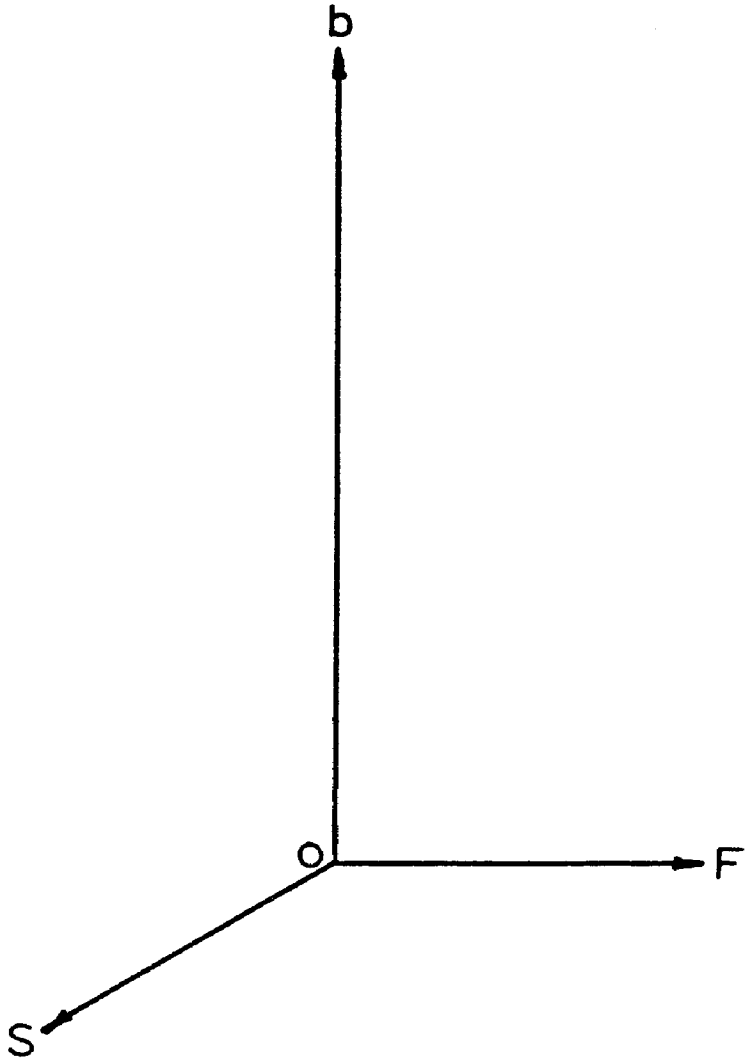

FIG.23 THREE PARAMETER COORDINATE SYSTEM

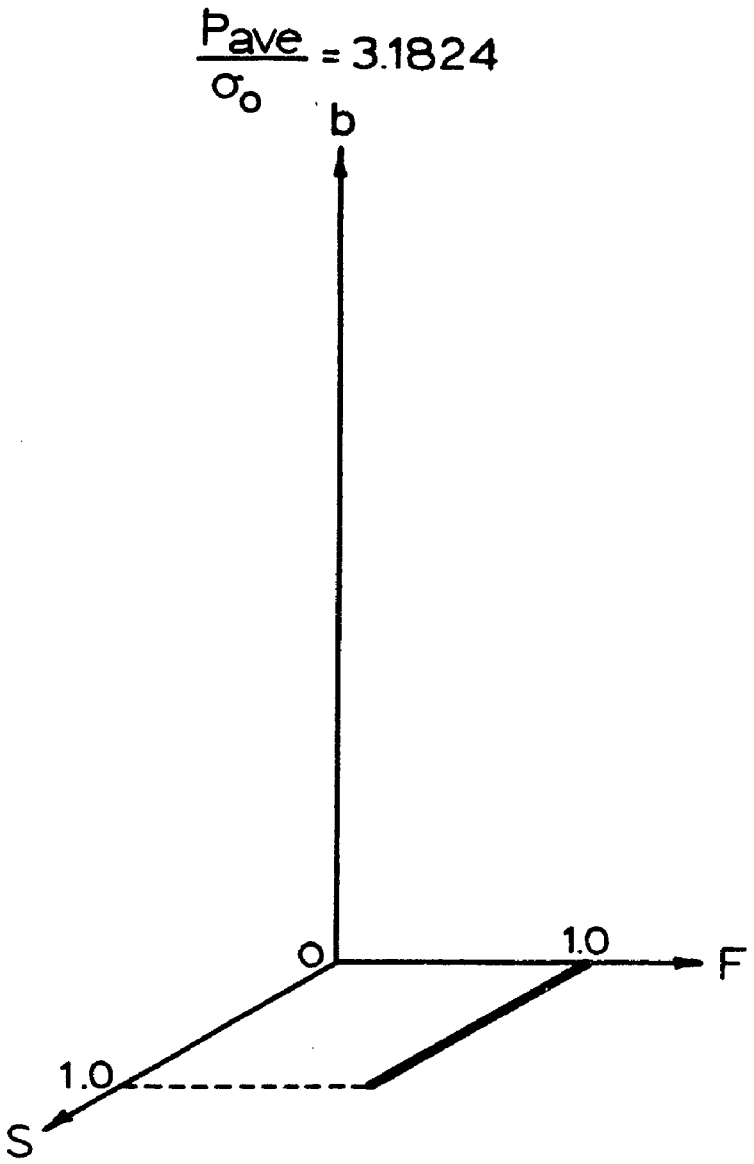

$D = \frac{t}{w} = 0.2$

$m = 1.0$

FIG. 24 PARALLEL FIELD

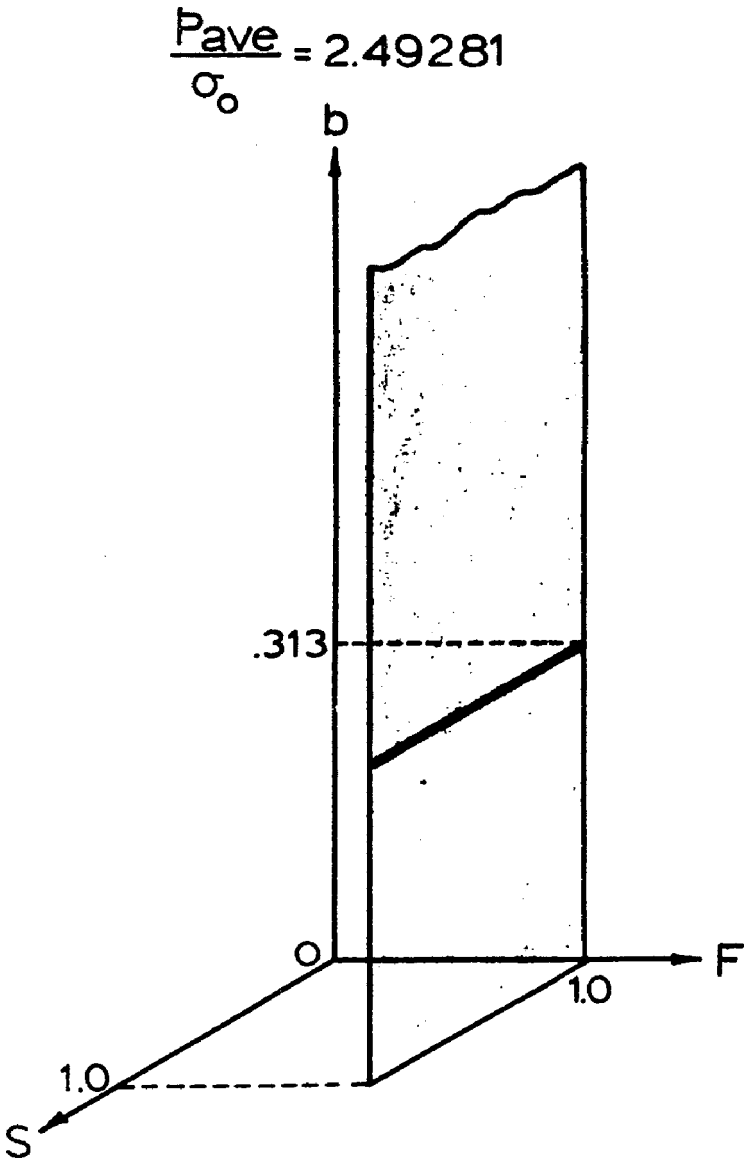

$$D = \frac{t}{w} = 0.2$$

$$m = 1.0$$

FIG. 25 BULGE FIELD

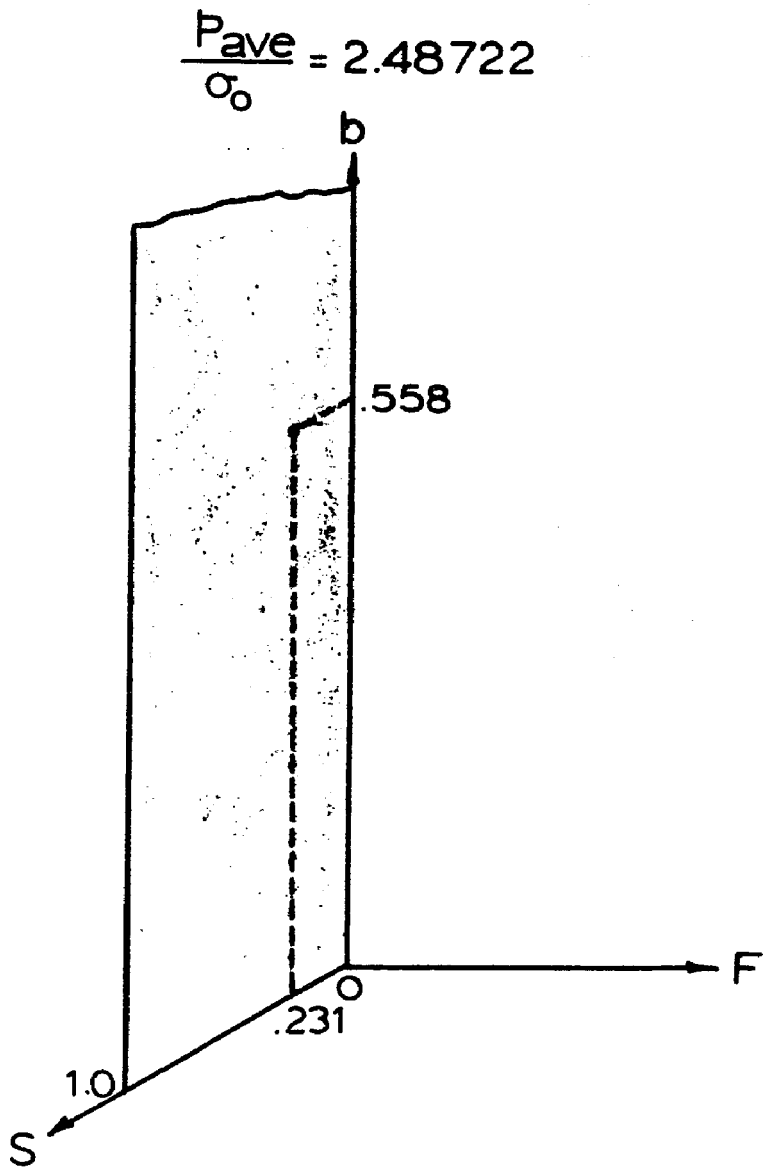

$D = \frac{t}{w} = 0.2$

$m = 1.0$

FIG. 26 2-PARAMETER FIELD

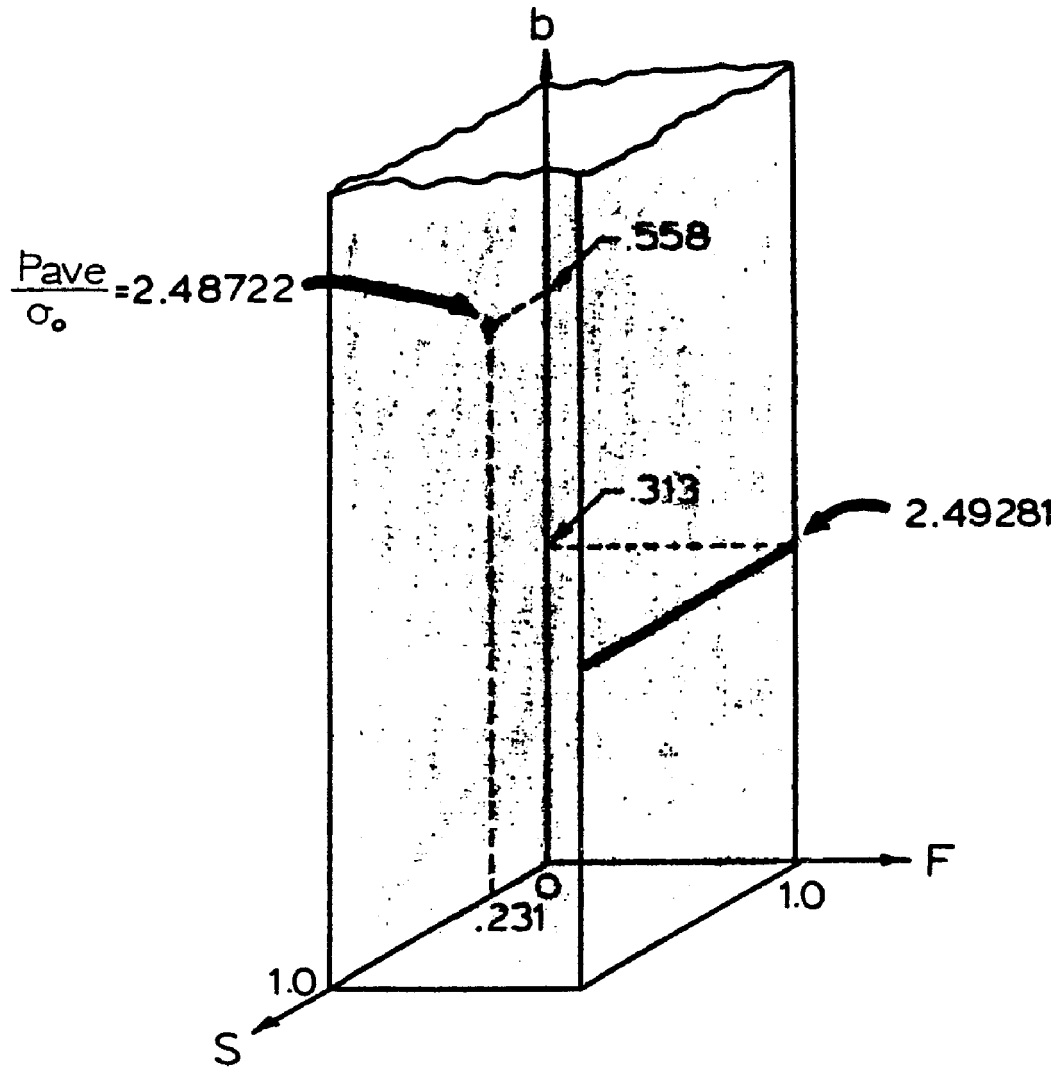

$D = \frac{t}{w} = 0.2$

$m = 1.0$

FIG. 27 3-PARAMETER FIELD

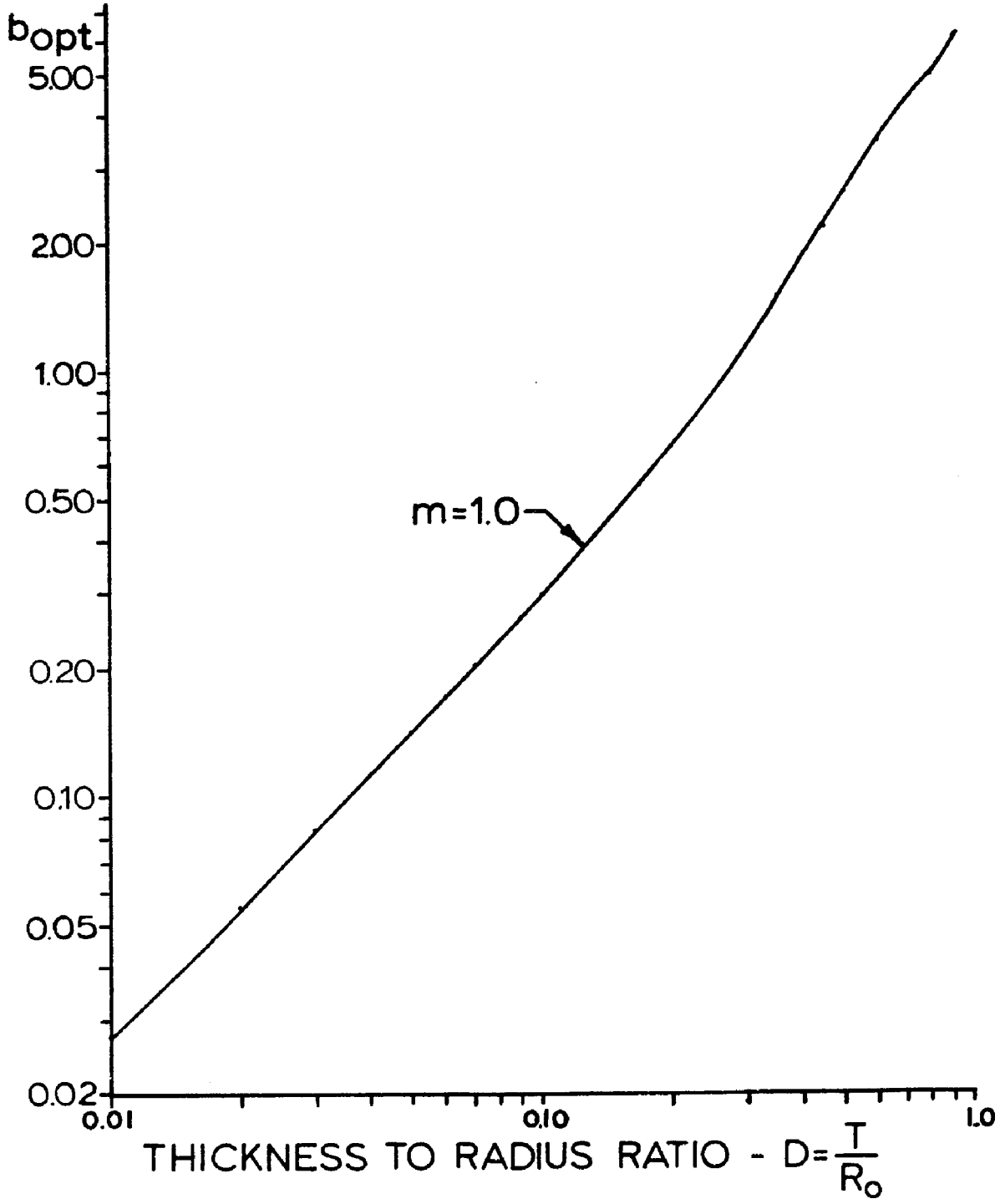

FIG. 28 OPTIMAL VALUE OF THE BULGE PARAMETER

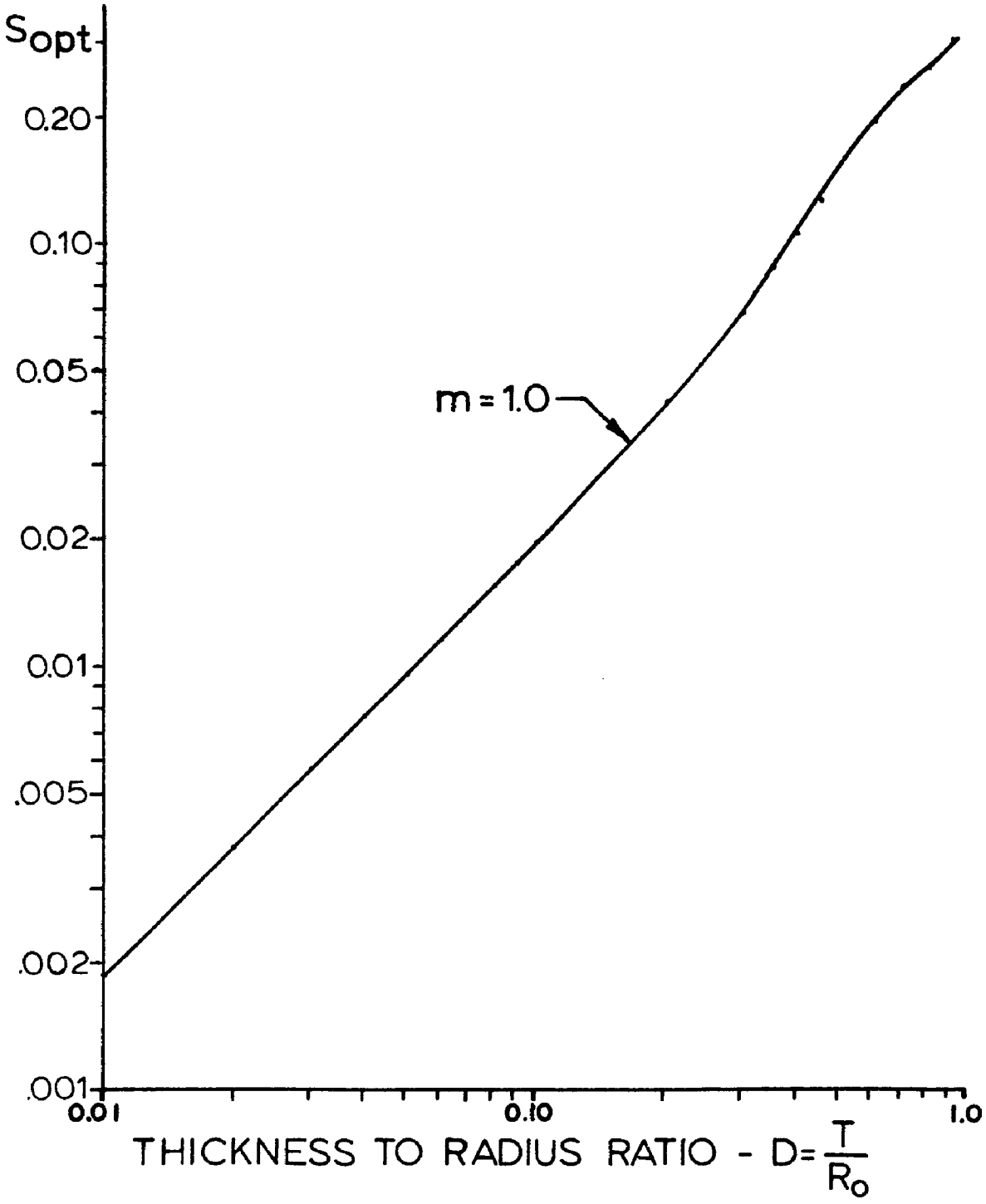

FIG. 29 OPTIMAL VALUE OF THE ZONE SIZE PARAMETER

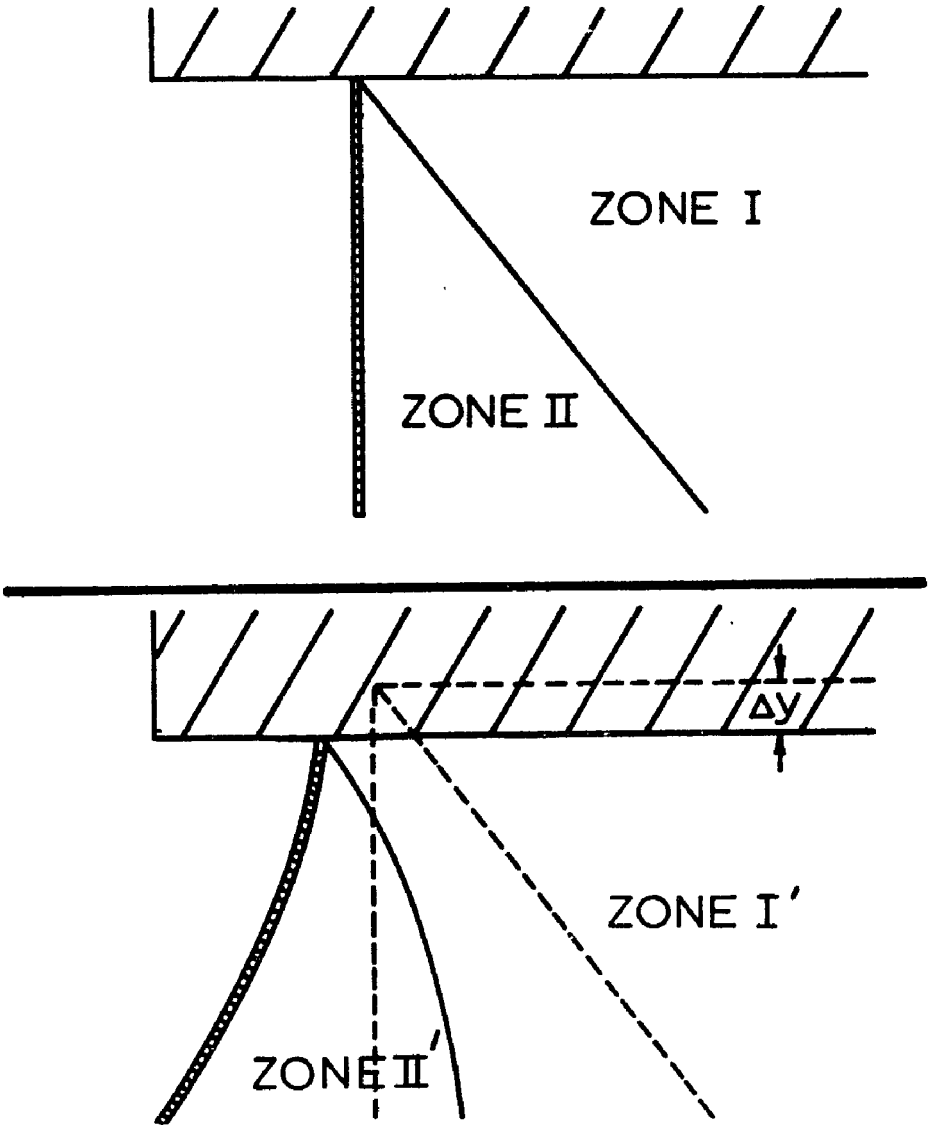

FIG. 30a SEQUENCE OF DEFORMATION

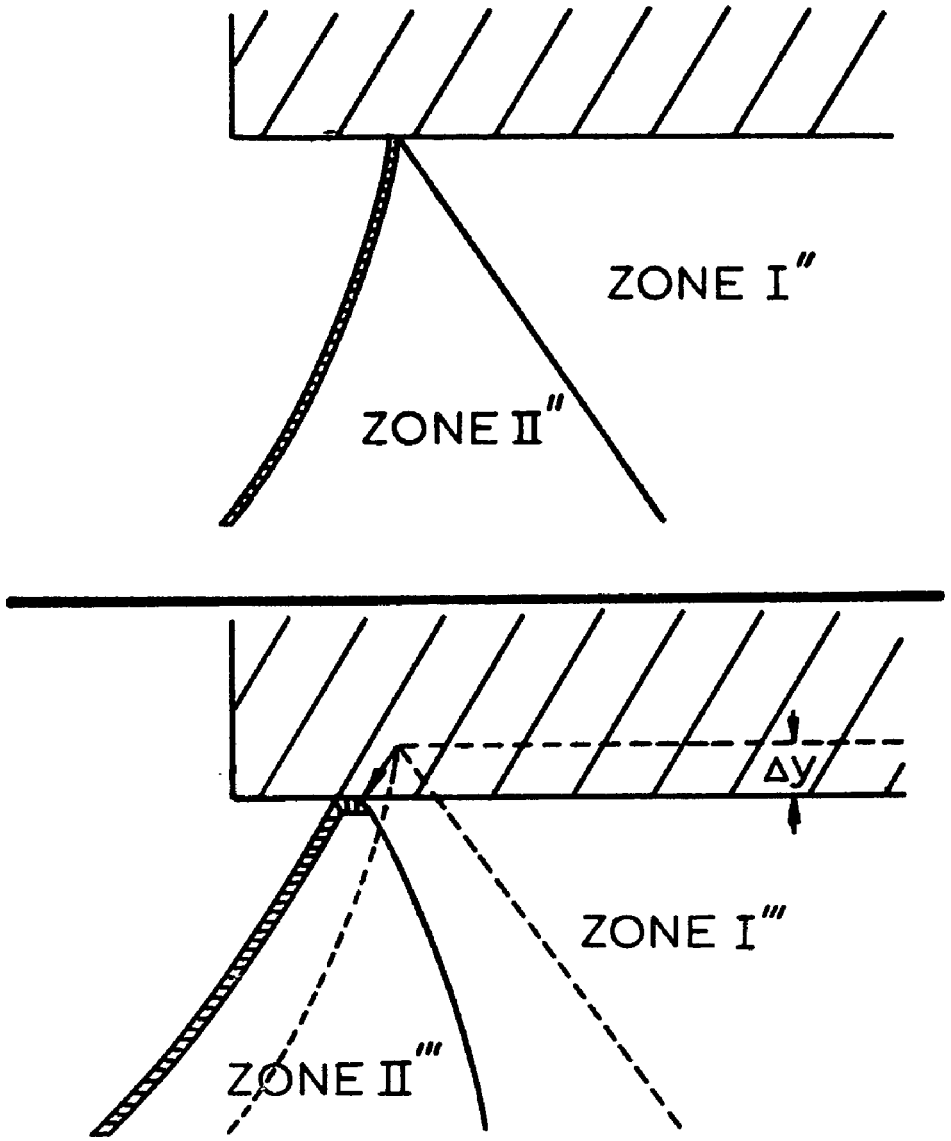

FIG. 30b SEQUENCE OF DEFORMATION

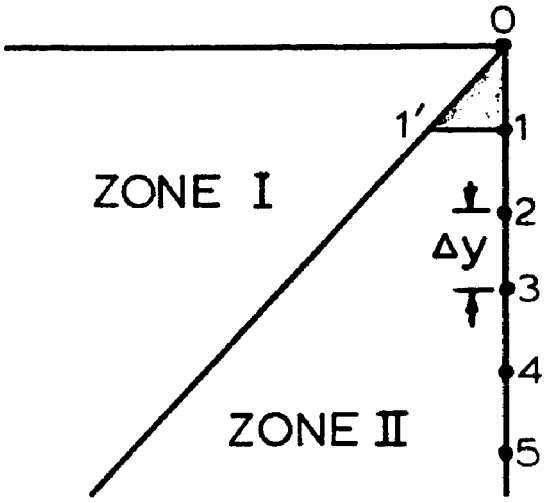

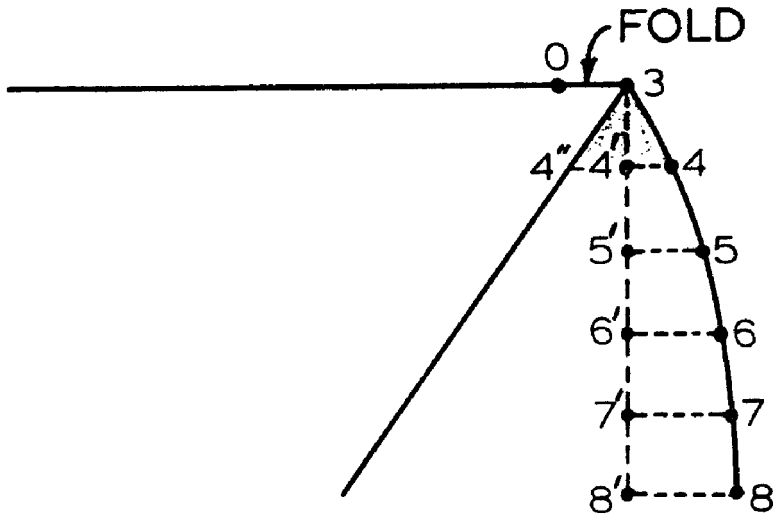

FIG. 31 DEFORMATION MODEL

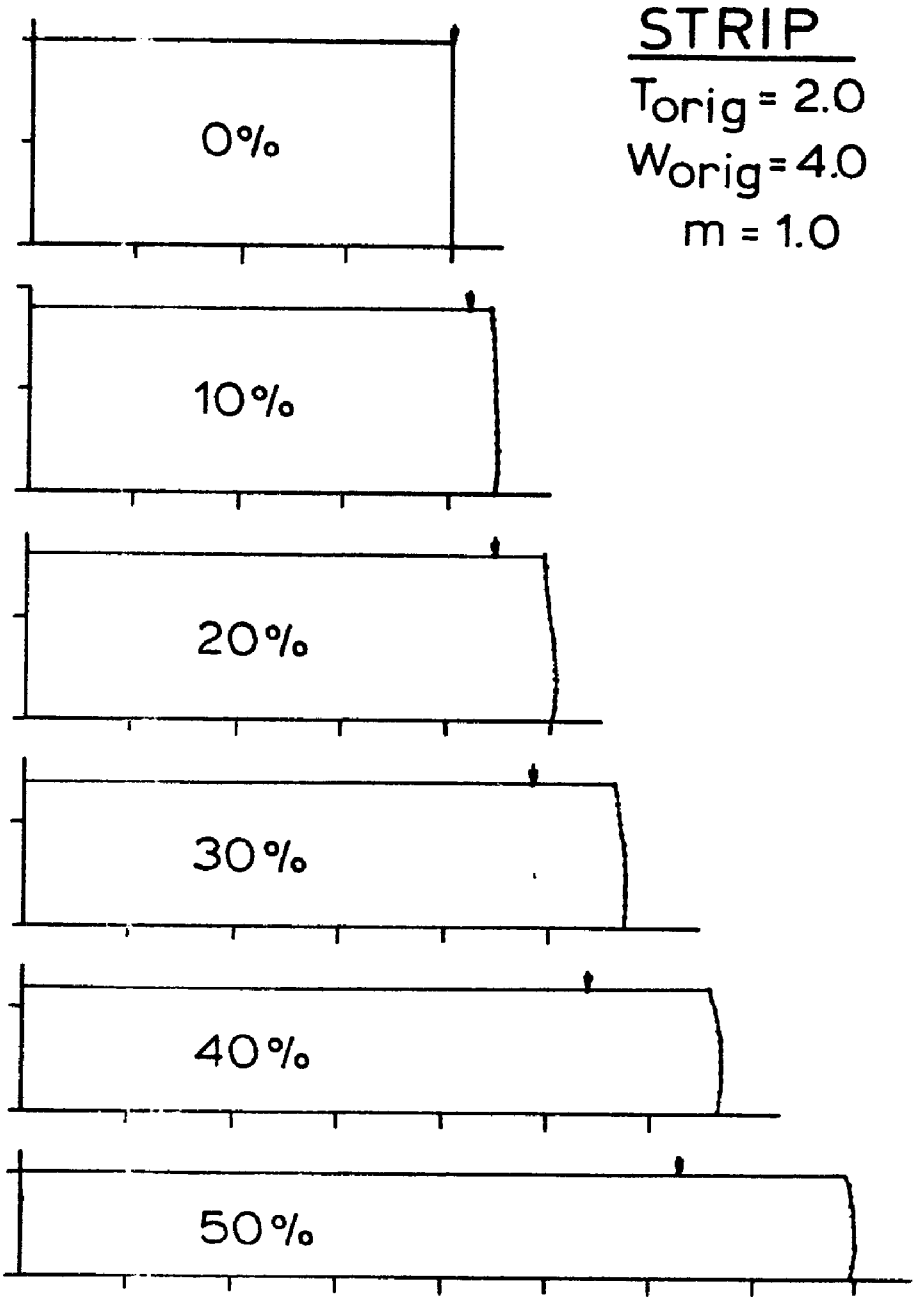

FIG. 32 DEFORMATION SEQUENCE FOR STRIP

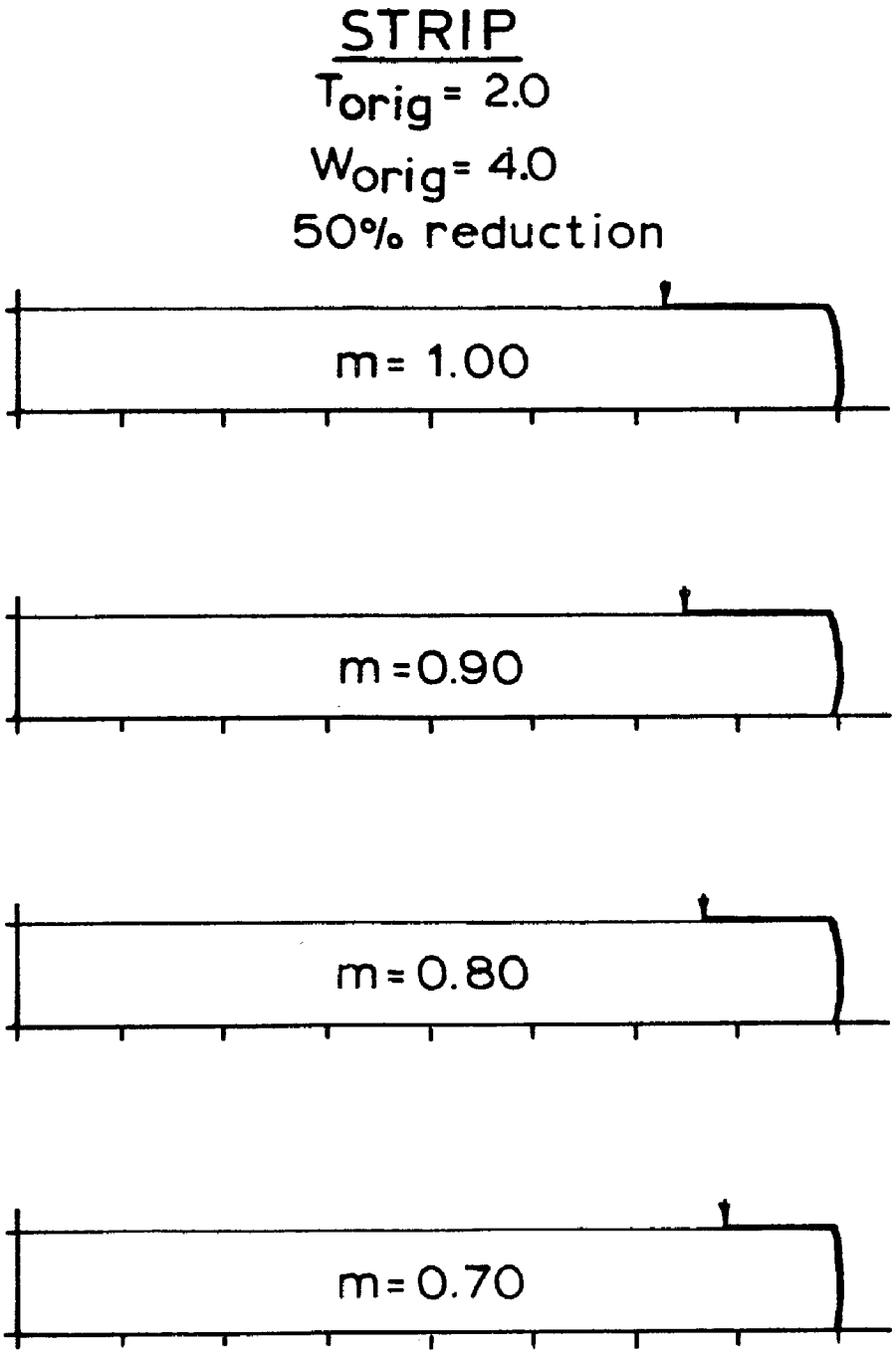

FIG. 33 EFFECT OF THE FRICTION FACTOR

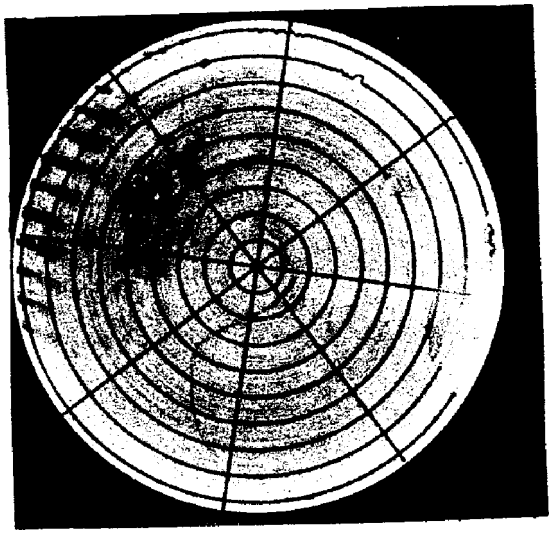

BEFORE DEFORMATION

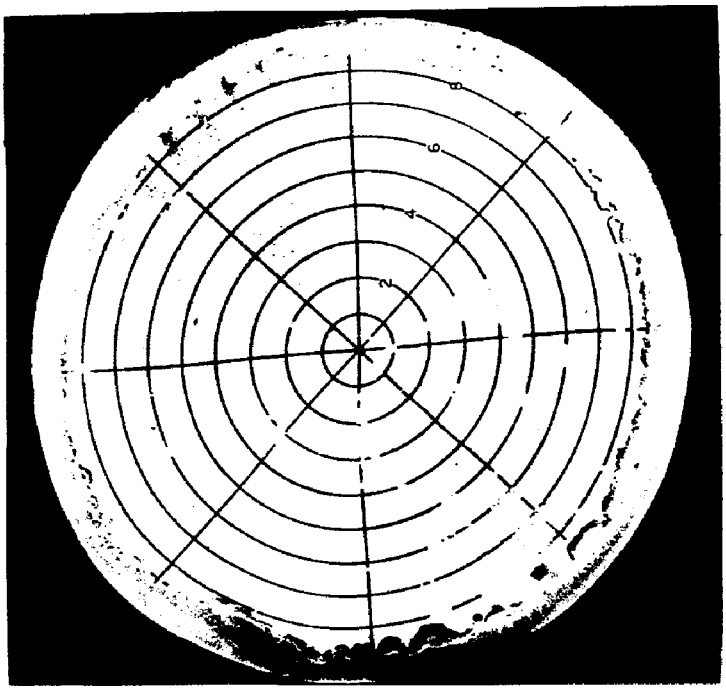

AFTER DEFORMATION

FIG.34 DEFORMATION OF PURE ALUMINUM DISC (LUBRICATED)

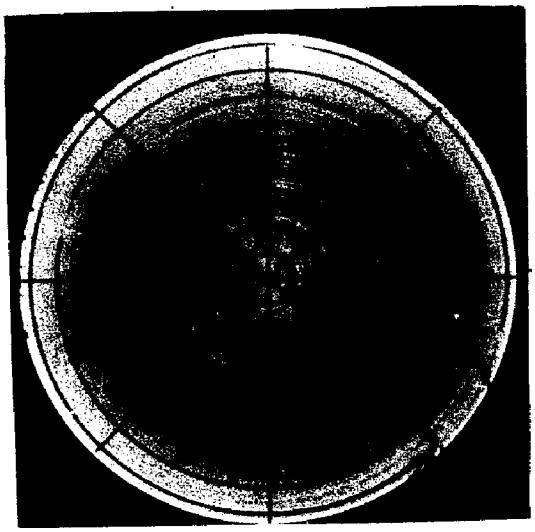

BEFORE DEFORMATION

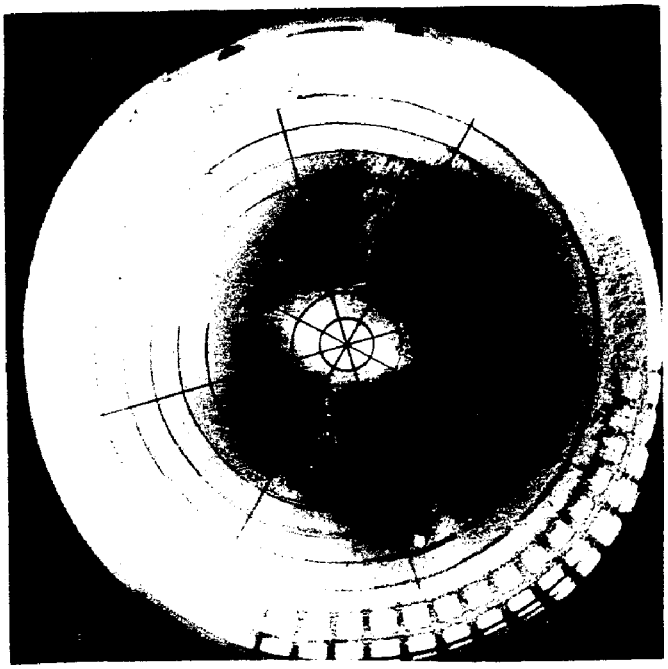

AFTER DEFORMATION

FIG. 35 DEFORMATION OF PURE ALUMINUM DISC (UNLUBRICATED)

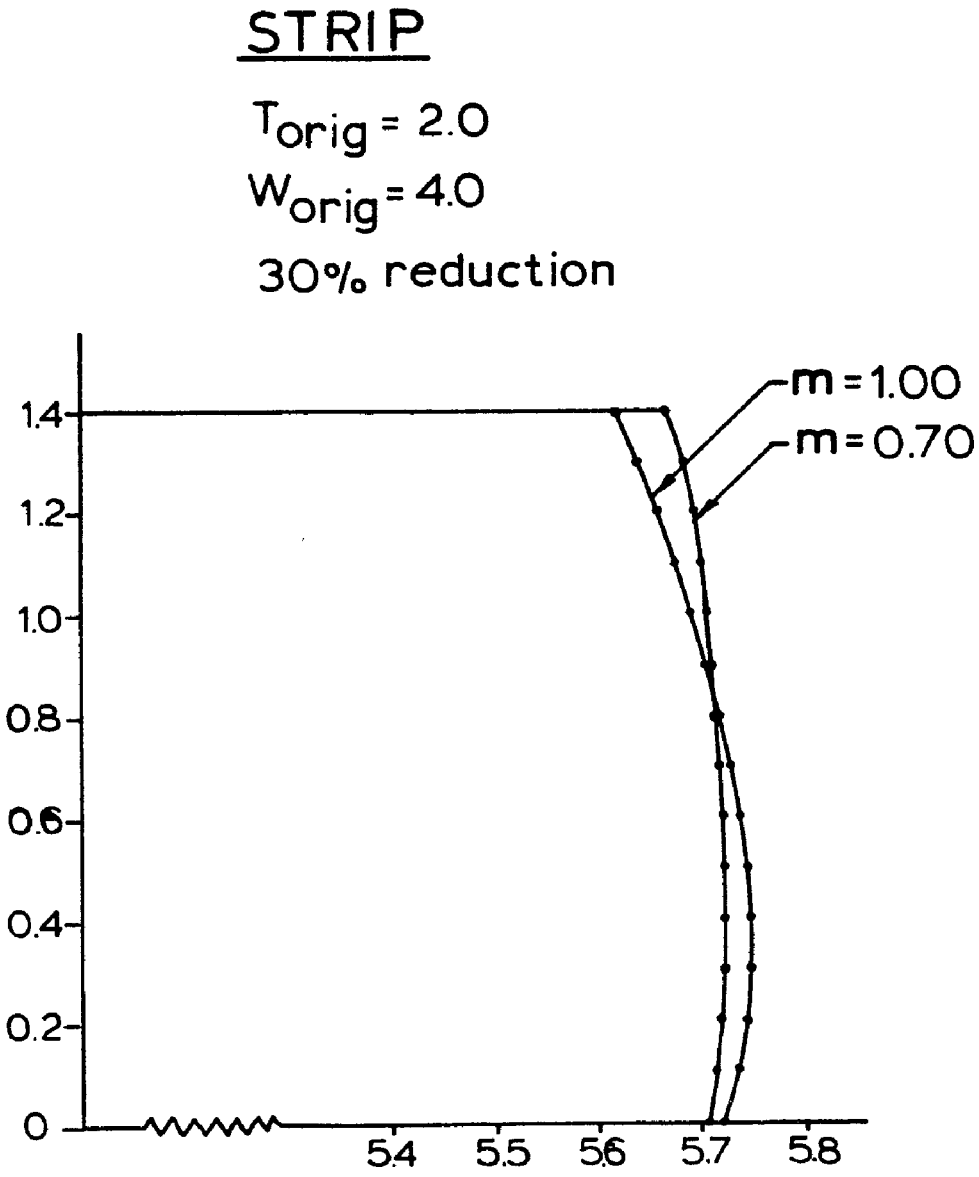

FIG.36 EFFECT OF THE FRICTION FACTOR

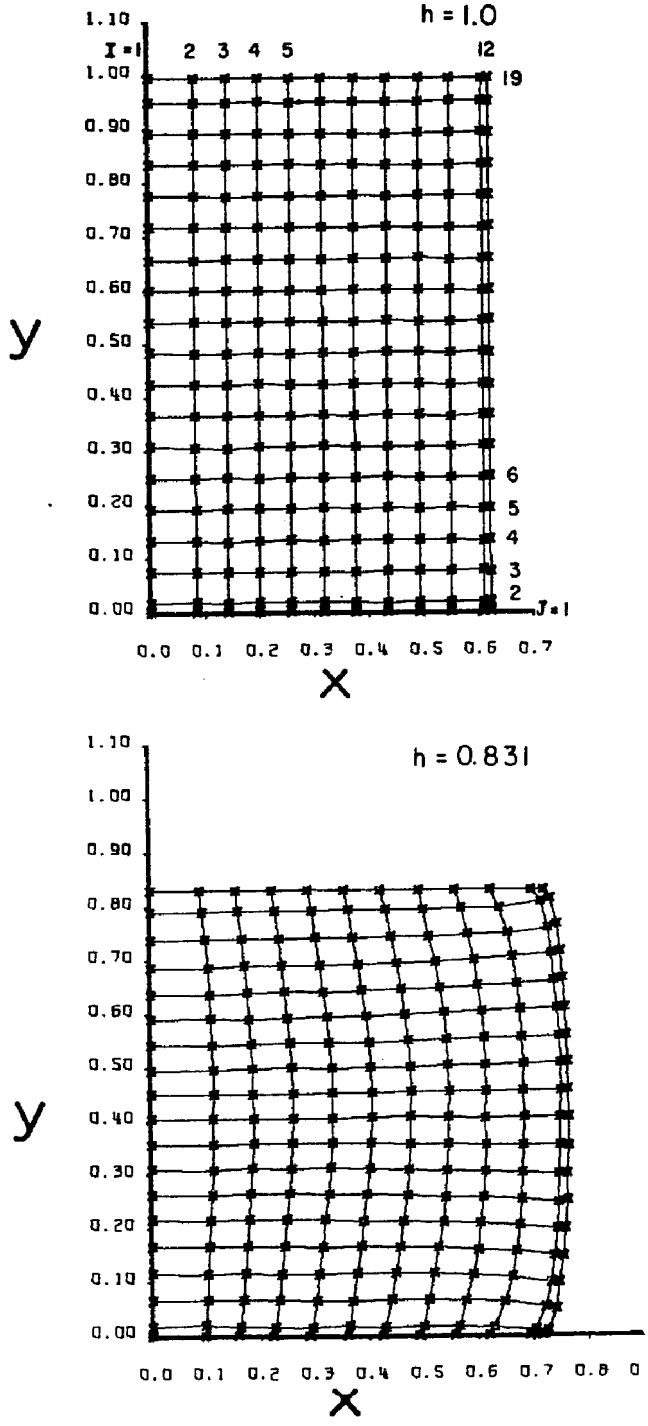

FIG. 37a DISTORTED GRID
PLANE-STRAIN (no lubricant)
From Ref [78]

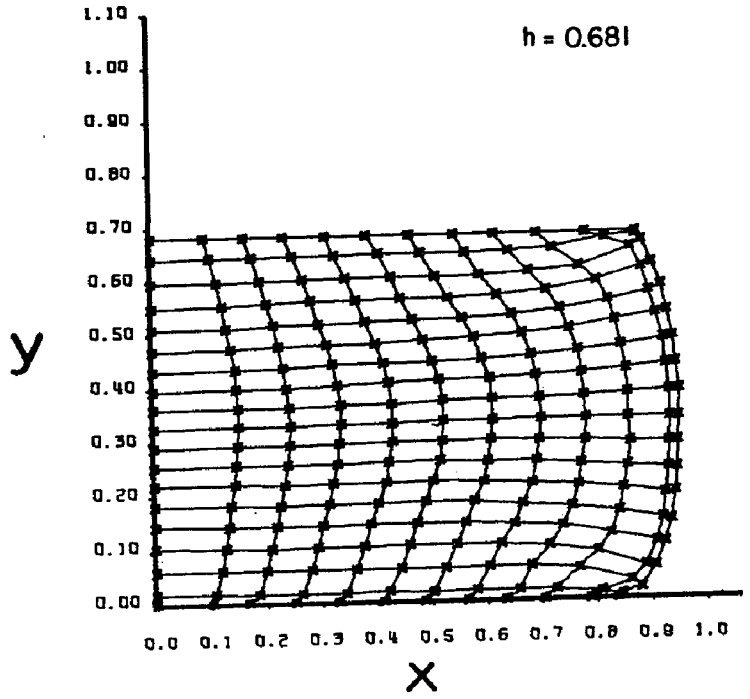

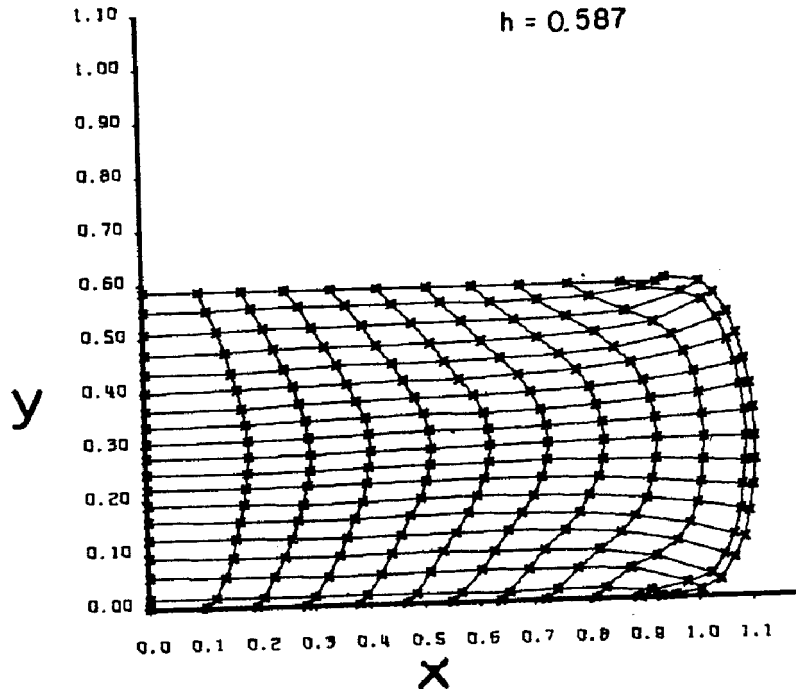

FIG. 37b DISTORTED GRID (continued)

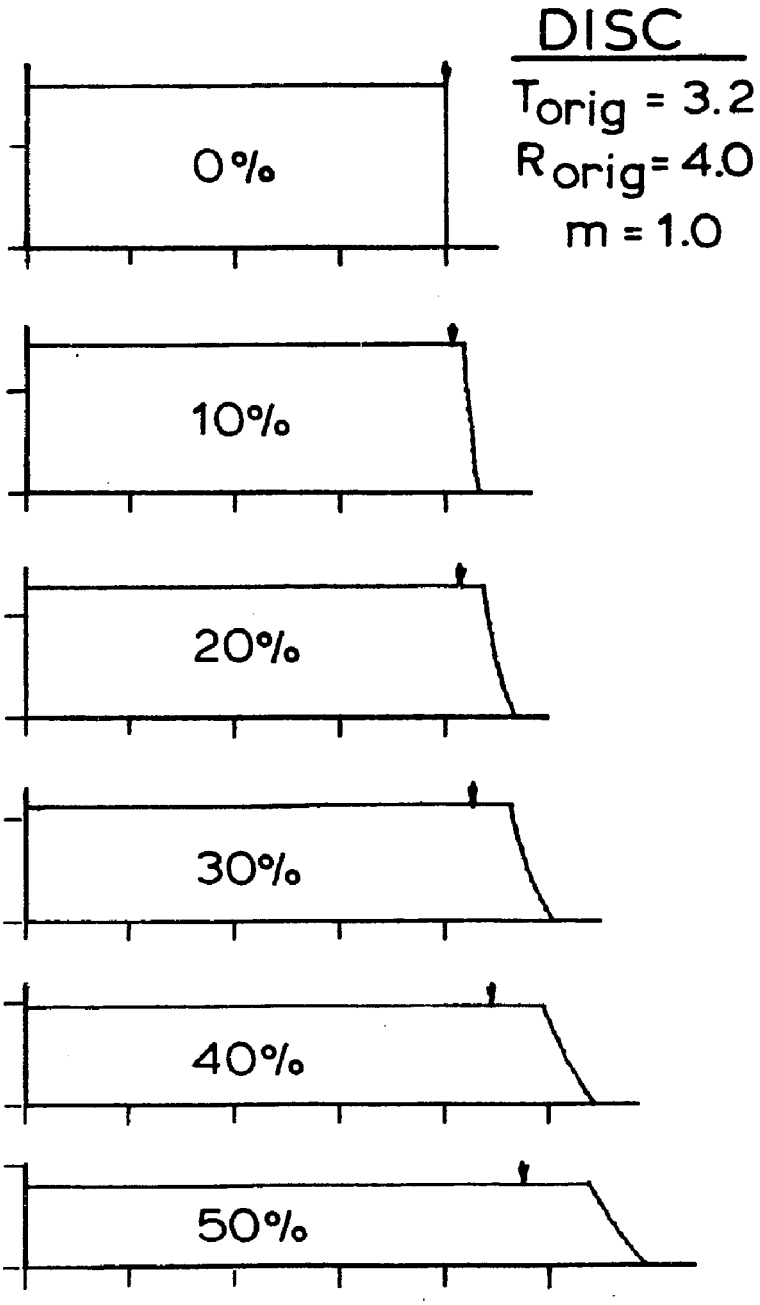

FIG. 38 DEFORMATION SEQUENCE FOR DISC

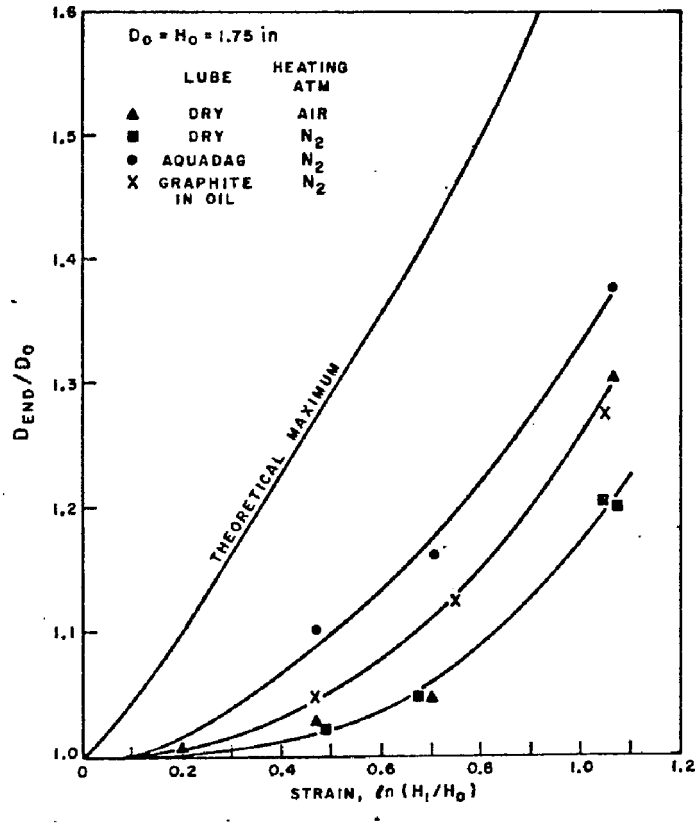

Variation of Original Top End-Face Diameter (D_o) with Strain for Simple Press Upsetting of Steel. Speed, 30 ipm.

theoretical by:

$$D_{end}^2 H_i = D_o^2 H_o$$

FIG. 39 EXPERIMENTAL RESULTS From Ref. [59]

REFERENCES

1. Kalpakjian, Serope, Mechanical Processing of Materials, D. Van Nostrand Co., Inc., 1967.

2. Jenson, Jon E., editor, Forging Industry Handbook, Forging Industry Association, 1966.

3. Avitzur, Betzalel, "Metal Forming: The Application of Limit Analysis", unpublished manuscript, Institute for Metal Forming, Lehigh University, July, 1973.

4. Hill, R., "A General Method of Analysis for Metal Working Processes", J. Mech. Phys. Solids, Vol. 11 (1963), pp. 305-326.

5. Tardif, H. P., "Deformation Studies in Metal Working Problems", Steel Processing and Conversion, Vol. 43 (Nov., 1957), pp. 626ff.

6. Kobayashi, Shiro and Thomsen, E. G., "Methods of Solution of Metal Forming Problems", Chapter 3 of the text: Fundamentals of Deformation Processing - Proceedings of the Ninth Sagamore Army Materials Research Conference, edited by Walter A. Backofen, et al., Syracuse University Press, 1964, pp. 43-69.

7. Dieter, George E., Jr., Mechanical Metallurgy, McGraw-Hill Book Company, New York, 1961.

8. Shah, S. N., et al., "Compression of Tall, Circular, Solid Cylinders Between Parallel Flat Dies", proceedings of the Int'l Conf. Prod. Engr., Tokyo, Aug., 1974, pp. 295-300.

9. Lee, C. H., and Kobayashi, Shiro, "New Solutions to Rigid-Plastic Deformation Problems Using a Matrix Method", J. Eng. Indust., Trans. ASME, Vol. 95 (1973), pp. 865-873.

10. Lee, C. H., and Kobayashi, Shiro, "General Matrix Method for Rigid-Plastic Deformation Problems", unpublished work, University of California - Berkeley, February, 1972.

11. Sauerwine, Fred R., "Limit Analysis of Hollow Disc Forging", Unpublished Ph.D. dissertation, Dept. of Met. and Mat. Sci., Lehigh University, 1971.

12. Thomsen, E. G., Yang, C. T., and Kobayashi, S., Mechanics of Plastic Deformation in Metal Processing, The MacMillan Company, New York, 1965.

13. Lee, C. H., and Altan, T., "Influence of Flow Stress and Friction Upon Metal Flow in Upset Forging of Rings and Cylinders", ASME Paper 71-WA/Prod-9, J. Eng. Indust., ASME Trans.

14. Sabroff, A. M., Boulger, F. W., and Henning, H. J., Forging Materials and Practices, Reinhold Book Corp., New York, 1968.

15. Prandtl, L., "Anwendungsbeispiele zu einem Henckyschen Satz über das Plastische Gleichgewicht", Zeits Angew. Math. u. Mech., Vol. 3 (1923), pp. 401-406.

16. Geiringer, H. and Prager, W., "Mechanik Isotroper Koerper im Plastichen Zustand", Ergeb. d. exact. Naturwiss, Vol. 13 (1934), pp. 310-363.

17. Siebel, E., "The Application to Shaping Processes of Hencky's Laws of Equilibrium", J. Iron and Steel Inst., Vol. 155 (1947), pp. 526-534.

18. Hill, R., The Mathematical Theory of Plasticity, Oxford University Press, New York, 1950, pp. 226-236.

19. Hill, R., Lee, C. H., and Tupper, S. J., "A Method of Numerical Analysis of Plastic Flow in Plane Strain and its Application to the Compression of a Ductile Material between Rough Plates," Trans. ASME, J. Appl. Mech., Vol. 18 (1951), p. 46ff.

20. Alexander, J. M., "The Effect of Coulomb Friction in the Plane-Strain Compression of a Plastic-Rigid Material", J. Mech. and Phys. Solids, Vol. 3 (1955), pp. 233-245.

21. Bishop, J. F. W., "On the Effect of Friction on Compression and Identation Between Flat Dies", J. Mech. and Phys. Solids, Vol. 6 (1958), pp. 132-144.

22. Shabaik, Aly H., "Prediction of the Geometry Changes of the Free Boundary during Upsetting by the Slip-Line Theory", Trans. ASME, J. Eng. Indust., Vol. 93, (1971), pp. 586ff.

23. Shabaik, A. H., "Effect of Friction and Degree of Deformation on Bulge Profile During Compression", Proceedings of the North American Metalworking Research Conference, May 14 and 15, 1973, McMaster Univ., Hamilton, Ontario, Canada; Volume 1: Metal Forming, pp. 221-238.

24. Johnson, W., "Over-Estimates of Load for Some Two-Dimensional Forging Operations", Proc. 3rd U.S. Congr. Appl. Mech., ASME, New York, 1958, pp. 571-579.

25. Johnson, W. and Kudo, H., "The Compression of Rigid-Perfectly Plastic Material Between Rough Parallel Dies of Unequal Width", Int. J. Mech. Sciences, Vol. 1 (1960), pp. 336-341.

26. Kudo, H., "An Upper-Bound Approach to Plane-Strain Forging and Extrusion", Parts I, II, III, Int. J. Mech. Sciences, Vol. 1 (1960), pp. 57ff, 229ff, and 366ff.

27. Avitzur, B., Metal Forming: Processes and Analysis, McGraw-Hill, New York, 1968.

28. Avitzur, B., "Limit Analysis of Disc and Strip Forging", Int. J. Machine Tool Design and Research, Vol. 9 (1969), pp. 165-195.

29. Siebel, E., "Die Formgebung im Bildsamen Zustand", Stahl u. Eisen, 1932, p. 25ff.

30. Shaw, Milton C., "Surface Conditions in Deformation Processes", Chapter 5 of the text: Fundamentals of Deformation Processing - Proceedings of the Ninth Sagamore Army Materials Research Conference, edited by Walter A. Backofen, et al., Syracuse University Press, 1964, pp. 107-130.

31. Kulkarni, K. M. and Kalpakjian, S., "A Study of Barrelling as an Example of Free Deformation in Plastic Working", Trans. ASME, J. Eng. Indust., Vol. 91 (1969), pp. 743-754.

32. Schroeder, W. and Webster, D. A., "Press-Forging Thin Sections: Effect of Friction, Area, and Thickness on Pressures Required", J. Appl. Mech., Vol. 16 (1949), pp. 289-294.

33. Kudo, H., "Some Analytical and Experimental Studies of Axi-symmetric Cold Forging and Extrusion - I", Int. J. of Mech. Sciences, Vol. 2 (1960), pp. 102-127.

34. Kudo, H., "Some Analytical and Experimental Studies of Axi-symmetric Cold Forging and Extrusion - II", Int. J. of Mech. Sciences, Vol. 3 (1961), pp. 91-117.

35. Kobayashi, Shiro, "Upper-Bound Solutions of Axisymmetric Forming Problems - I", Trans. ASME, May, 1964.

36. Kobayashi, S., and Thomsen, E. G., "Upper and Lower-Bound Solutions to Axisymmetric Compression and Extrusion Problems", Int. J. Mech. Sci., Vol. 7 (1965) p. 127ff.

37. Steck. E. and Schmid, K., "The Application of the Upper Bound Principal Upon Upsetting and Forging Operations" (in German), Industrie - Anzeiger, Vol. 87 (1965), p. 1751ff.

38. Lee, C. H. and Kobayashi, Shiro, "Analysis of Simple Upsetting of Solid Cylinders by the Finite Element Method", part 3 of: Analytical Prediction of Defects Occurrence in Simple and Complex Forgings by S. Kobayashi, et al., Technical Report AFML-TR-69-148, July, 1969, Air Force Materials Laboratory, Air Force Systems Command, W.P.A.F.B., Ohio.

39. Kobayashi, S., and Lee, C. H., "Deformation Mechanics and Workability in Upsetting Solid Circular Cylinders", Proceedings of the North American Metalworking Research Conference, May 14 & 15, 1973, McMaster Univ., Hamilton, Ontario, Canada; Vol. 1: Metal Forming, pp. 185-204.

40. "Principles of Forging Design", published by the Committee of Hot Rolled and Cold Finished Bar Producers, AISI, 633 Third Ave., N. Y., N. Y., 10017.

41. Avitzur, Betzalel, "Bulge in Hollow Disc Forging", Technical Report No. AFML-TR-69-261, Nov., 1969, Air Force Materials Laboratory, Air Force Systems Command, W.P.A.F.B., Ohio.

42. "Technical Evaluation of the Forging Industry", published by the Committee of Hot Rolled and Cold Finished Bar Producers, AISI, 633 Third Ave., N. Y., N. Y., 10017.

43. DePierre, V., et al., "Mathematical Calibration of the Ring Test with Bulge Formation", Technical Report No. AFML-TR-72-37, March, 1972, Air Force Materials Laboratory, Air Force Systems Command, W.P.A.F.B., Ohio.

44. Male, A. T., "The Friction of Metals Undergoing Plastic Deformation at Elevated Temperatures", Ph.D. thesis, Department of Industrial Metallurgy, University of Birmingham, England, October, 1962.

45. Male, A. T., and Cockcroft, M. G., "A Method for the Determination of the Coefficient of Friction of Metals Under Conditions of Bulk Plastic Deformation, J. Inst. Metals, 1964-65, Vol. 93, pp. 38-46.

46. Male, A. T., "Variations in Friction Coefficients of Metals during Compressive Deformation", J. Inst. Met., Vol. 94 (1966), pp. 121-125.

47. Burgdorf, M., "Investigation of Friction Values for Metal Forming Processes by the Ring Compression Method", Industrie - Anzeiger, Vol. 89 (1967), p. 799ff.

48. DePierre, V., Saul, G., and Male, A. T., "The Relative Validity of Coefficient of Friction and Interface Friction Shear Factor for Use in Metal Deformation Studies", AFML-TR-70-243, October, 1970. (See also ASME paper 72-7A-3)

49. Hawkyard, J. B., and Johnson, W., "An Analysis of the Changes in Geometry of a Short Hollow Cylinder During Compression", Int. J. Mech. Sci., Vol. 9 (1967), p. 163ff.

50. Saul, G., et al., "A New Method for the Determination of Material Flow Stress Values Under Metalworking Conditions", Metal Forming: Interrelation Between Theory and Practice, edited by A. L. Hoffmanner, Plenum Press, N. Y., 1971, p. 293ff.

51. Abdul, N. A., and Bramley, A. N., "Determination of Yield Stress-Strain Relations Using the Ring Compression Technique", Ref. SM/8, July, 1972, University of Leeds, Dept. of Mech. Engr., Leeds, England.

52. Male, A. T., and DePierre, V., "The Validity of Mathematical Solutions for Determining Friction from the Ring Compression Test", Trans. ASME, J. Lub. Tech., Vol. 92 (1970), pp. 389-395.

53. Avitzur, Betzalel, "Bulge in Hollow Disc Forging", Technical Report No. AFML-TR-69-261, Nov., 1969, Air Force Materials Laboratory, Air Force Systems Command, W.P.A.F.B., Ohio.

54. Liu, J. Y., "An Analysis of Deformation Characteristics and Interfacial Friction Conditions in Simple Upsetting of Rings", ASME Paper No. 71-WA/Prod-12.

55. DePierre, V., and Gurney, F., "A Method for Determination of Constant and Varying Friction Factors During Ring Compression Tests", report of Air Force Materials Laboratory, contract USAF-F33615-71-C-1163.

56. "Improved Analysis for Hollow Disc Forging", Lehigh University Institute for Metal Forming proposal submitted to the United States Army Research Office - Durham, Nov. 17, 1971.

57. Kobayashi, Shiro, and Shabaik, A. H., "Analytical Prediction of Defect Occurrence in Simple and Complex Forging" - progress report to USAF Systems Engineering Group, W.P.A.F.B., contract AF-33615-68-C-1314.

58. Jain, Sulekh C., "Friction and Lubrication in Hot Forging: A Look at the Current State of the Art", Proceedings of the North American Metalworking Research Conference, May 14 & 15, 1973, McMaster Univ., Hamilton, Ontario, Canada; Vol. 1: Metal Forming, pp. 143-163.

59. "Metal Flow in Closed Die Forging of Steel", Committee of Hot Rolled and Cold Finished Bar Producers, AISI, 633, Third Ave., N. Y., N. Y., 10017: Part I - Fundamental Study by J. A. Schey, et al.; Part II - Speed and Lubrication Effects by J. A. Schey, et al.

60. Unksov, E. P., An Engineering Theory of Plasticity, Butterworth, London, 1961.

61. Kobayashi, Shiro, "Deformation Characteristcis and Ductile Fracture of Steel SAE 1040 in Simple Upsetting of Solid Cylinders and Rings", part 1 of: Analytical Prediction of Defects Occurrence in Simple and Complex Forgings, by S. Kobayashi, et al., Technical Report AFML-TR-69-148, July, 1969, Air Force Materials Laboratory, Air Force Systems Command, W.P.A.F.B., Ohio.

62. Lee, C. H., and Kobayashi, Shiro, "Analysis of Axisymmetric Upsetting and Plane-Strain Side-Pressing of Solid Cylinders by the Finite Element Method", Trans. ASME, J. Eng. Indust., Vol. 93 (1971), pp. 445ff.

63. Kobayashi, Shiro, and Oh, S. I., "Fracture Criterion for Materials in Plastic Deformation Processes", Technical Report AFML-TR-74-159, August, 1974, Air Force Materials Laboratory, Air Force Systems Command, W.P.A.F.B., Ohio.

64. Specimen provided through the courtesy of Mr. V. DePierre, Technical Manager for Metallurgical Processing, Metals and Processing Branch, Metals and Ceramics Division, Air Force Materials Laboratory, Wright-Patterson Air Force Base, Dayton, Ohio.

65. Unpublished picture provided by Mr. V. DePierre, Technical Manager for Metallurgical Processing, Metals and Processing Branch, Metals and Ceramics Division, Air Force Materials Laboratory, Wright-Patterson Air Force Base, Dayton, Ohio.

66. Pearsall, G. W., and Backofen, W. A., "Frictional Boundary Conditions in Plastic Compression", Trans. ASME, J. Eng. Indust., Vol. 85 (1963), pp. 68-76.

67. Prager, W., and Hodge, P. G., Jr., Theory of Perfectly Plastic Solids, John Wiley, New York, 1951.

68. The CRC Handbook of Mathematical Tables, Second Edition, edited by Robert C. Weast, et al., The Chemical Rubber Company, Cleveland, Ohio, 1964.

69. van Rooyen, G. T., and Backofen, W. A., "A Study of Interface Friction in Plastic Compression", Int. J. Mech. Sci., Pergamon Press Ltd., Vol. 1 (1960), pp. 1-27.

70. Kobayashi, Shiro, "Tentative Analysis for Bulge and Strain: Future Work" - Progress report, August, 1969.

71. Parkins, R. N., Mechanical Treatment of Metals, American Elsevier Publishing Co., Inc., New York, 1968.

72. Dwight, H. B., Tables of Integrals and Other Mathematical Data, The Macmillan Company, New York, Fourth Edition, 1961.

73. Tarnovskii, I., et al., Deformation of Metals During Rolling, Pergamon Press, New York, 1965.

74. Kudo, H., and Aoi, K., "Effect of Compression Test Conditions upon Fracturing of a Medium Carbon Steel--Study on Cold Forgeability Test: Part II", J. Japan Soc. for Tech. of Plasticity, Vol. 8 (1967), p. 17ff.

75. Nagamatsu, A., et al., "On the Non-Uniform Deformation of Material in Axially Symmetric Compression Caused by Friction", Bulletin of the JSME, Vol. 14 (1971), pp. 331-338.

76. Hsu, T. C., "A Study of the Compression Test for Ductile Materials", Materials Research and Standards (A.S.T.M.), December, 1969, p. 20ff.

77. Berkowitz, Lawrence and Kuhn, Howard, A., "A Simplified Minimum Internal Energy of Deformation Postulate and its Application to Metalforming Processes", Proceedings of NAMRC-II, Second North American Metalworking Research Conference, Society of Manufacturing Engineers, May, 1974, pp. 336-349.

78. Shabaik, A. H., and Kobayashi, Shiro, "Plastic Flow Observations in Plane-Strain and Axisymmetric Compression", part 2 of: Analytical Prediction of Defects Occurrence in Simple and Complex Forgings, by S. Kobayashi, et al., Technical Report AFML-TR-69-148, July, 1969, Air Force Materials Laboratory, Air Force Systems Command, W.P.A.F.B., Ohio.

APPENDIX A

THE TWO-ZONE THREE-PARAMETER SOLUTION FOR STRIP

Introduction

As was noted in the text, a two-zone three-parameter solution was developed for the strip geometry involving a significant increase in mathematical complexity and substantial use of approximation and numeric integration. Investigation of the results, however, showed that no significant benefit was obtained through the more complex approach. Since the basic concept of building toward a generalized, all-inclusive solution is indeed a valid and attractive one, the details of the solution are included here as a reference for possible re-evaluation and improvement.

Figure 22 presents the basic velocity field to be applied in the solution. Zone I will obey the exponential bulge velocity field used in the Zone I region of the two-parameter solution and presented as Equation (3). In Zone II, the velocity field will be characterized by the general form:

$$\begin{aligned} \dot{U}_x &= \dot{U}_x\,(x,y) \\ \dot{U}_y &= \frac{-F}{1-e^{-b}}\,\dot{U}\,(1 - e^{-by/t}) \\ \dot{U}_z &= 0 \end{aligned} \qquad \text{(A-1)}$$

The upper-bound relation of Equation (1) will be applied and the two-zone description of Equation (2) and following will still apply.

Internal Power of Zone I and Interface Friction

Since the Zone I region of the three-parameter solution is identical to that of the previously presented two-parameter solution, all powers relating to the Zone I region may be represented by their previous relations. Equation (19) presents an upper-bound approximation of the internal power of deformation for Zone I, which appears in an exact form with a remaining integral in Equation (50). Friction losses along the workpiece-platen interfaces can be computed explicitly by Equation (26).

Velocity Field of Zone II

Paralleling the techniques presented in the two-zone two-parameter solution, flow continuity and volume constancy are now applied to characterize the velocity field of Zone II. Approaching the interzone boundary from the Zone I region, the velocity component normal to the interface remains unchanged and is therefore represented by Equation (28). In the Zone II region, however, there are now two non-zero velocity components, $\dot{U}_x$ and $\dot{U}_y$. Equation (A-1) has already specified the form of $\dot{U}_y$ to be assumed throughout the entire volume of Zone II. The $\dot{U}_x$ component, however, must be chosen to assume a form consistent with velocity continuity normal to the interface and volume constancy throughout the entire region. Elementary vector analysis will show that the form of $\dot{U}_x$ at the interzone boundary must be:

$$\dot{U}_{xII}\Big|_{bdy} = \frac{\dot{U}\xi}{(1-e^{-b})t}\left\{e^{-by/t}\left(\frac{bw}{\xi} - b + \frac{by}{t} - 1 + F\right) + 1 - F\right\} \tag{A-2}$$

A simple check here shows that if F is set equal to one, the values for $\dot{U}_x$ zone I and $\dot{U}_x$ zone II become identical at the interzone boundary as required.

To extend the form of $\dot{U}_x$ to the entire volume of Zone II, the strain rates field of Equation (4) is now evaluated using the velocity field of Equation (A-1), and the results are then subjected to the volume constancy relation of Equation (30). Thus, volume constancy requires:

$$\frac{\partial \dot{U}_x}{\partial x} - \frac{Fb}{(1-e^{-b})}\frac{\dot{U}}{t}e^{-by/t} = 0 \tag{A-3}$$

$$\dot{U}_x = \frac{xFb}{(1-e^{-b})}\frac{\dot{U}}{t}e^{-by/t} + f(y)$$

To evaluate f(y) the expression of Equation (A-3) is evaluated at the boundary where $x = w - \xi + \xi y/t$ and the result is equated to the previously developed form of Equation (A-2). Solving for f(y) and substituting into Equation (A-3) the velocity field for the volume of Zone II becomes:

$$\dot{U}_x = \frac{\dot{U}}{(1-e^{-b})} \left\{ \frac{xbF}{t} e^{-by/t} + (1 - F) \right.$$

$$\left. [e^{-by/t} (\frac{bw}{t} - \frac{b\xi}{t} + \frac{by\xi}{t^2} - \frac{\xi}{t}) + \frac{\xi}{t}] \right\}$$

$$\dot{U}_y = \frac{-F}{(1-e^{-b})} \dot{U} (1 - e^{-by/t})$$

$$\dot{U}_z = 0 \qquad \text{(A-4)}$$

A check shows that if F = 1, $\dot{U}_x$ assumes the value of the one-zone bulge solution and if F = 0, the form is identical to that of the two-parameter approach. Thus, the form of Equation (A-4) appears valid.

Zone II - Internal Power of Deformation

From the velocity field of Equation (A-4), the strain rates components of Equation (4) can now be explicitly evaluated to produce:

$$\dot{\varepsilon}_{xx} = -\dot{\varepsilon}_{yy} = \frac{\dot{U}}{(1-e^{-b})} \frac{bF}{t} e^{-by/t}$$

$$\dot{\varepsilon}_{xy} = \frac{\dot{U}}{2(1-e^{-b})} e^{-by/t} \frac{\xi b^2}{t^2} \left\{ \frac{-xF}{\xi} + (1-F) [1 - \frac{w}{\xi} + \frac{2}{b} - \frac{y}{t}] \right\} \text{(A-5)}$$

$$\dot{\varepsilon}_{zz} = \dot{\varepsilon}_{yz} = \dot{\varepsilon}_{zx} = 0$$

As before, the limits of F = 1 and F = 0 produce results corresponding to the bulge and two-parameter solutions respectively.

The internal power of deformation in Zone II can now be computed by the relation of Equation (6):

$$\dot{W}_{iII} = \frac{2}{\sqrt{3}} \sigma_o \int_V \sqrt{\frac{1}{2} \dot{\varepsilon}_{ij} \dot{\varepsilon}_{ij}} \, dV \qquad (6)$$

Substituting the strain rates of Equation (34) and integrating over the volume of Zone II, the expression becomes:

$$\dot{W}_{iII} = \frac{2\sigma_o}{\sqrt{3}} \int_V \sqrt{\dot{\varepsilon}_{xx}^2 + \dot{\varepsilon}_{xy}^2} \, dV$$

$$\dot{W}_{iII} = \frac{8\sigma_o \dot{U} b}{\sqrt{3}(1-e^{-b})t} \int_{y=0}^{y=t} e^{-by/t}$$

$$\left\{ \int_{x=w-\xi+\xi y/t}^{x=w} \sqrt{F^2 + \frac{1}{4} \frac{\xi^2 b^2}{t^2} \left\{ \right\}^2} \, dx \right\} dy$$

where:

$$\left\{ \right\}^2 = \left\{ -\frac{xF}{\xi} + (1 - F) \left[1 - \frac{w}{\xi} + \frac{2}{b} - \frac{y}{t} \right] \right\}^2 \qquad (A\text{-}6)$$

Considering the integral with respect to x, manipulation can produce the form:

$$\frac{1}{2}\,\frac{\xi b}{t}\int_x \sqrt{ax^2 + cx + f}\;dx \qquad \text{(A-7)}$$

where:

$$a = \frac{F^2}{\xi^2}$$

$$c = \frac{-2F\,(1 - F)\,[\;]}{\xi}$$

$$f = (1 - F)^2\,[\;\;]^2 + \frac{4t^2F^2}{\xi^2\,b^2}$$

$$[\;] = 1 - \frac{w}{\xi} + \frac{2}{b} - \frac{y}{t}$$

Integral tables can be consulted to show that:

$$\int_x \sqrt{ax^2 + cx + f}\;dx = \frac{(2ax + c)\sqrt{ax^2 + cx + f}}{4a} \qquad \text{(A-8)}$$

$$+ \frac{4af - c^2}{8a}\int_x \frac{dx}{\sqrt{ax^2 + cx + f}} \quad \text{and} \quad \int_x \frac{dx}{\sqrt{ax^2 + cx + f}}$$

$$= \frac{1}{\sqrt{a}}\,\ell n\left|2\sqrt{a}\,\sqrt{ax^2 + cx + f} + 2ax + c\right| = \frac{1}{\sqrt{a}}\sinh^{-1}\left\{\frac{2ax + c}{\sqrt{4af - c^2}}\right\} \qquad \text{(A-9)}$$

Evaluating the integral of Equation (A-7) and substituting the result into Equation (A-6) yields:

$$\dot{W}_{iII} = \frac{4\sigma_o \dot{U} \xi b^2}{\sqrt{3}\,(1-e^{-b})t^2} \int_{y=0}^{y=t} e^{-by/t} \left\{ \frac{1}{4a} \left[(2aw + c)\sqrt{aw^2+cw + f}\right.\right.$$

$$\left. - (2a\left[w - \xi + \xi \frac{y}{t}\right] + c) \sqrt{a\left[w-\xi+\xi \frac{y}{t}\right]^2 + c\left[w-\xi+\xi \frac{y}{t}\right] + f}\,\right]$$

$$\left. + \frac{4af - c^2}{8a} \frac{1}{\sqrt{a}} \left[\sinh^{-1}\left\{\frac{2aw+c}{\sqrt{4af-c^2}}\right\} - \sinh^{-1}\left\{\frac{2a\left[w-\xi+\xi \frac{y}{t}\right]+c}{\sqrt{4af - c^2}}\right\}\right]\right\} dy$$

(A-10)

Substituting for a, c, and f as per Equation (A-7), expanding all terms, and grouping by like powers of y produces:

$$\dot{W}_{iII} = \frac{4\sigma_o \dot{U} \xi b^2}{\sqrt{3}(1-e^{-b})t^2} \left\{ \int_{y=0}^{y=t} e^{-by/t} \left(\frac{\xi}{2} + \frac{\xi}{b} - \frac{\xi}{2F} + \frac{w}{2F} - \frac{\xi}{bF}\right)\right.$$

$$\sqrt{\frac{F^2w^2}{\xi^2} + \frac{4t^2F^2}{\xi^2b^2} - \frac{2wF(1-F)(1- \frac{w}{\xi} + \frac{2}{b})}{\xi} + (1-F)^2(1- \frac{w}{\xi} + \frac{2}{b})^2}$$

$$\left. + \frac{y}{t}\left\{\frac{2wF(1-F)}{\xi} - 2(1- \frac{w}{\xi} + \frac{2}{b})(1-F)^2\right\} + \left(\frac{y}{t}\right)^2 (1 - F)^2}\; dy\right.$$

(cont.)

$$+\int_{y=0}^{y=t} e^{-by/t}\, y\, \left(\frac{\xi}{2tF} - \frac{\xi}{2t}\right) \sqrt{\frac{F^2w^2}{\xi^2} + \frac{4t^2F^2}{\xi b^2} - \frac{2wF(1-F)\left(1-\frac{w}{\xi}+\frac{2}{b}\right)}{\xi}}$$

$$\sqrt{+\,(1-F)^2\left(1-\frac{w}{\xi}+\frac{2}{b}\right)^2 + \frac{y}{t}\left\{\frac{2wF(1-F)}{\xi} - 2\left(1-\frac{w}{\xi}+\frac{2}{b}\right)(1-F)^2\right\} + \left(\frac{y}{t}\right)^2 (1-F)^2}\; dy$$

$$-\int_{y=0}^{y=t} \left(\frac{\xi}{b} - \frac{\xi}{2F} + \frac{w}{2F} - \frac{\xi}{bF}\right) e^{-by/t} \sqrt{\frac{F^2}{\xi^2}(w-\xi)^2 - \frac{2F(1-F)\xi\left(\frac{w}{\xi}-1\right)\left(1-\frac{w}{\xi}+\frac{2}{b}\right)}{\xi}}$$

$$\sqrt{+\,(1-F)^2\left(1-\frac{w}{\xi}+\frac{2}{b}\right)^2 + \frac{4t^2F^2}{\xi^2 b^2} + \frac{y}{t}\left\{\frac{F^2 2(w-\xi)\xi}{\xi^2} - \frac{2F(1-F)\xi\left(2-2\frac{w}{\xi}+\frac{2}{b}\right)}{\xi}\right.}$$

$$\sqrt{\left. -\,(1-F)^2\, 2\left(1-\frac{w}{\xi}+\frac{2}{b}\right)\right\} + \left(\frac{y}{t}\right)^2 \left\{\frac{F^2\xi^2}{\xi^2} + \frac{2F(1-F)\xi}{\xi} + (1-F)^2\right\}}\; dy$$

$$-\int_{y=0}^{y=t} y\, e^{-by/t}\, \left(\frac{\xi}{2tF}\right) \cdot \sqrt{\frac{F^2(w-\xi)^2}{\xi^2} - \frac{2F(1-F)\xi\left(\frac{w}{\xi}-1\right)\left(1-\frac{w}{\xi}+\frac{2}{b}\right)}{\xi}}$$

(cont.)

$$+ (1-F)^2\left(1 - \frac{w}{\xi} + \frac{2}{b}\right)^2 + \frac{4t^2F^2}{\xi^2 b^2} + \left(\frac{y}{t}\right)\left\{\frac{F^2 2\,(w-\xi)\xi}{\xi^2} - \frac{2F(1-F)\xi\left(2-2\,\frac{w}{\xi} + \frac{2}{b}\right)}{\xi}\right.$$

$$\left. - (1-F)^2\,2\left(1 - \frac{w}{\xi} + \frac{2}{b}\right)\right\} + \left(\frac{y}{t}\right)^2\left\{\frac{F^2\xi^2}{\xi^2} + \frac{2F(1-F)\xi}{\xi} + (1-F)^2\right\}\,dy$$

$$+ \int_{y=0}^{y=t} e^{-by/t}\left(\frac{2Ft^2}{\xi b^2}\right)\sinh^{-1}\left\{\left(\frac{\xi b}{2t} + \frac{\xi}{t} - \frac{\xi b}{2Ft} + \frac{bw}{2Ft} - \frac{\xi}{Ft}\right) + y\left(\frac{\xi b}{2Ft^2} - \frac{\xi b}{2t^2}\right)\right\}dy$$

$$- \int_{y=0}^{y=t} e^{-by/t}\left(\frac{2Ft^2}{\xi b^2}\right)\sinh^{-1}\left\{\left(\frac{\xi}{t} - \frac{\xi b}{2Ft} + \frac{wb}{2Ft} - \frac{\xi}{Ft}\right) + y\left(\frac{\xi b}{2Ft^2}\right)\right\}\,dy \qquad \text{(A-11)}$$

Successfully evaluating or approximating the various integrals of Equation (A-11) provided the major hurdle of the three-parameter solution. As a first attempt, the equation was divided into its six component integrals and an effort was made to produce valid upper-bound approximations (of the nature of those presented in Figure 14 and discussed in the text of the two-parameter strip solution) for each component. This approach, however, proved far too complex when all of the various possibilities had to be considered.

For example, consider the first integral of Equation (A-11). The most troublesome component is obviously the $\sqrt{\ }$ term, which when investigated from $y = 0$ to $y = t$ for a range of process variables shows characteristics similar to those in Figure 14a. Thus, should the multiplying coefficient be positive, a straight line connecting the endpoints would be a valid upper-bound approximation. Should the multiplying coefficient of $\xi/2(1 + 2/b - 1/F + 1/SF - 2/bF)$ be negative, a definite possibility since b, F, and S are all floating variables subject to optimization, the characteristics of the $\sqrt{\ }$ term for upper-bound approximation must be considered as those of $-\sqrt{\ }$ and become similar to Figure 14b. Moreover, in the case of our present $\sqrt{\ }$ relation, the maximum value may be either at $y = 0$, $y = t$, or at some interim point. Thus, from just the first integral, four cases must be considered: 1) coefficient positive, 2) coefficient negative, max. at $y = 0$, 3) coefficient negative, interim maximum, and 4) coefficient negative, max. at $y = t$. At the expense of increased complexity, a straight-line tangent to the mid-point can reduce cases 2) through 4) to a single case, but the basic problem still exists.

The coefficient of the second integral is always positive, so only one case need be considered and a linear end-point connection is a valid approximation. The third integral has all four possible cases, and the fourth integral involves all three cases for a negative coefficient.

In the expressions for the fifth and sixth integrals, the $\sinh^{-1}$ function appears with the argument being a function of y and the parameters of the process. The basic function has an ever increasing value with varying curvature and an inflection point at the origin, but for the present forms, the range of consideration is flexible. Thus, in the range of integration, the function may be either entirely negative, partially negative and part positive, or entirely positive. Since a valid upper-bound approximation requires the overestimation of all positive components and the underestimation of negative terms, the first $\sinh^{-1}$ term must be assumed constant at its maximum value ($y/t = 1$) and the second term, constant at its value when $y/t = 0$.

The preceding technique with its multiple cases and numerous combinations thereof produces a solution that is far from attractive in its format and usefulness. As a result, a second approach was adopted to achieve a workable approximation to Equation (A-11). Under most conditions, the troublesome functions showed a near-linearity in the range of integration and can be closely approximated by a straight line connecting the end-points. The upper-bound quality of the solution may be sacrificed, but only a single solution is produced for each term and one expression finally approximates the internal power of Zone II.

Using a straight line between the end-points to approximate the square root components of the first four integrals of Equation (A-11) and approximating the final two integrals in the same manner

as in the previous approach, the Zone II internal power may be approximated as follows:

$$\dot{W}_{iII} = \frac{2\sigma_o \dot{U} w}{\sqrt{3}} \left\{ \frac{S^2 b}{(1-e^{-b})D} \right\} \left\{ \left[\left(1 + \frac{2}{b} - \frac{1}{F} + \frac{1}{SF} - \frac{2}{bF}\right) \right.\right.$$

$$\sqrt{\left\{ \frac{1}{S} - (1-F)\left(1 + \frac{2}{b}\right) \right\}^2 + \frac{4F^2D^2}{b^2S^2}} + \left(\frac{1}{F} - \frac{1}{SF} + \frac{2}{bF} - \frac{2}{b}\right)$$

$$\sqrt{\left(1 - \frac{1}{S} + \frac{2}{b} - \frac{2F}{b}\right)^2 + \frac{4D^2F^2}{b^2S^2}} + \frac{4F^2D^2}{b^2S^2} \left\{ \sinh^{-1}\left(\frac{S}{D} + \frac{b}{2FD} - \frac{S}{FD}\right) \right.$$

$$\left. \left. - \sinh^{-1}\left(\frac{S}{D} + \frac{b}{2FD} - \frac{S}{FD} - \frac{bS}{2FD}\right) \right\} \right] (1-e^{-b})$$

$$+ \left[\sqrt{\left\{ \frac{1}{S} - \frac{2}{b}(1-F) \right\}^2 + \frac{4F^2D^2}{b^2S^2}} + \left(\frac{2}{F} + \frac{2}{bF} - 2 - \frac{2}{b} - \frac{1}{SF}\right) \right.$$

$$\sqrt{\left\{ \frac{1}{S} - (1-F)\left(1 + \frac{2}{b}\right) \right\}^2 + \frac{4F^2D^2}{b^2S^2}} + \left(\frac{2}{b} + \frac{1}{SF} - \frac{2}{F} - \frac{2}{bF}\right)$$

$$\left. \sqrt{\left(1 - \frac{1}{S} + \frac{2}{b} - \frac{2F}{b}\right)^2 + \frac{4D^2F^2}{b^2S^2}} \right] \left(\frac{1}{b} - \frac{e^{-b}}{b} - e^{-b}\right)$$

(cont.)

$$+\left[-\sqrt{\left\{\frac{1}{S}-\frac{2}{b}(1-F)\right\}^2+\frac{4F^2D^2}{b^2S^2}}+(1-F)\right.$$

$$\sqrt{\left\{\frac{1}{S}-(1-F)\left(1+\frac{2}{b}\right)\right\}^2+\frac{4F^2D^2}{b^2S^2}}$$

$$\left.+\frac{1}{F}\sqrt{\left(1-\frac{1}{S}+\frac{2}{b}-\frac{2F}{b}\right)^2+\frac{4D^2F^2}{b^2S^2}}\right]\left(\frac{2}{b^2}-e^{-b}\left(\frac{2}{b^2}+\frac{2}{b}+1\right)\right]\Bigg\} \quad \text{(A-12)}$$

Since all other terms in the total power expression are rather straight-forward, it becomes clear that any improvements of the three-parameter solution would likely involve modification of either the Zone II velocity field or boundaries in a manner so as to reduce the present complexity.

Interzone Shear Losses

The interzone shear losses can be computed through use of Equation (20) in a manner similar to that presented in the two-parameter strip solution. The only difference is a change in $|\Delta v|$ due to the modification of the Zone II velocity field. Vector analysis applied to the velocity fields of Equations (3) and (A-1) will show that the tangential velocity discontinuity along the interzone boundary assumes the form:

$$|\Delta v| = (1-F)\frac{\sqrt{\xi^2 + t^2}}{t}\left\{\frac{\dot{U}\,(1-e^{-by/t})}{(1-e^{-b})}\right\} \qquad \text{(A-13)}$$

This term is simply (1-F) times the value of $|\Delta v|$ for the two-parameter solution (see Equation (43)). Since the added coefficient is a constant throughout the integration, the final result is simply (1-F) times that previously obtained in Equation (47), or:

$$\dot{W}_{sI-II} = \frac{4\sigma_o \dot{U} w}{\sqrt{3}(1-e^{-b})D}(1-F)\left\{(S^2+ D^2)\,(1 - \frac{1}{b} + \frac{e^{-b}}{b})\right\} \qquad \text{(A-14)}$$

Power to Overcome Imposed Body Tractions

The power required to overcome external pressure on the free surface area remains unchanged in the transition from two to three parameters. The velocity distribution along the free surface may vary, but the net volume of material expanding against the pressure must still equal the volume being displaced by the platens. Thus,:

$$\dot{W}_p = 4\,p\,\dot{U}\,w \qquad \text{(A-15)}$$

Total Power Required and Relative Average Forging Pressure

Equation (49) provides the form of the summation to compute the total power requirement. $\dot{W}_{iI}$, $\dot{W}_f$, and $\dot{W}_p$ all remain unchanged with respect to their forms in the two-parameter solution. $\dot{W}_{iI}$ is approximated by Equation (A-12) and $\dot{W}_{sI-II}$ is presented exactly in Equation (A-14). The form for the relative average forging pressure remains unchanged as Equation (52).

VITA

Ronald A. Kohser was born on May 22, 1947, in Pittsburgh, Pennsylvania, the son of Elinora F. and John C. Kohser.

Upon graduation from Shaler Senior High School, Glenshaw, Pennsylvania, he entered Lehigh University in September, 1965, where he received a Bachelor of Arts degree in June, 1969, with a major in physics. While pursuing undergraduate work, he received the Malcolm K. Gordon, Jr. Memorial Physics Prize, was awarded membership in Phi Beta Kappa, and graduated with Highest Honors and Interdepartmental Honors.

After his fifth consecutive summer of employment with the United States Steel Corporation, he entered Iowa State University and received a Master of Science degree in physics one year later in August, 1970.

The following month, he began graduate study in the Metallurgy and Materials Science Department of Lehigh University, pursuing a Ph.D. under the guidance of Dr. Betzalel Avitzur. During this study, he served as a teaching intern in laboratory courses relating to metal forming and fabrication, phase diagrams and transformations, and electronic properties and crystal structure, and assisted in numerous research efforts.

He is married to the former Barbara Ann Fritz of Bethlehem, Pennsylvania, and they are currently expecting their first child.